

GEOLOGIC MAP OF THE LAKE CHAPLAIN 7.5-MINUTE QUADRANGLE, SNOHOMISH COUNTY, WASHINGTON

by Joe D. Dragovich, Christina L. Frattali,
Megan L. Anderson, Shannon A. Mahan,
James H. MacDonald, Jr., Bruce A. Stoker,
Daniel T. Smith, Curtis J. Koger,
Recep Cakir, S. Andrew DuFrane,
and Kirsten B. Sauer

WASHINGTON
DIVISION OF GEOLOGY
AND EARTH RESOURCES
Map Series 2014-01
December 2014

*This geologic map was funded in part by the USGS
National Cooperative Geologic Mapping Program,
award no. G13AC00173*



WASHINGTON STATE DEPARTMENT OF
Natural Resources
Peter Goldmark - Commissioner of Public Lands

DISCLAIMER

Neither the State of Washington, nor any agency thereof, nor any of their employees, makes any warranty, express or implied, or assumes any legal liability or responsibility for the accuracy, completeness, or usefulness of any information, apparatus, product, or process disclosed, or represents that its use would not infringe privately owned rights. Reference herein to any specific commercial product, process, or service by trade name, trademark, manufacturer, or otherwise, does not necessarily constitute or imply its endorsement, recommendation, or favoring by the State of Washington or any agency thereof. The views and opinions of authors expressed herein do not necessarily state or reflect those of the State of Washington or any agency thereof.

This map product has been subjected to an iterative internal review process by agency geologists, cartographers, and editors and meets Map Series standards as defined by Washington Division of Geology and Earth Resources.

INDEMNIFICATION

Research supported by the U.S. Geological Survey, National Cooperative Geologic Mapping Program, under USGS award number G13AC00173. The views and conclusions contained in this document are those of the authors and should not be interpreted as necessarily representing the official policies, either expressed or implied, of the U.S. Government.

WASHINGTON STATE DEPARTMENT OF NATURAL RESOURCES

Peter Goldmark—*Commissioner of Public Lands*

DIVISION OF GEOLOGY AND EARTH RESOURCES

David K. Norman—*State Geologist*

John P. Bromley—*Assistant State Geologist*

Washington State Department of Natural Resources Division of Geology and Earth Resources

<i>Mailing Address:</i>	<i>Street Address:</i>
MS 47007	Natural Resources Bldg, Rm 148
Olympia, WA 98504-7007	1111 Washington St SE
	Olympia, WA 98501

Phone: 360-902-1450

Fax: 360-902-1785

E-mail: geology@dnr.wa.gov

Website: <http://www.dnr.wa.gov/geology>

Publications List:

[http://www.dnr.wa.gov/ResearchScience/Topics/
GeologyPublicationsLibrary/Pages/pubs.aspx](http://www.dnr.wa.gov/ResearchScience/Topics/GeologyPublicationsLibrary/Pages/pubs.aspx)

Washington Geology Library Searchable Catalog:

[http://www.dnr.wa.gov/ResearchScience/Topics/
GeologyPublicationsLibrary/Pages/washbib.aspx](http://www.dnr.wa.gov/ResearchScience/Topics/GeologyPublicationsLibrary/Pages/washbib.aspx)

Washington State Geologic Information Portal:

<http://www.dnr.wa.gov/geologyportal>

Suggested Citation: Dragovich, J. D.; Frattali, C. L.; Anderson, M. L.; Mahan, S. A.; MacDonald, Jr., J. H.; Stoker, B. A.; Smith, D. T.; Koger, C. J.; Cakir, Recep; DuFrane, S. A.; Sauer, K. B., 2014, Geologic map of the Lake Chaplain 7.5-minute quadrangle, Snohomish County, Washington: Washington Division of Geology and Earth Resources Map Series 2014-01, 1 sheet, scale 1:24,000, 51 p. text.

© 2014 Washington Division of Geology and Earth Resources
Published in the United States of America

Contents

Introduction	1
Description of Map Units.....	2
Quaternary Sedimentary Deposits	3
Holocene Nonglacial Deposits	3
Pleistocene Glacial and Nonglacial Deposits	5
Vashon Stade of the Fraser Glaciation.....	5
Pre-Fraser Glacial and Nonglacial Deposits.....	9
Tertiary Volcanic, Intrusive, and Sedimentary Rocks	14
Mesozoic Low-Grade Metamorphic Rocks of the Western Mélange Belt	15
Holocene to Tertiary Tectonic Zones	19
Geochemistry	20
Quaternary Sand Deposits.....	20
Western Mélange Belt	21
Isostatic Gravity and Aeromagnetic Analyses.....	23
Metamorphism and Structure of the Western Mélange Belt	26
The Lake Chaplain Nappe	27
Tertiary to Recent Faults and Folds	28
Overview.....	28
Cherry Creek Fault Zone	29
Ancient Alluvium and the Neotectonics of the Skykomish River Valley	30
Pleistocene Alluvium	30
Structural Control of the Skykomish River Valley	31
Regional Overview	31
Monroe Syncline.....	31
The Explorer Falls Basin	32
Acknowledgments.....	33
References Cited	33
Appendix A. Infrared and Optically Stimulated Luminescence Age Data	38
Appendix B. Seismicity in and near the Lake Chaplain 7.5-minute Quadrangle	40
Appendix C. U-Pb Detrital Zircon Geochronology	43
Appendix D. Geochemical Data	48

FIGURES

Figure 1. Regional tectonic map of the central Puget Lowland and Cascade foothills showing the Lake Chaplain quadrangle	2
Figure 2. Photo of recessional deltaic deposits (unit Qgod) in the Sultan River fluvial-deltaic complex in the south-central part of the map area.	6
Figure 3. Photo of probable fault cutting advance outwash deposits (unit Qgav) at significant site 10M west of Lake Chaplain.	9
Figure 4. Photo of peaty organic-silt rip-up clast in advance outwash (unit Qgav) at age site 37C west of the Sultan River	10
Figure 5. Photo of compact, laminated to thinly bedded sand and silt exposed in a steep 6-ft (2 m)-high road cut slope directly west of Marsh Creek (age site 37B)	11
Figure 6. Close-up photo of the deposits west of Marsh Creek showing the ptigmatic folding of silt beds between thicker beds of fine- to medium-grained sand	11
Figure 7. Photo of liquefaction-deformed Whidbey Formation nonglacial sand.....	12

Figure 8. Vanadium (V) vs. Scandium (Sc) provenance diagram for Quaternary sand samples and metasedimentary rocks from the WMB.....	21
Figure 9. Chondrite-normalized Lanthanum/Lutetium (La/Lu) vs. Lead/Ytterbium (Pb/Yb) diagram for Quaternary sand samples.....	21
Figure 10. Roser and Korsch discriminant function diagram for Quaternary samples and metasedimentary rocks from the WMB.....	22
Figure 11. Thorium/Ytterbium (Th/Yb) vs. Niobium/ Ytterbium (Nb/Yb) diagram, adapted for WMB meta-igneous samples	22
Figure 12. Thorium (Th)-Hafnium (Hf)-Tantalum (Ta) discrimination diagram, adapted for WMB meta-igneous samples	23
Figure 13. Rubidium (Rb)-[Yttrium (Y)+Niobium (Nb)] discrimination diagram for granitoid rocks, adapted for WMB “granitic” samples	23
Figure 14. Regional gravity map and major structures along the Monroe syncline.....	25
Figure 15. Lake Chaplain nappe diagram.....	26
Figure 16. Stereonets of Western mélange belt (WMB) structural data	27
Figure 17. Photo of greenschist facies, volcanoclastic to tuffaceous phyllite, and semischist (unit KJph _w)	29
Figure 18. Photo of strong metamorphic fabric at site 6A.....	29
Figure B1. Earthquake epicenters in and around the Lake Chaplain and Lake Roesiger 7.5-minute quadrangles	42
Figure C1. ²⁰⁶ Pb/ ²³⁸ U age distributions and concordia plot for sample 37A	47
Figure C2. ²⁰⁶ Pb/ ²³⁸ U age distributions and concordia plot for sample 35J.....	47

TABLES

Table 1. Sedimentary provenances for Quaternary deposits of the Lake Chaplain, Sultan, Lake Joy, Monroe, Carnation, North Bend, Fall City, and Snoqualmie areas.....	3
Table A1. Infrared stimulated luminescence (IRSL) and optically stimulated luminescence (OSL) data.....	38
Table B1. Earthquake focal mechanisms in the Lake Chaplain and surrounding area.....	40
Table C1. Detrital zircon U-Pb data for sample 37A (unit QCo).....	43
Table C2. Percentage area of major geologic units in the Skykomish River basin.....	45
Table C3. Detrital zircon U-Pb data for sample 35J (unit KJms _w).....	45
Table D1. X-ray fluorescence data	48
Table D2. Inductively coupled plasma mass spectrometry data	50

MAP SHEET

Geologic map of the Lake Chaplain 7.5-minute Quadrangle, Snohomish County, Washington

Figure M1. Aeromagnetic anomaly and gravity map

Figure M2. Geophysical cross sections

Geologic Map of the Lake Chaplain 7.5-minute Quadrangle, Snohomish County, Washington

by Joe D. Dragovich¹, Christina L. Frattali¹, Megan L. Anderson², Shannon A. Mahan³,
James H. MacDonald, Jr.⁴, Bruce A. Stoker⁵, Daniel T. Smith⁶, Curtis J. Koger⁷, Recep Cakir¹,
S. Andrew DuFrane⁸, and Kirsten B. Sauer⁹

¹ Washington Division of
Geology and Earth Resources
MS 47007
Olympia, WA 98504-7007

² Colorado College
Department of Geology
14 E Cache La Poudre St
Colorado Springs, CO 80903

³ U.S. Geological Survey
Box 25046, MS 974
Denver Federal Center
Denver, CO 80225-5046

⁴ Florida Gulf Coast University
Department of Marine and
Ecological Science
Fort Myers, FL 33965

⁵ Earth Systems
19729 207th Ave SE
Monroe, WA 98272

⁶ King County Department of
Natural Resources and Parks
Water and Land Resource Division
201 S Jackson St
Seattle, WA 98104

⁷ Associated Earth Sciences, Inc.
911 5th Ave, Suite 100
Kirkland, WA 98033

⁸ University of Alberta
Department of Earth and
Atmospheric Sciences
1-26 Earth Sciences Building
Edmonton, Alberta, Canada T6G 2E3

⁹ University of Nevada, Reno
Department of Geological Sciences
and Engineering
1664 N Virginia St
Reno, NV 89503

INTRODUCTION

The Lake Chaplain 7.5-minute quadrangle is directly north of Sultan and northeast of Monroe. The Sultan River flows northeast to southwest across the quadrangle forming a major bedrock-lined canyon along much of its length. It joins the Skykomish River directly south of the map area at Sultan. The Culmback Dam is east of the quadrangle at Spada Lake, and the Lake Chaplain reservoir is in the northwest part of the map area. These facilities supply water for three-quarters of Snohomish County, including the City of Everett. The Lake Chaplain quadrangle is the eighth in a series of 7.5-minute quadrangle geologic maps along the eastern margin of the Puget Lowland. Each map represents a year-long effort to document surficial and bedrock geology and geologic structures in the lower Snoqualmie and Skykomish river basins of King and Snohomish Counties—a densely populated region that is seismically active. The Lake Chaplain quadrangle abuts two recently completed quadrangles—Sultan and Monroe (Dragovich and others, 2011a,b, 2013) and is a northward continuation of the mapping in these quadrangles.

To enhance our mapping, we have added detailed field observations and several types of geologic analyses to existing data, including prior geologic mapping (for example, Booth, 1990; Tabor and others, 1993). We include geotechnical findings from Snohomish County road engineering studies, and surface and subsurface information from geotechnical companies. The map sheet presents the geologic map, cross sections, correlation diagram, and geophysical maps and models of the cross sections. Appendix A contains optically stimulated luminescence (OSL) and infrared stimulated luminescence (IRSL) age information for Quaternary deposits. See http://crustal.usgs.gov/laboratories/luminescence_dating/experts.html for a discussion of the relationship between radiocarbon, calendric and OSL/IRSL ages. Appendices B and C provide earthquake and U-Pb zircon age data, respectively. Appendix D provides geochemical data for sand and rocks.

We follow the nomenclature of Booth (1990) for many glacial features. For example, ‘Glacial Lake Skykomish’ describes the proglacial lake occupying much of the Skykomish Valley during Vashon Stade deglaciation. Our fault, fold, and geomorphic feature names shown on the map, such as the Monroe syncline and the various glacial recessional complexes, are informal. We use the informal term ‘Olympia beds’ in the same manner as Pessl and others (1989) to describe the deposits of the Olympia nonglacial interval.

Major active or potentially active structures in and near the quadrangle include the southern Whidbey Island fault zone (SWIF), Cherry Creek fault zone (CCFZ), Carnation fault, Monroe fault, and Monroe syncline (Fig. 1). The map area is northeast of the Rattlesnake Mountain fault zone (RMFZ) and the SWIF, fault zones that cut late Pleistocene strata in King and Snohomish Counties. The active CCFZ is conjugate to the SWIF and was responsible for the shallow 1996 Duvall earthquake (M5.4). Both of these structures are responding to north–south crustal compression across the Puget Lowland (Wells and others, 1998). The newly named Explorer Falls basin is a probable Pleistocene graben in the northwest part of the map area.

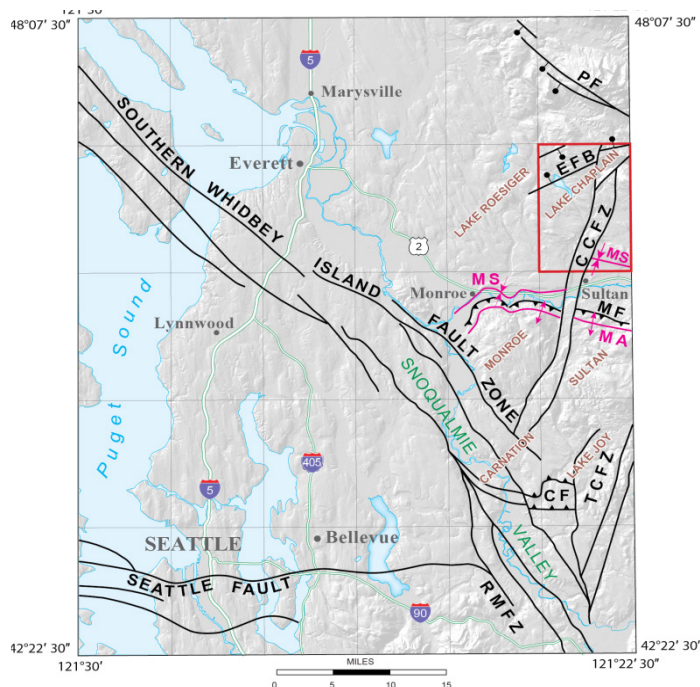


Figure 1. Simplified regional tectonic map of the central Puget Lowland and Cascade foothills showing the Lake Chaplain 7.5-minute quadrangle (red rectangle). The Cherry Creek fault zone (CCFZ) is mapped northward into the Lake Chaplain quadrangle from previous mapping in the Sultan, Lake Joy, and Carnation quadrangles (Dragovich and others, 2011a,b, 2012, 2013). The Tokul Creek fault zone (TCFZ) is similar to the CCFZ. They are likely left-lateral conjugates to the southern Whidbey Island fault zone. MF, Monroe fault; CF, Carnation fault; MS, Monroe syncline; MA, Monroe anticline; RMFZ, Rattlesnake Mountain fault zone; EFB, Explorer Falls basin. The bedrock high south of the Monroe fault and north of the Carnation fault is likely uplifted between these two opposing reverse faults. The Seattle fault zone and the SWIF are significantly simplified from Dragovich and others (2002) and Sherrod and others (2008). We also show the Pilchuck River fault (PF) of Tabor and others (2002) north of the map area. The PF and EFB might be related extensional structures that preserve Paleogene to Pleistocene basin sediments.

DESCRIPTION OF MAP UNITS

We use the Udden-Wentworth scale (Pettijohn, 1957) to classify unconsolidated sediments, Dickinson's (1970) terminology for sandstones, and Le Maitre and others' (2002) and Frost and others' (2001) terminology for igneous rocks. Clinopyroxenes are collectively described as 'augite' but may include other petrographically similar varieties. We use the time scales of the U.S. Geological Survey Geologic Names Committee (2010) and Wolfe and others (1998). Description of weathering rinds on basaltic clasts follows the methodology of Colman and Pierce (1981). We used the landslide classification system of Varnes (1978a,b). Quaternary sand deposit provenances are defined by compositional data derived from sand point-count data, petrographic observations, and sand geochemistry, as well as field data and observations (Table 1). Thin-section point-count data on the sand-size fractions helped differentiate several glacial and nonglacial units. An important compositional discriminator for Quaternary strata studied for this report is the ternary system composed of monocrystalline quartz (Qm_x); quartz-mica tectonite, polycrystalline quartz, and chert (Qp_x); and potassium feldspar (PF_x). The normalized $Qm_xQp_xPF_x$ data provided below were obtained from petrographic examination of 34 sand samples from the Lake Chaplain quadrangle as well as from Dragovich (2007) and Dragovich and others (2009b, 2010a,b, 2012, 2013). Percentages given for individual mineral or lithic grains are not normalized and represent the total clast population. See *Geochemistry* for a presentation and discussion of major and trace element composition of the Western mélange belt and Quaternary sand deposit samples. In that section, we show that some geologic units have distinctive geochemical characteristics consistent with other compositional metrics such as petrologic data.

Table 1. Sedimentary provenances for Quaternary deposits of the Lake Chaplain, Sultan, Lake Joy, Monroe, Carnation, North Bend, Fall City, and Snoqualmie quadrangles (Dragovich, 2007; Dragovich and others, 2009a,b,c, 2010a,b, 2011a,b, 2012, 2013, this study). Geologic units from the Lake Chaplain quadrangle are black; others from adjacent quadrangles are gray. Provenance is defined by composition from sand point-count data, petrographic observations, sand geochemistry, and field data. Nonglacial Pleistocene geologic units were deposited in fluvial depositional environments similar to modern (Holocene) rivers of the same provenance. RMFZ, Rattlesnake Mountain fault zone; SWIF, southern Whidbey Island fault zone.

Group	Geologic unit(s)	Sedimentary provenance and facies notes
SP (Snoqualmie or Skykomish river basin provenance)	Qa (Snoqualmie and Skykomish Rivers), Qc_o , Qc_{ws} , Qc_h , Qc_{pf} , Qc_{ph}	Snoqualmie and Skykomish river basin or central Cascade (nonglacial) provenance from eastern erosional sources. The major bedrock sources for SP sediments are Tertiary intrusive rocks such as the widely exposed Snoqualmie, Index, and Grotto batholiths. Ancient (Pleistocene) and modern Skykomish River alluvial facies are similar in composition to ancient and modern Snoqualmie River alluvial facies. All of these nonglacial units contain abundant monocrystalline quartz, K-spar, and plagioclase, and minor but distinct granitic lithic grains, biotite, pyroxene, and hornblende. The Monroe synclinal basin hosts a substantial thickness of these SP-provenance deposits and Dragovich and others (2009a,b,c, 2010a,b, 2011a,b, 2012, 2013, this study) postulate structural control for parts of these major river valleys by faults such as the RMFZ–SWIF or Monroe fault. (See <i>Ancient Alluvium and the Neotectonics of the Skykomish River Valley</i> .) In this study we map thick deposits of ancient Pilchuck River sediment (unit Qc_{ph}) exposed in the Explorer Falls basin. This graben contains early to middle Pleistocene sediment—with a distinctive Cascade granitic provenance—similar to SP-provenance deposits to the south. Although ancient Pilchuck River alluvium is generally more weathered than SP deposits to the south, they are compositionally indistinguishable.
LP (local provenance; Lake Chaplain and nearby quadrangles)	Qa (Tolt River, Youngs–Elwell Creek, and Sultan River), Qc_o , Qc_{hmp} , Qc_{phl}	Nonglacial provenance from local sources carried by low-order rivers flowing generally west, away from the Cascade foothills. Sediments are locally sourced and contain significant volcanic lithic grains, meta-argillite, and metasandstone, primarily derived from the volcanic rocks of Mount Persis and Western mélange belt (WMB). The fluvial network for these deposits includes both the modern and ancient Tolt River, Sultan River, and Youngs–Elwell Creek basins (40–100 mi ² ; 104–259 km ²). Modern Tolt River alluvium is compositionally and sedimentologically similar to ancient Tolt River alluvium and alluvial fan deposits (Dragovich and others, 2010a,b, 2012). Like the modern Tolt River fan at Carnation, ancient Tolt River alluvium interfingers with ancient Snoqualmie River alluvium locally, and may include alluvial fan deposits. Ancient Youngs–Elwell Creek alluvium likely interfingers with ancient Skykomish River alluvium (unit Qc_o) southwest of Sultan, similar to the modern interaction of the Skykomish River with the Youngs–Elwell Creek alluvial system (Dragovich and others, 2013). Similarly, ancient alluvium (unit Qc_{phl}) containing locally derived metasedimentary clasts—such as meta-argillite and phyllite—distinctly interfingers with Cascade-provenance alluvium (unit Qc_{ph}) in the Explorer Falls basin. SP-provenance unit Qc_{ph} occupies the valley axis and interfingers with locally-derived LP-provenance unit Qc_{phl} sediments towards the basin margin.
PG (Puget Group provenance)	Qc_{wp}	Deposits with a Puget Group provenance (Whidbey Formation in the southwest Carnation Quadrangle) are lithic rich and contain abundant andesite, and recycled arkosic (feldspathic) sandstone and siltstone clasts from the Tukwila, Renton, and Tiger Mountain Formations. Local rivers eroded these bedrock lithologies and transported them northward and northeastward into the lowlands, similar in style, but different in direction, to the local rivers of the ‘LP’ group. Deposits of both LP- and PG-provenance are locally derived, but differ because their source regions have distinctive and unique lithologies that provide paleogeographic information about ancient sediment dispersal systems. Fluvial PG sediments likely interfinger with SP fluvial sediments southwest of the map area near Carnation.
NP (northern provenance)	Qglr , Qgos , Qgod , Qgof , Qgic , Qgik , Qgog , Qgtv , Qgav , Qglv , Qgt_p , Qgop , Qgl_p , Qgd_d , Qgd_{pd}	Northern provenance sediments were deposited during continental glaciations and contain various lithic clast types, including high-grade metamorphic clasts, and have a high polycrystalline/monocrystalline quartz ratio and less K-spar when compared to more local Cascade Range sources. Sand grain types tend to be polymictic or varied due to the complexity of the northern provenance area. See Booth (1990) for further discussion of the provenance and depositional environments of NP glacial deposits. These sediments are locally mixed with some sediments of eastern and northeastern Cascade provenance (particularly for some Vashon Stade recessional deposits transported by ice-marginal meltwater).

Quaternary Sedimentary Deposits

HOLOCENE NONGLACIAL DEPOSITS

- af Artificial fill and modified land**—Mixed earth materials and natural deposits at the Lake Chaplain reservoir and powerhouse. Includes sand and gravel fill.
- Qp Peat**—Loose or soft peat, muck, and organic silt and clay, locally with diatomite and thin beds of Mazama ash (Rigg, 1958). Peat occurs in abandoned river-channel depressions where it is interstratified with alluvial deposits (for example, in the Sultan River valley) or deposited in upland depressions and kettles over low-permeability glacial deposits such as till or poorly sorted ice-contact deposits. Most of these deposits were mapped using lidar, topographic maps, and the previous mapping of Booth (1990). Rigg (1958) cored the Winters Lake peat deposit in the center of the quadrangle and documented a 20-ft

(6 m)-thick stratigraphic sequence of sphagnum, fibrous, and sedimentary peat interbedded with wood, muck, diatomite, and ash.

- Qa Alluvium**—Sand, silt, boulder to cobble gravel, gravelly sand, and sandy pebble gravel; unit locally includes some peat and organic sediments; clasts subrounded to rounded; some subangular to angular clasts in Sultan River alluvium; loose; well stratified and sorted; plane-bedded sand, wood debris, and detrital wood are common; sand typically light olive gray. Unit **Qa** and older Holocene alluvium (unit **Qoa**) are mapped in both the Skykomish and Sultan river valleys in the southernmost part of the quadrangle. The Skykomish River contains lenses of cobble-gravel-rich channel deposits—typical of its high-energy, braided-river depositional style—within low-energy overbank sediment sequences that contain mostly sand, silt, and peat. Most of the channel gravel is composed of intrusive, volcanic, and metasedimentary clasts, with a large fraction of granitic clasts. Unit **Qa** sand (~70–72% SiO₂) contains monocrystalline quartz, plagioclase, K-spar (~5–10%), hornblende (≤ 10%), and less, but significant, amounts of pyroxene, granitic lithic grains, and mica, with rare garnet or metamorphic lithic grains. This combination of minerals and lithic grains (and their relative proportions) are indicative of sediment eroded from the central Cascade Range and transported by the ancient Snoqualmie or Skykomish rivers ('SP' provenance; Table 1). Sultan River alluvium consists of cobble and boulder gravel containing a large fraction of Western mélange belt detritus, and is typical of more local sources ('LP' provenance; Table 1). Subsurface information suggests that Sultan River alluvium is 10 to 80 ft (3–24 m) thick. Due to map scale, we do not show alluvium along the Sultan River canyon or the Pilchuck River in the northeastern portion of the map area.
- Qoa Older alluvium**—Generally boulder to cobble gravel, sand, silt, and minor peat and organic sediments; subrounded to rounded clasts; loose; well stratified and sorted; plane-bedded sand, wood debris, and detrital wood common. Unit **Qoa** is inset against Pleistocene deposits and elevated above the modern Sultan or Skykomish River flood plains (Booth, 1990). Unit **Qoa** terraces were mapped using field mapping and lidar elevation information. These fluvial deposits are similar to the channel deposits of units **Qa** and **Qgof**, and thus could be either (1) earliest Holocene river deposits (unit **Qa**), or (2) latest Pleistocene fluvial outwash (unit **Qgof**) graded to a waning Glacial Lake Skykomish water surface. In the latter 'outwash scenario' these perched **Qoa** deposits would be fluvial-deltaic outwash deposited on the periphery of a shallowing Glacial Lake Skykomish at the close of the last glaciation, similar to the 'Monroe fan' of Dragovich and others (2011a). Alternatively, it is possible that Holocene neotectonic uplift or tilting may have contributed to the isolation of these alluvial deposits as valley marginal terraces.
- Qls Landslide deposits (Holocene to latest Pleistocene)**—Diamicton or boulder gravel with minor sand or gravel beds where locally modified by stream processes; loose or soft; typically poorly sorted and unstratified; clasts are angular to subangular where derived from bedrock, but are mostly rounded where the landslide originated in Quaternary deposits. Mapped landslides include rock falls, lateral spreads, slump-earthflows, debris slumps, and larger debris-flow deposits, but also a few areas of thick colluvium. This unit may include chaotic, stratified slump blocks or debris-flow aprons originating in unstable Vashon recessional deposits perched on hillsides. Some landslides may have initiated during late Pleistocene deglaciation. We show only the most prominent landslide complexes in the study area. In the Explorer Falls basin in the northwest part of the study area (significant site 36L), the unique Pleistocene stratigraphy and structure of a tilted mid-to-early Pleistocene basin has created hydrologic conditions conducive to landsliding—the westerly tilt of this bedrock-bounded basin has resulted in convergent groundwater flow through highly weathered sediments (Cross Section B). Groundwater flow through highly weathered and clayified sediments has resulted in both deep-seated and shallow landslides along the incised upper basin walls as well as a large, active alluvial fan complex. See Sarikhan and Pringle (2005) and Sarikhan and Vaugeois (2007) for detailed mapping and analyses of mass-wasting features in the Sultan basin, particularly along the Sultan River.
- Qaf Alluvial fan deposits (Holocene to latest Pleistocene)**—Diamicton, alluvial gravel, boulder gravel, and sand; loose, poorly to moderately sorted; moderately stratified to massive. The reduced gradient where streams emerge from confining valleys causes some sediment load to be deposited as a fan. Unit **Qaf**

deposits were distinguished from unit Qls deposits by their location and regular lobate shape visible on lidar imagery or aerial photographs, although many of the alluvial fans also contain significant debris flow deposits. Some fans may have initiated as fan deltas that graded to Glacial Lake Skykomish at the close of the last glaciation, similar to the ‘Monroe fan’ at the City of Monroe (Dragovich and others, 2011a). We attribute the large alluvial fan complex in the Explorer Falls basin to the unique hydrology of this Pleistocene basin (see unit Qls).

PLEISTOCENE GLACIAL AND NONGLACIAL DEPOSITS

Vashon Stade of the Fraser Glaciation

Deposits of the Vashon Stade of the Fraser Glaciation are widely distributed across the study area. Glacial ice and meltwater deposited drift and carved the southern Puget Lowland into a complex geomorphology that provides insight into late Pleistocene glacial processes. Vashon deposits are typically fresh to only slightly weathered; basalt clasts have very thin (commonly <0.5 mm) or no weathering rinds.

Vashon Recessional Deposits

Puget lobe continental ice advanced south across the Puget Lowland from British Columbia and flowed southeast to east across the Cascade Range foothills and up major west-draining river valleys. The ice sheet covered the map area—including Blue Mountain at 3,028 ft elevation in the northeast part of the map area—and terminated along the Cascade Range front 3 to 6 mi to the east (Booth, 1990). Vashon deglaciation in the map area began ~14,000 yrs BP along the Cascade foothills directly to the east, and the map area was ice free by ~13,500 yrs BP (Porter and Swanson, 1998). The Puget lobe ice front receded across the map area in a northwesterly direction, leaving Vashon recessional deposits. These deposits are horizontally and vertically complex due to facies changes generated by dynamic glacial depositional environments. During ice recession, a series of ice-marginal lakes and connecting glaciofluvial channels formed in the wake of the retreating ice lobe. The geometry, inset relationships, and elevation of the recessional deposits reflect successive lowering of the base level as lower valleys became ice-free and emerging spillways migrated westward and northward. This resulted in younger inset or terraced recessional deposits graded to these spillways (Knoll, 1967; Booth, 1990; Porter and Swanson, 1998).

Booth (1990) subdivided recessional outwash deposits into six stages of deglaciation and emphasized the importance of both ice-marginal and subglacial meltwater paths. For example, some of the southwest-trending valleys traversing the glacial uplands are the result of meltwater erosion and sedimentation in subglacial tunnels and open recessional valleys. Our mapping confirms that ice-marginal meltwater followed several elevated pathways during glacial recession and deposited fluvial, deltaic, lacustrine, and ice-contact sediments. Glacial Lakes Snoqualmie and Skykomish were ice-dammed lakes that inundated the Skykomish and Snoqualmie valleys during deglaciation and merged as ice tongues receded down the Snoqualmie and Skykomish valleys to the Monroe area (Mackin, 1941; Booth, 1990; Dragovich and others, 2007, 2009a,c, 2010a,b, 2011a,b, 2012, 2013). The elevation of glacial lakes controlled the location of recessional outwash and smaller lakes in the region. For example, the Sultan River fluvial-deltaic complex is graded to Glacial Lake Skykomish. As observed in adjacent quadrangles, many terraces record ancient southwest-trending recessional meltwater pathways that descend to Glacial Lake Skykomish elevations. Unit Qgof inset fluvial terraces and outwash channel landforms are the result of fluvial incision or erosion in response to dropping glacial lake levels during deglaciation. The glacial recessional sand is polycrystalline quartz-rich and compositionally distinct from the Pleistocene nonglacial SP-provenance alluvium (Table 1).

Qglr Recessional glaciolacustrine deposits—Silt, clayey or sandy silt, and silty sand, typically with scattered dropstones; local lenses or beds of sand or gravel; loose or soft; massive or laminated to thinly bedded; locally displays varve-like rhythmites. Upward-fining sequences record waning lake sedimentation in small proglacial lakes. Upward-coarsening sequences may begin as glacial-lake deposits (units Qglr and Qgos) and grade into overlying deltaic (unit Qgod) and fluvial (unit Qgof) deposits as a result of progradation of the outwash complexes into Glacial Lake Skykomish or smaller ice-marginal glacial lake environments. Glacial Lake Skykomish sediments were deposited at various elevations in the map area, and record a westward-receding glacial ice margin and a lower Glacial Lake Skykomish level. For example, the units Qglr and Qgos around Marsh Creek and near the Lake Bronson ice-contact complex appear to be early Glacial Lake Skykomish deposits (elevation ~720–800 ft). The Kellogg Lake kame-delta complex also terminates in glacial-lake deposits at an elevation (660–760 ft)

slightly lower than the delta top. The Sultan River fluvial-deltaic complex and Pipeline Road kame-delta complex also grade into distal glaciolacustrine deposits below the delta front elevation of ~480 ft. In the Pilchuck River valley in the northeast corner of the map area, Booth (1990) maps recessional glaciolacustrine deposits. Our mapping confirms that the valley contains recessional deposits, but expands the glacial types to include recessional sand deposits (unit Qgos) as well as advance lake deposits (unit Qglv). Broecker and others (1956) reported a radiocarbon date of 11,900 yrs BP from peat overlying soft blue clay (unit Qglr) in the Lake Joy quadrangle (Dragovich and others, 2012), indicating that the area was ice free before that time.

Qgos Outwash sand—Sand and pebbly sand with some interbeds of silty sand, silt, or gravel; sand (~73% SiO₂) is typically dark blue-gray and weathers brown-gray; loose or soft; varies from unstratified to weakly stratified; locally plane-bedded, laminated, and, rarely, crossbedded. Vertical and horizontal fining trends indicate mostly shallow-water glaciolacustrine deposition along delta fronts or as a sandy lake facies adjacent to silty glaciolacustrine deposits (unit Qglr). In some cases, sandy deposits (unit Qgos) may be higher-energy lake facies that represent former shorelines or sandy turbidite flows into finer grained lake facies. Unit Qgos is complexly interbedded with recessional lake deposits (unit Qglr), fluvial outwash deposits (unit Qgof), and deltaic or kame-deltaic deposits (unit Qgod). Most of the lateral and vertical fining trends—from gravel to sand to silt across these complexes—are best explained as textural changes resulting from simple deltaic progradation into a glacial lake environment; sand (unit Qgos) coarsens upward into sand and gravel (unit Qgod), which fines downward or laterally into silty lake deposits (unit Qglr). Some trough crossbeds at significant site 17D—in the Lake Bronson ice-contact complex outwash sand deposits—indicate southeasterly fluvial paleoflow toward the glacial-lake deposits mapped near Marsh Creek. In this area, we observed very thick sequences of sand and gravel that probably represent near-ice fluvial or fluvial-fan sequences along a glacial-lake proximal ice front.

Qgod Deltaic outwash and kame deltas—Sandy cobble gravel, gravel, and pebbly sand; sand is typically dark blue-gray to light gray and weathers to yellowish brown or brownish gray; loose; moderately to well sorted and well stratified in thin to very thick beds. Deltas have high-amplitude planar foreset beds graded to temporary ice-dammed lake levels. We have mapped several small deltas and larger delta complexes in the map area, including the Kellogg Lake and Pipeline Road kame-delta complexes and the Sultan River fluvial-deltaic complex. The high-amplitude planar foreset beds are well-exposed along the Sultan River delta complex front (Fig. 2). Sand at this front contains significant amounts of lithic grains and monocrystalline quartz, polycrystalline quartz (~10%), and plagioclase with much epidote, but low K-spar (~2%), and rare hornblende detrital grains. These recessional deltaic sand deposits have a strong ‘Sultan River’ provenance: abundant local mélange belt metachert, metasandstone, phyllite, meta-argillite, and greenstone grains and some foliated metamorphic exotic lithic grains (see NP in Table 1). Delta front gravel consistently grades to more distal delta front sand (unit Qgos) and glacial-lake silt



Figure 2. Recessional deltaic deposits (unit Qgod) in the Sultan River fluvial-deltaic complex in the south-central part of the map area (middle of sec. 29, T28N R8E). The high-amplitude foreset beds in the sand and gravel pit dip ~25° to the east-southeast and are the result of delta front deposits prograding into Glacial Lake Skykomish. Topset fluvial beds above this site indicate that the lake level was graded to a delta-top elevation of ~440 ft. The high proportion of sand in the deposits indicates deposition on the mid- to mid-lower delta front, consistent with a dip below 32° (angle of repose for these deposits). These delta-front deposits grade to lower delta-front or lacustrine sand (unit Qgos) directly south and southeast. We suggest that some of the gravel-cobble beds are grain-flow mass-wasting deposits that were originally deposited higher on the delta slope but slid to the lower delta slope during deglaciation as a result of delta front over-steepening.

(unit Qglr) in most areas. The delta complexes are graded to Glacial Lake Skykomish and are sediment accumulations adjacent to ice-contact complexes or have pitted outwash plains or other evidence for ice-proximal deposition (units Qgik and Qgof).

- Qgof Fluvial outwash deposits**—Cobble and boulder gravel, gravel, pebbly sand, and interbeds of sand and rare silt; sand is gray-brown and weathers olive-yellow; loose; moderately to well stratified and commonly contains medium to very thick subhorizontal beds that have local bar or ripple crossbedding, imbricated gravel, scour structures, and rip-up clasts. This unit generally lacks ice-contact sedimentary structures and other geomorphic and stratigraphic evidence for nearby ice, but some unit Qgof outwash grades laterally into pitted outwash plains that are suggestive of isolated kettle lakes. For example, the Sultan River valley outwash is mildly pitted, and suggests near-glacier deposition similar to the kame complexes in the map area (also see unit Qgik). Unit Qgof is commonly the topset beds of deltas (unit Qgod). A falling Glacial Lake Skykomish elevation controlled subaerial fluvial outwash incision and deposition over much of the map area. This incision is geomorphically prominent—lidar data reveals that fluvial outwash deposits above the Sultan River contain as many as twelve erosional inset terraces. These terraces are the result of meltwater incision into older glacial deposits as the base level of Glacial Lake Skykomish dropped during deglaciation. Outwash drainage channels and terraces are as high as 1,600 ft elevation in the northeast part of the map area, with prominent terrace levels at 1,180, 900, 830, 800, 600, 430, 400, and 270 ft elevation in the Sultan River valley. See Booth (1990) and Dragovich and others (2013, 2011a,b) for a discussion of the timing and elevation of the various controlling outlet lakes and connecting channels south of the map area.
- Qgic Ice-contact deposits, undivided**—Cobble to boulder gravel and gravel, locally containing diamicton, silty pebbly gravel, sand, pebbly sand, and silt; loose or soft; moderately stratified, medium to very thickly bedded, with varied sorting; abrupt grain-size changes are common. Ice-contact primary structures include oversteepened and contorted bedding and other ice-shear features, all of which produce strata of varied dip. Diamicton was deposited in a variety of settings, including melt-out, debris flow, and dropstone-rich lacustrine environments. The upper surface of the deposit is typically hummocky and contains numerous kettle depressions. The Lake Bronson ice-contact complex has several mappable ice-contact facies, including fluvial-deltaic kames (unit Qgik), glaciofluvial outwash, and hummocky dead-ice facies. An arcuate deposit directly east of significant site 17D might be a moraine. Locally, dead-ice deposits of the complex (unit Qgic) grade from kame deposits to recessional outwash fluvial and deltaic deposits (units Qgik and Qgod) and glacial-lake facies (units Qglr and Qgos). We interpret the ice-contact deposits adjacent to the Pipeline Road kame-delta complex as an ice margin that abutted a prograding kame complex. Taken together, the north–northeast-trending belt of ice-contact complexes implies an ice margin that waned or stagnated along the highlands during ice recession, similar to events that occurred south of the map area (Dragovich and others, 2013). The geometry and mutual relationships of these features—ice-contact deposits, kames, and fluvial outwash—form an arcuate lobe in the southern part of the map area, where ice-contact deposits generally young to the west. Also, as inferred by Booth (1990), geomorphic relations imply that an ice tongue extended up the Skykomish River valley during recession. This ice tongue probably persisted until Glacial Lakes Skykomish and Snoqualmie merged, after the ice margin decayed past the Monroe area (Dragovich and others, 2011a,b, 2013). Some of the smaller and isolated deposits of unit Qgic mapped outside the large ice-contact complexes are probably locations where active ice lobes were stable long enough for debris to accumulate, but do not necessarily represent ice stagnation. See Booth (1990) or Knoll (1967) for a discussion of the temporal and spatial relations of deglaciation, and Booth (1984, 1986, 1990) for a subglacial depositional model. Unit Qgic is locally divided into:
- Qgik Kames**—Cobble and boulder gravel, gravel, sand, and pebbly sand, and rare lenses of diamicton (mostly flow till or melt-out till from buried sediment-laden ice blocks); sand is typically dark yellowish gray to gray; loose; moderately to well stratified, medium to very thickly bedded, and commonly display till or silt rip-up clasts, cut-and-fill structures, and localized oversteepened or slumped bedding. This unit includes both fluvial and, locally, deltaic kame deposits. Kames were mapped where sedimentary structures, geomorphology, and (or) geologic setting imply lateral ice buttressing. Fluvial kame deposits in the Kellogg

Lake and Pipeline Road kame-delta complexes laterally grade into or overlie divided kame deltas (unit Qgod) and (or) proglacial-lake deposits (units Qgos and Qglr), forming upward-coarsening deposits. The Pipeline Road kame-delta complex probably formed after the Sultan River fluvial-deltaic complex, given the slightly lower elevation and westward position of the delta top near Pipeline Road. In other areas, receding or wasting ice impinged upon highlands, leaving small isolated kame deposits. Kames are also part of the more geomorphically complex ice-contact complexes in the area, including the Lake Bronson ice-contact complex, which Booth (1990) mapped mostly as kame deposits. (See unit Qgic for named ice-contact complexes.)

Qgog Outwash gravel deposits, undivided—Boulder–pebble gravel to pebbly sand; loose; massive to crudely bedded; mostly ice-contact deposits, including kame outwash deposits, but may include any of the gravelly Vashon recessional facies. We were unable to assign a depositional environment to unit Qgog deposits because they are poorly exposed. Unit Qgog along Woods Creek in the southwest part of the map area may have been formed by subglacial meltwater.

Vashon Advance Proglacial and Subglacial Deposits

Throughout the map area, drumlins and flutes show that Puget lobe ice advanced from northwest to southeast. Ice advance over this part of the lowland occurred about 14,500 radiocarbon years ago and blocked ancient rivers, creating extensive temporary lakes across much of the map area (Mackin, 1941; Booth, 1990). This general chronology is consistent with our new OSL/IRSL age for advance outwash of 14.1 to 16.4 ka at age site 37C. Most advance outwash consists of proglacial-fluvial-deltaic sediment, although some may be kame or other ice-contact sediments, or subglacial ice-tunnel sediments deposited between advancing ice and restricting highlands. Facies relationships among river and delta deposits (unit Qgav) and lake deposits (unit Qglv), as well as their thickness and widespread distribution indicate that one or more large proglacial lakes progressively occupied significant portions of the map area during ice advance (Knoll, 1967; Dragovich and others, 2007, 2009a,c, 2010b, 2011a, 2012, 2013). Similar to relations in the Sultan area, a complex series of advance deposits formed in front of the advancing ice as it interacted with the steep Cascade foothills and deep paleovalleys in the map area. Bedding in advance outwash and lake deposits generally has a southeast primary dip that reflect either (1) glaciofluvial or deltaic deposition of foreset beds on the lee side of fluvial bars that slope away from the advancing ice front into temporary glacially dammed lakes, or (2) steep-gradient, high-energy braided streams. Vashon-age strata on the geologic map show subtle bedding that slopes away from the advancing ice and probably does not indicate significant tectonic tilting. This differs from Pleistocene ('ancient') alluvial nonglacial deposits (for example, unit Qco), which were originally deposited as subhorizontal fluvial sandy and silty flood deposits. Advance outwash sediment (average composition ~Qm₄₀Qp₅₄PF₆) is polycrystalline-quartz-rich and contains a polymict variety of lithic sedimentary, igneous, and metamorphic grain types (unnormalized ~60–70%) that are distinctly different from nonglacial deposits that have an SP provenance (less monocrystalline quartz, plagioclase, and little or no K-spar (0–3%) or mica; Table 1). Petrographic and geochemical analyses of advance outwash sand (~65% SiO₂) indicate a complex provenance involving local and northern sources.

Qgtv Lodgment till—Unstratified mixture of clay, silt, sand, and gravel (diamicton), with rare lenses of sand and gravel; grayish blue to very dark gray, locally slightly weathered to mottled yellow-brown; sand-silt matrix-supported; unsorted; dense; accreted at the base of the Vashon ice and thus typically displays a friable shear fabric. Clasts are both local and northern-sourced and rounded to subangular. Angular clasts are present where this unit directly overlies bedrock. Till is generally 5 to 50 ft (1.5–15 m) thick and unconformably overlies advance deposits, older Quaternary deposits, or bedrock. Older tills were observed at significant sites 11A and 15T along the easternmost part of the study area on Blue Mountain—consistent with mapping by Booth (1990)—as well as under Vashon till in the southwestern part of the map area. Basalt clast weathering rinds in these older tills are about 2 mm thick. We tentatively correlate these older tills with the Possession Glaciation; these deposits were mapped extensively in the Monroe quadrangle to the southwest by Dragovich and others (2011a,b).

Qgav Advance outwash deposits—Sand and pebble gravel, sand and cobble gravel, and local silt; dense; sand beds are dark green-gray, weathering to yellowish brown, light yellowish brown, or pale brown; typically well sorted; mostly thinly to very thickly bedded with local silt interbeds, rip-up clasts,



Figure 3. Probable fault cutting advance outwash deposits (unit Qgav) at significant site 10M west of Lake Chaplain. Note the light weathering of these well-sorted gravel deposits. They are likely fluvial channel deposits that locally contain lag boulders and interbeds of pebbly coarse sand and form multistory beds (~20 ft thick). Imbricated cobbles in these dense glaciofluvial deposits indicate a paleoflow direction to the southeast. The fault strikes N30W, dips 72°NE, and has 1.5 ft (46 cm) of apparent dip-slip offset (top of the offset gravel bed shown with the black and red markers left and right of the fault respectively). The oblique dip of the fault into the hill (away from the viewer) is not consistent with a deep-seated slump failure plane, which typically dip toward the open slope (toward the viewer). View is to the east.

deltaic and bar foreset beds, and cut- and fill- structures. Advance outwash is intricately interlayered with, conformably overlies, or may locally underlie glacial-lake deposits (unit Qglv). Unit Qgav is most commonly overlain by Vashon lodgment till (unit Qgtv) along a sharp contact. Composite sections of fluvial-deltaic advance outwash and glacial-lake deposits are thick where fluvial-deltaic deposits prograded into restricted proglacial lakes during ice advance. Stratigraphic relationships suggest proglacial lakes occupied the Pilchuck River valley, Lake Chaplain area, and Skykomish River valley during ice advance. A steeply dipping northwest-trending fault displaces advance outwash at significant site 10M along the western margin of the quadrangle as shown in Figure 3. Radiocarbon dates for this unit from south and west of the map area are 14,450 to 14,560 yr BP, (17,313–17,426 cal yr BP) (Porter and Swanson, 1998; Associated Earth Sciences, Inc, 2003; Dragovich and others, 2007). We obtained OSL and IRSL ages of 14.1 ± 0.59 ka and 16.4 ± 0.64 ka from age site 37C directly west of the Sultan River in the south-central part of the map area, consistent with this chronology (Appendix A). Figure 4 shows a rip-up clast of peat in this deposit. We obtained a radiocarbon age of $14,900 \pm 50$ yr BP (17,985–18,250 cal yr BP) from plant material derived from this peat rip-up, which is consistent with the IRSL age within 2 sigma uncertainty. The older IRSL age is consistent with the observation that advance outwash scoured the older nonglacial deposits, resulting in the partial SP composition of the sand at site 37C (Appendix A).

Qglv Advance glaciolacustrine deposits—Silt, clayey silt, pebbly silt, and diamicton, locally with very thin to thick beds of sand; stiff to hard, or dense to very dense; stratification and sorting is varied, but commonly massive or thinly bedded, laminated, or varved; typically contains scattered dropstones and beds or lenses of massive till-like diamicton that may be iceberg melt-out till or flow till. Some exposures are mostly diamicton with thin, wispy interbeds of silt or laminated silt and sand. Unit Qgav typically overlies unit Qglv regionally—as a result of simple progradation of fluvial and deltaic outwash over proglacial lake deposits—but there are local exceptions where this order is reversed; elsewhere, the two units are complexly interbedded. We suspect that some of the more complexly layered advance outwash and lake sections are the result of partial draining of proglacial lakes that created stratigraphic repetition and inset relations. Some outcrops expose contorted or folded bedding, sand dikes, or other liquefaction features. Inclined to recumbently folded sand, silt, and clay beds were found at significant sites 34S (sec. 18, T28N R8E) and 111D (sec. 15, T29N R8E); these folds verge east-southeast, subparallel to the Vashon ice-flow direction, and thus have an orientation and geometry consistent with a glacial ice-shear. Unit Qglv includes some of the transitional beds of Booth (1990) and correlates with the Lawton Clay mapped elsewhere in the Puget Lowland. See Pessl and others (1989) for a regional description of the ‘transitional beds’.

Pre-Fraser Glacial and Nonglacial Deposits

QC₀ Deposits of the Olympia nonglacial interval (Olympia beds), ancient Skykomish River facies
QC₀? (Pleistocene)—Sand, sandy silt, silty sand, and silt, with some clay, organic silt-clay, minor peat and a few gravel beds; typically yellow, gray-brown, or brown-gray with distinctive dark gray-orange oxidation; dense; laminated to very thickly bedded and well stratified. Unit QC₀ contains charcoal,



Figure 4. Peaty organic-silt rip-up clast in advance outwash (unit Qgav) at age site 37C west of the Sultan River, in the south-central part of the map area. The outcrop is directly below Pipeline Road in a 15-ft-deep rill that exposes stratified sand, sandy gravel, and gravel. We obtained OSL/IRSL ages of 14.1 and 16.4 ka at this site (Appendix A). A radiocarbon age from this rip-up clast of $14,900 \pm 50$ yr BP (cal yr BP 17,985–18,250) is roughly consistent with the OSL/IRSL age. Mapping around this outcrop and petrographic analyses of sand deposits to the north (on Pipeline Road) indicate that nonglacial strata with an SP provenance (Table 1) probably occurs laterally below this outcrop (see unit Qco? on map).

disseminated detrital organic matter, trough-and-ripple crossbedding, and local graded beds. Deposits typically preserve moderate to intense liquefaction features, such as sand dikes, chaotic or folded bedding, flutes, and rare dish structures. (See chaotic bedding Figs. 5 and 6.) These features are likely Pleistocene in age and represent earthquake-induced liquefaction of saturated ancient Skykomish valley alluvium *prior* to compaction by the Vashon ice load. Thick exposures of fluvial overbank deposits form upward-fining sequences of pebbly sand, sand, and silt—typical of meandering river systems—are common. Channel deposits are regionally common in Olympia beds but were rarely observed in the Lake Chaplain quadrangle. Unit Qc₀ represents ancient Skykomish River alluvium in the Skykomish valley around Monroe and Sultan (SP in Table 1). This alluvium is compositionally very similar to the ancient Snoqualmie River alluvium (Qm₄₀₋₈₂Qp₁₀₋₄₆PF₈₋₂₆) mapped south of Monroe and in the Carnation, Lake Joy, Fall City, Snoqualmie, and North Bend quadrangles (Dragovich and others, 2009a,b,c, 2010a,b, 2011). See Dragovich and others (2007) for additional SP point count data. Compared to glacial deposits, SP alluvial sand contains more K-spar (8–15%), limited amounts of polycrystalline quartz, and has the same provenance as units Qc_{ws} and Qc_{ph}. Sand from this unit is 72–74% SiO₂, is geochemically similar to modern and ancient alluvium, and was predominantly derived from an intermediate to slightly primitive arc source with mixing from older accreted sedimentary and metamorphic sources (Appendix D; Dragovich and others, 2010a,b, 2011b, 2013). The Olympia beds are inferred to be 200 ft (60 m) thick on Cross Section B, along the core of the Monroe syncline, and are similar in thickness to the beds in the core of the Monroe syncline directly to the south (Dragovich and others, 2013).

Our new OSL and IRSL ages for the Olympia beds and Whidbey Formation (unit Qc_{ws}) confirm that the Monroe synclinal core contains Olympia beds in the southeastern part of the Lake Chaplain quadrangle. We obtained new OSL and IRSL ages of 40.5 ± 3.1 and 48.3 ± 4.0 ka from the Olympia beds at age site 37A along the northern limb of the Monroe syncline in the southeastern part of the map area



Figure 5 (left). Compact, laminated to thinly bedded sand and silt exposed in a steep 6-ft (2-m)-high road cut slope directly west of Marsh Creek in the east-central part of the map area (age site 37B). We obtained OSL and IRSL ages of 32.4 and 29.8 ka at this site (Appendix A) and correlated these deposits with the Olympia beds (unit Qco). The deposits were intensely liquefied and display chaotic or wavy bedding, with local tight to isoclinal rootless folds. Note the brown-orange cast to these deposits, typical of SP provenance nonglacial beds in the region (Table 1). The sand has a Cascade provenance.

Figure 6 (below). Close-up photograph of the deposits showing the ptygmatic folding of silt beds between thicker beds of fine- to medium-grained sand. See sample 16K in Appendix D for geochemical analyses at this site.



(Appendix A). Detrital zircon ages from this same site (Appendix C) show that these Olympia beds contain significant Cascade Range batholithic detritus, consistent with the geochemistry of sand sample 30U, also from this site.

We obtained OSL and IRSL ages of 32.3 ± 2.5 and 29.9 ± 2.6 ka from high-elevation SP strata in the Marsh Creek area at age site 37B in the east-central part of the map area (Appendix A). The chronology of the Evans Creek alpine glaciation provided by Riedel and others (2010) documents alpine ice advances in the Skagit Valley between 30.3 and 19.5 cal ka, with an intervening period of glacial recession about 24.9 cal ka. This 30.3 ka age is statistically identical to our 32.4 and 29.8 ka OSL ages for Olympia beds near Marsh Creek, suggesting that sedimentation is related to alpine glaciation. We map these deposits as Olympia beds given their distinct SP fluvial stratigraphy and provenance, but note that these may be the first geochronologically constrained Evans Creek outwash mapped in the Skykomish valley. An alpine glaciation interpretation also explains the high elevation of these Cascade-provenance Olympia beds. Associated Earth Sciences (2001, 2002, 2004, 2007) and Dragovich and others (2007, 2009a,b,c, 2010a,b, 2012, 2013) obtained radiocarbon and OSL/IRSL ages that vary from 17.5 to 51.5 ka from 55 organic and sediment samples of Olympia beds south and southwest of the map area. These beds were assigned to the Olympia nonglacial interval (~15–60 ka). Olympia beds include some of the transitional beds of Booth (1990) and correlate with the deposits of the Olympia nonglacial interval of Pessl and others (1989).

QCws Whidbey Formation, Skykomish River facies (Pleistocene)—Sand, silt, and silty sand with lesser pebbly sand, clay, gravel, organic sediment including peat, and a few lenses of (cobble) gravel; sand is yellow-gray or brown and weathers to a distinctive orange-gray; dense or hard; well sorted and stratified; mostly laminated to thickly bedded sand and silt with thin beds or laminae of clay locally; commonly planar bedded; may contain charcoal, disseminated organic matter, trough-and-ripple crossbedding, graded beds, flutes, flames, sand dikes, and dish structures; folds and chaotic bedding are evident in areas that experienced liquefaction (Fig. 7). These SP-provenance sand beds are generally lithic poor and contain abundant monocrystalline quartz (~20%) with minor, but significant K-spar (5–10%), granitic

lithic clasts, hornblende, opaque minerals, and mica, similar to units Qa, Qco, and Qcph (SP in Table 1). Some sand contains augite and epidote with subordinate polycrystalline quartz and volcanic and metamorphic lithic clasts. Geochemically, these deposits were derived from an intermediate arc source with minor sedimentary or metamorphic input (Dragovich and others, 2010a,b, 2011a,b, 2012, 2013). Microscopically, sand appears to be more weathered at some sites than the younger Olympia bed deposits, but is distinctly less weathered than mid to early Pleistocene alluvium in unit Qcph.

Dragovich and others (2011b) obtained an IRSL age of 123 ± 8.24 ka from Whidbey Formation SP deposits north of Monroe. South and southwest of the area, OSL ages of 101 ± 4.47 ka and 107 ± 9.87 ka (Dragovich and others, 2011a,b) are consistent with infinite radiocarbon ages south of Monroe. Dragovich and others (2012) obtained two infinite radiocarbon dates of $>43,500$ yr BP and IRSL ages of 85.8 ± 7.4 , 79.3 ± 6.9 , 113 ± 9.0 , and 143 ± 4.5 ka from SP-provenance deposits inset above the Tolt River in the Lake Joy quadrangle to the south. Ages of 122 to 128 ka were also obtained from unit Qcws in the Carnation quadrangle by Dragovich and others (2009a,c). As part of this study, we obtained new OSL/IRSL ages of 75.4 ± 2.3 and 80.4 ± 7.0 ka at age site 38A in the northern part of the Sultan quadrangle (Appendix A), about 2,700 ft (825 m) directly south of the quadrangle boundary.

We correlate unit Qcws with the Whidbey Formation (~80,000–130,000 yr BP) on the basis of age, composition, and stratigraphic position. See Dragovich and others (2007, 2009a,c) and Capps and others (1973) for previous Whidbey Formation mapping south and west of the Monroe quadrangle. Available local and regional structure, combined with nonglacial SP deposit age information, suggests that the younger Olympia beds overlie Whidbey Formation along the core of the east–west-trending Monroe syncline in the southeastern part of the map area. (See Cross Section B and *Monroe Syncline*).



Figure 7. Liquefaction-deformed Whidbey Formation nonglacial sand. Note the overturned folds, flame structures, and generally chaotic bedding. Site consists of multiple outcrops along a 15-ft (5 m)-high road cut, ~2,700 ft (823 m) directly south of age site 38A in the Sultan quadrangle (Dragovich and others, 2013). See Appendix A for OSL/IRSL ages obtained from sand at this site. SP deposits (Table 1) at this location contain well-sorted, angular to subangular sand grains dominated by monocrystalline quartz, K-spar (~10%), plagioclase, hornblende, pyroxenes, and mica, with significant opaque mineral content in this overbank sand facies. See site 17A in Appendix D for geochemical analyses of sand at this site.

Qcph Pre-Hamm Creek nonglacial deposits (Pleistocene)—Boulder to cobble gravel, pebble gravel, gravelly sand, and sand with minor silt; sand is typically yellowish brown to brown, oxidized, and strongly weathered; thin to very thickly bedded; well stratified; may contain cross bedding, graded beds, charcoal, logs, or disseminated organic matter; liquefaction features occur in some outcrops. Petrographic inspection of several sand samples revealed significant angular to subangular monocrystalline quartz (~25%), conspicuous biotite and white mica (~15–25%), K-spar (~5–10%), and plagioclase, with minor but significant hornblende and lithic grains of granite, phyllite, metasandstone, meta-argillite, metachert, and foliated quartz-mica aggregates. Additionally, some sand samples have minor epidote, greenstone, and greenschist. Sand (67–78% SiO₂) has a strong granitic-metamorphic

provenance from local *mélange* basement and Tertiary plutonic rocks. The abundant mica is likely from two-mica-granite Cascade sources—such as the Index and Bald Mountain plutons—with some micaceous fragments from foliated *mélange* belt rocks such as phyllite. As in other SP-provenance samples, some granitic lithic grains contain plagioclase, K-spar, and hornblende. The sand also contains minor but conspicuous polycrystalline quartz, most likely derived from metachert that is common in the *mélange* belts to the east.

These sediments were derived from eastern sources and are compositionally similar to Skykomish River (SP-provenance) sediments and are informally termed ‘ancient Pilchuck River alluvium’ in Table 1. This ancient Pilchuck alluvium intertongues with locally derived ancient alluvium (unit Q_{Cphl}), on the northern and southern edges of the Explore Falls basin (Table 1). Interbedding of these two lithologies can be observed or confidently inferred at many sites, including significant sites 36L and 36N in the southern part of the basin. Weathering rinds on basaltic clasts are 2 to 5 mm thick. As also noted below for unit Q_{Cphl} , the high (4–6%) loss on ignition (LOI) of the sand geochemical samples (Appendix D) is because of the moderate to intense weathering of the sand grains that produce the clay and other microcrystalline or cryptocrystalline weathering products we observed petrographically.

We obtained OSL and IRSL ages of more than 125 and 550 ka at age site 37D along the western part of the basin (Appendix A). Our new OSL/IRSL ages from this unit, the deep and persistent weathering characteristics, and its significant westerly tilt all suggest that the unit entirely predates the Hamm Creek nonglacial interval of Troost and others (2005) that spans 243 to 188 ka (MIS 7)(Morrison, 1991). We informally name this basin the Explorer Falls basin after a prominent waterfall near its center. The distribution of outcrops, kinematics of bounding faults, and the thickness of basin sediments (~700 to 800 ft; Cross Section A) all suggest that the basin is a graben tilted to the west as a result of Cascade Range uplift. Additionally, the significant westerly tilt of these ancient fluvial deposits suggests a long-lived basin.

We also obtained OSL and IRSL ages of 21.6 ± 1.3 ka and 71.9 ± 6.1 ka at age site 37E along the eastern part of the basin at an elevation of 1,900 ft (580 m). These deeply weathered sandy silt deposits have the same eastern Cascade provenance as the basin sediments to the west of this elevated site. Sediments at this site are significantly tilted to the west and intensely weathered such that the original silty sand now contains abundant clay weathering products. The extreme weathering, structure, and abundant mica-rich SP-provenance of the sand does not appear to correlate with the determined OSL age. See Appendix A for a discussion of resetting mechanisms responsible for the errant age of this probably early Pleistocene deposit. Dragovich and others (2013) obtained an infinite IRSL age of more than 300 ka from overbank facies of silty fine- to medium-grained SP-provenance sand about 2,900 ft (884 m) south of the map area and above the west bank of the Sultan River. This age, along with the distribution of the Olympia beds and Whidbey Formation, suggests that a lowermost Pleistocene nonglacial SP unit (Table 1) occupies part of the Monroe syncline in some areas. We map these deposits as unit Q_{Cph} on Cross Sections A and B (compare unit Q_{Cph} with unit Q_{Cpf} and Q_{gnpf} of Dragovich and others [2011a,b, 2013] in the Monroe and Sultan quadrangles and unit Q_{pf} of Booth [1990]).

Q_{Cphl} **Pre-Hamm Creek continental deposits, locally derived facies (Pleistocene)**—Pebbly sand, sandy pebble gravel, with lesser gravel and rare silt; locally contains peat, logs or organic sediments; thinly to thickly bedded with lenticular interbeds common; well-sorted; angular to subangular; yellow-gray or brown and weathers to a distinctive reddish yellow-gray. These deposits are lithic rich and contain 80 to 95% WMB-derived meta-argillite, phyllite, and metasandstone lithic clasts, with minor greenstone and a few metagabbro clasts locally. The deposits also contain 10 to 15% monocrystalline and polycrystalline quartz and plagioclase. Unlike unit Q_{Cph} , these locally derived sediments lack distinct Cascade-provenance detritus such as K-spar and granitic lithic grains. Like unit Q_{Cph} , weathering of the deposits is observed at outcrop- and thin-section scale, with conspicuous 2-to-6-mm-thick weathering rinds on basalt and basaltic greenstone gravel clasts and abundant brown sand- and silt-sized cryptocrystalline weathering products observed petrographically. These sediments were deposited as alluvial fan and alluvial sediments along the northern and southern margins of the Explorer Falls basin and are interbedded with the Cascade-provenance fluvial sediments of unit Q_{Cph} along the central part of this graben structure (Cross Section A; Table 1)(see unit Q_{pf} of Booth [1990] and unit Q_{Cph} for the middle to early Pleistocene age assignment for this unit). We also include phyllite-rich fluvial nonglacial

sediments near the Sultan River and significant site 48L in unit Qc_{phl}. These deposits are not part of the Explorer Falls basin, and although weathered, might be younger than the Hamm Creek nonglacial interval.

Qgn_{pf} Pre-Fraser glacial and nonglacial deposits, undivided (Pleistocene to Pliocene?)(cross sections only)—Dense to very dense gravel, boulder gravel, sand, silt, clay, and diamicton; locally contains peat or organic sediments. The few wells that reached this undivided unit first likely drilled through wood-bearing nonglacial SP strata of unit Qc_{ph} (Cross Section B). Knoll (1967), Booth (1990), and Dragovich and others (2007, 2009c, 2010a,b, 2012) also describe outcrops of old and undivided glacial and nonglacial deposits elsewhere in the Snoqualmie/Skykomish valley area, including the highly weathered tills and outwash in unit Qgn_{pf} of Dragovich and others (2009a,b) south of the map area. Geophysical analyses of magnetic data along Cross Section B and the southernmost part of Cross Section A suggest that the Monroe synclinal basin in the southern part of the map area is dominated by moderately magnetically susceptible SP strata (Table 1) of units Qc_o, Qc_{ws}, and Qc_{ph} and does not contain appreciable low-susceptibility pre-Fraser glacial deposits. This interpretation is consistent with the prevalence of SP-provenance strata in deep water-well logs within the Monroe synclinal basin. (See *Isostatic Gravity and Aeromagnetic Analyses* for further information.)

Tertiary Volcanic, Intrusive, and Sedimentary Rocks

Ei Dikes (Eocene)—Basaltic to andesitic dikes intrude the Western mélange belt and are well exposed in the central part of the map area. Dike orientation and wall rock structure suggest that some dikes intruded along pre-existing minor faults of the northeast-trending Cherry Creek fault zone. Adjacent to the dikes, the mélange belt country rocks display steeply dipping and northeast-trending slickensided fracture planes with sub-horizontal slickenlines consistent with the regional kinematics of the Cherry Creek fault zone.

ØEc Sedimentary rocks, undivided (Oligocene to Eocene)—Poorly exposed feldspathic sandstone with lesser conglomerate, siltstone, and coal; sandstone is very pale brown to light gray and weathers to brownish yellow. Predominant rock type is a compositionally and texturally mature sandstone composed of well sorted, subangular to subrounded monocrystalline quartz (~40%), K-spar (~25%), and plagioclase (~20%), with some polycrystalline quartz, muscovite, and biotite. This unit is well exposed in the Lake Roesiger area directly west of the quadrangle (Tabor and others, 1993; Danner, 1957) where it thickens into the Everett basin (Dragovich and others, 2010a,b). This unit is mapped in the northwestern and southwestern parts of the map area as thin erosional remnants (see Cross Sections A and B). The unit is inferred in four additional areas: (1) Richard Roesiger's "Little Pittsburgh" coal prospect at significant site 'Coal' along the northern part of the Explorer Falls graben, as noted on unpublished early land survey maps (Pat Schreiner, Everett Water Filtration Plant, written commun., 2013); (2) in the southern part of the graben—south of significant site 36N—where it is mapped on the basis of float; (3) at depth directly north of the Woods Creek fault where well log data suggest sandstone and coal resting unconformably on top of WMB metagabbro; and (4) at depth along the northern limb of the Monroe syncline and the easternmost edge of the thick Everett basin (Cross Section A and B). Minard (1981) indicated that sandstone and conglomerate north of Monroe appear to be continuous with shallow-marine rocks of Oligocene age to the west and considered these Tertiary sedimentary rocks as correlative with the Blakely Formation. He also reported that a few kilometers west of the quadrangle, the sedimentary rocks unconformably overlie volcanic rocks that are probably continuous with the volcanic rocks of Mount Persis. Similar sedimentary rocks 18 km (11 mi) northwest of the quadrangle are described as the Oligocene Riverside formation by Danner (1957) and as the upper Eocene to lower Oligocene Bulson Creek unit of Lovseth (1975) by Whetten and others (1988). Although more detailed compositional data is needed, the granitic provenance of fluvial sandstone is similar to the compositionally mature quarto-feldspathic sandstone of the lower Chuckanut Formation of Evans and Ristoe (1994), mapped north of the study area. See units Ts, Evc_p, ØEc, ØEn, and M_{vc} of Dragovich and others (2010a,b, 2011a,b, 2013) for mapping of Tertiary sedimentary rocks southwest of the map area.

Mesozoic Low-Grade Metamorphic Rocks of the Western Mélange Belt

The metamorphic basement in the map area is the Western mélange belt (WMB) of Frizzel and others (1987) and Tabor and others (1993). The metamorphic grade of the WMB in the map area generally increases northeastward from the prehnite-pumpellyite facies to the greenschist facies. (See *Metamorphism and Structure of the Western Mélange Belt* below). Most WMB metasedimentary rocks were deposited as turbidites along an accretionary wedge (Jett, 1986; Frizzel and others, 1987; Jett and Heller, 1988). Although the WMB is regionally a tectonic amalgamation of various original tectonic environments, we document that most of the WMB in the map area originated as Cretaceous to Jurassic arc volcanics and near-arc turbidites. (See units KJmv_w, KJigb_w, and KJit_w and *Geochemistry*.) Conversely, the feldspathic metasedimentary rocks in unit KJms_w in the southeastern part of the map area originated as turbidites eroded from a two-mica granitic source.

KJm_w Western mélange belt of Tabor and others (1993), undivided (Cretaceous to Jurassic)—Meta-argillite, metasandstone, greenstone, metagabbro, metachert, with less metadiabase, metatonalite, slate, and phyllite, minor marble with meta-quartz-diorite and hornblendite, (banded) amphibolite, and rare ultramafic rocks observed regionally (Fuller, 1925; Danner, 1957; Tabor and others, 1993; Dragovich and others, 2007, 2009a,b,c, 2010a,b, 2011a,b, 2012, 2013). Locally divided into:

KJmv_w Metavolcanic rocks—Greenstone derived from metamorphosed basaltic to andesitic tuff, basaltic andesite to dacitic volcanic flows (55–70% SiO₂), with regionally common basalt flows and rare volcanic breccia; greenish gray to dark greenish black. Tabor and others (2000) described boudins of metamorphosed quartz-porphyry dikes in faintly foliated greenstone south of the study area. Regionally metamorphosed flows are mostly massive to moderately foliated metabasaltic andesite and a lesser metabasalt or meta-andesite variation that locally displays amygdaloidal and pillow textures and eutaxitic flow structure (Dragovich and others, 2009a,b,c, 2013). Amygdaloidal metadacitic greenstone flows, characteristic of island-arcs, are relatively abundant and contain microlitic and eutaxitic plagioclase microphenocrysts, with a few large plagioclase phenocrysts (60–75% total plagioclase) in a homogeneous clear matrix containing interstitial quartz and accessory sphene or opaque minerals. Metamorphosed basaltic to andesitic flows typically contain plagioclase microlites (~40–60%) in a light green chloritized or saussuritized matrix. Some flows contain small interstitial quartz grains; more mafic flows contain relic cumuloaphyric mafic and plagioclase phenocrysts with scattered microphenocrysts of plagioclase, locally with some chloritized or saussuritized pyroxene. We mapped massive ‘apple green’ metatuffs widely in the map area. These tuffs are also mapped as separate bodies of thick to very thick unit KJmv_w greenstone or as discrete very thin to thick beds in metasedimentary rocks. These metatuff beds are dacitic to rhyolitic (crystal) vitric tuffs (~77% SiO₂) with some mapped as linear unit KJmv_w bodies in metasedimentary rocks. Large embayed relict volcanic quartz grains (≤2 mm) were observed locally. Most of the vitric tuffs are completely recrystallized granoblastic rocks that lack relict grains and contain some interstitial chlorite and opaque minerals, but a few contain relict subhedral to euhedral crystals of quartz and plagioclase (≤3 mm) in a recrystallized clear quartzose matrix (40–50%). Metamorphic minerals in greenstones include chlorite, epidote, prehnite, and calcite. Pumpellyite is probable in the metabasaltic greenstones and, with the other index minerals, indicates a prehnite-pumpellyite metamorphic facies for the low-grade portion of the WMB. Veins containing euhedral prehnite and (or) epidote are common. Compared with unit KJsh_w, greenstones lack actinolite. The geochemistry and stratigraphy of the meta-igneous rocks indicate that the WMB contains portions of an accreted volcanic island-arc consistent with volcanic provenance of most metasedimentary rocks in the map area. This is also consistent with the composition of the metatuff, which is mostly calc-alkaline, both locally and regionally (Dragovich and others, 2009a,b,c). Dragovich and others (2013) document an alkali oceanic-island basalt (OIB) provenance for one very thick mafic mugearitic (basaltic trachyandesite) flow interbedded with metachert south of the map area.

KJsh_w Greenschist—Foliated metavolcanic rocks derived mostly from metamorphosed basaltic to dacitic tuff (≤77% SiO₂) and volcanic flows (~49–70% SiO₂); greenish gray to dark greenish

black. Some flows are amygdaloidal with probable pillows. Greenschist is stratigraphically and compositionally similar to the lower metamorphic grade greenstones (unit KJmv_w) but is strongly foliated with local interbeds of volcanic-clast-rich foliated metasandstone or phyllite. Metatuffaceous greenschist beds are generally thinner than the flows, but form thin to very thick interbeds in phyllite. A probable greenschist dacitic flow with small interstitial quartz grains was also observed. Unlike greenstone, most greenschist contains schistose-quartzose metamorphic segregations parallel to the foliation; these leucosomal segregations are more than 1 cm thick, forming gneissic bands in a few areas. Greenschist flows commonly contain plagioclase microlites in a light green matrix with abundant epidote and chlorite and some metamorphic actinolite, typically pseudomorphing faint relict minerals. Metatuffaceous greenschist is compositionally similar to flows of both mafic and felsic varieties. These rocks lack relict minerals and contain a granoblastic matrix of recrystallized quartz and feldspar similar to the 'apple green' metatuff of unit KJmv_w. We noted veins of euhedral quartz and calcite ± epidote and prehnite in several samples. Geochemically, greenstone (unit KJmv_w) and greenschist have a similar island-arc tectonic environment. (Also see volcanoclastic rocks in units KJms_w and KJph_w.) A greenschist metamorphic facies is indicated for these metavolcanic rocks by the presence of chlorite, epidote, and calcite, locally with actinolite. The higher-grade portion of the WMB contains greenschist (unit KJsh_w) and phyllite (unit KJph_w) and appears to lack pumpellyite. The higher grade portions of the mélange belt are best understood by inspection of greenschist and phyllite on the map relative to greenstone and metasedimentary rocks.

KJms_w Metasedimentary rocks—Marine feldspathic to feldspatholithic subquartzose metasandstone, silty metasandstone, meta-argillite, metatuff, and minor metachert, marble and (chert pebble) metaconglomerate; typically greenish gray, dark or bluish gray, or gray-green; weathers brown; meta-argillite is typically black or greenish blue-black to dark gray. Danner (1957) mapped metamorphosed limestone in the mélange southeast of the map area and we also observed marble east of the map area. Relative to the WMB as a whole, metachert in the map area is relatively rare and was found only at significant sites 50G and 19W. The metachert is locally banded with meta-argillite interbeds and is dominantly composed of recrystallized polygonal quartz with relict recrystallized radiolarian fossils. The chert bands are undeformed to strongly contorted. In metasandstone and meta-argillite, relict sand grains are subrounded to angular; graded bedding and load casts are locally preserved.

The metasandstone can be divided into two distinct groups in the map area: (1) *feldspathic metasandstone* forming the arkosic facies of Tabor and others (1993) and Jett and Heller (1988), and (2) *feldspatholithic to lithofeldspathic metasandstone*, that generally parallel the lithic petrofacies of Jett and Heller (1988). Our geochemical, petrographic, stratigraphic, and detrital-zircon data further indicate that these two distinct sandstone petrofacies have a distinct granitic or volcanic provenance, respectively.

The feldspathic metasandstones contain angular to subangular relict grains of K-spar (3–20%), plagioclase, and monocrystalline quartz, with significant detrital biotite, muscovite, some lithic grains, and minor polycrystalline quartz and opaque minerals. These metasandstones are likely derived from felsic two-mica granites. The general angularity of the grains suggests 'first cycle' sediments or sediments that generally lack reworking and were derived from a homogeneous, perhaps proximal, intrusive source. Our field observations indicate that the mapping of the potassium-bearing metasandstones in the southeast part of the map area by Tabor and others (1993) accurately portrays the distribution of the arkosic facies. The metabasalt noted in several wells in this area is possibly flows or dikes in the arkosic sandstone facies (Cross Section B).

The feldspatholithic to lithofeldspathic metasandstones in the quadrangle generally contain monocrystalline quartz, plagioclase, and volcanic lithic grains, with lesser polycrystalline quartz and very little or no relict K-spar. Volcanic lithic grains have prevalent felty or microlitic textures indicative of andesitic to dacitic volcanism in the adjacent arc (Jett and Heller, 1988). Metasandstones in this facies are typically moderately sorted wackes that

are both compositionally and texturally immature, consistent with their near-arc volcanic provenance.

Tuffaceous feldspatholithic metasandstones contain significant relict quartz and plagioclase and likely originated as reworked crystal-vitric tuffs. Also, vitric and crystal-vitric metatuff interbeds are generally prominent in the volcanic metasedimentary rocks and contain relict plagioclase and quartz phenocrysts, locally with pyroxene, in a green but transparent chloritic matrix. These widespread metatuff beds record a major pyroclastic contribution to the WMB rocks which also contain volcanic flows (see unit KJmv_w) and arc gabbro and volcanoclastic lithologies. These moderately foliated and partially recrystallized prehnite-pumpellyite facies rocks have a synkinematic metamorphic fabric defined by subparallel white mica and relict clasts. Metamorphic minerals are white mica, epidote or clinozoisite, chlorite \pm pumpellyite, and prehnite.

Meta-argillite is easily eroded and does not form prominent outcrops in many areas. Tabor and others (1993, 2000) indicate that meta-argillite forms the matrix around tectonic bodies in the *mélange*—such as metagabbro knockers—and this is confirmed by our mapping in many areas. However, very thick sequences of less-deformed strata are locally and regionally well exposed in the WMB, and in these locations meta-argillite forms stratified thin to thick interbeds within metasandstone (Dragovich and others, 2013). A homoclinal sequence of this well-stratified metasedimentary rock is well exposed on Blue Mountain where volcanic metasedimentary and metavolcanic rocks are distinctly interbedded. The stratigraphic style, including partial Bouma sequences, indicates that the metasedimentary rocks were deposited as turbidites along an accretionary wedge. Tabor and others (1993, 2000) and Frizzell and others (1987) reported Kimmeridgian to Valanginian (157–134 Ma; Cretaceous–Jurassic) radiolarian ages from metachert beds south of the map area. Tabor and others (1993) also found an Early Cretaceous *Buchia* fossil in meta-argillite beds along the Sultan River 2,330 ft (710 m) east of the map area at age site USGS-1F. The age of these bivalves is restricted to the Tithonian (Danner, 1957, Tabor and others, 1993). See unit KJph_w for further fossil information.

We obtained new detrital-zircon ages from the potassium-rich feldspathic metasandstone (arkosic facies) at age site 35J in the southeastern part of the map area (Appendix C). The ages range from 69 to 2,190 Ma, and the weighted average of the youngest age population ($n = 21$ zircons) is 74 ± 1 Ma. South of the study area near Snoqualmie, Dragovich and others (2009a,b) obtained a minimum U-Pb detrital-zircon population age of ~ 96 Ma from feldspathic metasandstone. This minimum age is broadly similar to the mean age of 87.3 ± 1 Ma from the youngest zircons in a meta-arkosic sandstone 3.6 mi east-southeast of the southeast corner of the Lake Chaplain quadrangle (Brown, 2012). Our new ~ 74 Ma maximum depositional age is significantly younger than previous age estimates for the WMB and indicates: (1) that the arkosic sandstone petrofacies is locally as young as latest Cretaceous, and (2) that accretionary *mélange*-belt formation and sedimentation ended in the latest Cretaceous, which is substantially younger than previously documented (Sauer and others, 2014). The sediment composition and latest Cretaceous age suggests a two-mica granitic source, such as the Idaho batholith, for these sediments. See petrofacies mapping of Tabor and others (1993) and Jett (1986), and metasandstone geochemistry of Dragovich and others (2009b,c) for further information.

KJph_w Phyllite—Phyllite, phyllitic metasandstone, meta-argillite, slate, and minor semischist rock types, including local foliated metatuff interbeds; dark bluish gray, weathers to bluish gray; moderately to well-stratified; thin to very thickly bedded; sequences of phyllite have well-developed schistosity that is transposed parallel to bedding. The fabric is defined by subparallel chlorite or white mica, relict grains, and quartzose metamorphic segregations as much as 1 to 1.5 mm thick in most samples. The phyllitic primary foliation is crenulated or microfolded in some outcrops, and mylonitization was observed near some faults, including thrusts. Unit KJph_w includes feldspathic to feldspatholithic metasandstones, meta-argillite and metasiltstones similar to the lithic petrofacies found in unit KJms_w. It typically contains

relict subrounded to angular grains of monocrystalline quartz, plagioclase, locally abundant volcanic lithic clasts (~5–40%) locally with some polycrystalline quartz, sedimentary lithic grains, and detrital augite and biotite. The volcanic petrography of the relict sand grains, along with the occurrence of foliated metatuff beds in the phyllite, suggests a recrystallized volcanoclastic protolith for most of the metasandstones. We suspect these metaclastic rocks are most similar to the lithic facies of Jett and Heller (1988), yet some are more quartzofeldspathic and probably derived from a crystal-vitric tuffaceous source. Metamorphic minerals include sericite, chlorite, albite, calcite, sodic plagioclase, and opaque minerals. Prehnite is common in matrix veins, and actinolite is observed in a few compositionally immature metasedimentary rocks. Overall, these minerals are consistent with a greenschist metamorphic facies for these phyllitic rocks. The phyllite unit is mapped mainly in the northeastern part of the map area where it is interbedded with greenschist (unit KJsh_w). There is a general increase in metamorphic grade to the northeast across the WMB (Tabor and others, 1993). This regional grade increase is interrupted by local grade increases created by thrusting and reverse faulting juxtaposing low- and medium-grade rocks.

The island-arc setting for the metamorphosed intrusives, tuffs, and flows—and the volcanic nature of most metasedimentary rocks in the study area—indicates deposition proximal to a volcanic arc as turbidites in an accretionary complex for most of the mélange belt protoliths, including most of the phyllitic rocks. Tabor and others (1993) assigned earliest Cretaceous and Late Jurassic ages from sheared and deformed “*Buchia concentria*” and “*Aucella* sp. (*Buchia* sp.)”. At age site USGS 2F and 3F in the northeastern part of the map area near the Sultan River. Danner (1957, p. 422) reports that a collection of *Aucellus*, possible *Terebellina* tubes, and radiolarians suggests an Early Cretaceous to Late Jurassic depositional age for the phyllitic metasediments near age site WRD-4F. Tabor and others (1993, p. 14) summarized WMB fossil age information as follows: “A *Buchia* from matrix argillite and graywacke beds (table 1, no. 1F-3F) appears to be restricted to the Tithonian (Danner, 1957, p. 410), and more definitive radiolarian samples indicate ages from Kimmeridgian to Valanginian (Frizzell and others, 1987) that, in numerical age, range from 156 to 131 Ma based on the time scale of Harland and others (1982).”

KJigb_w Metagabbro—Metagabbro with minor metatrandhjemite and rare meta-quartz-diorite; feldspathic hornblendite and gneissic amphibolite are reported regionally; greenish gray; medium to coarse grained; hypidiomorphic granular massive to slightly foliated; locally schistose or gneissose with occasional flaser gneissic fabric. Metagabbro (44–53% SiO₂) generally contains actinolized hornblende (~50–70%) and plagioclase (~35%) with opaque minerals including magnetite. Tabor and others (1993) reported that mafic metagabbro near Woods Creek west of the map area contains hypersthene and clinopyroxene relicts. Metadiabase dikes (53% SiO₂) intruded metagabbro locally. Metadiabase is composed of plagioclase, uraninite/actinolite, chlorite, epidote, opaque minerals, and secondary blebs or veinlets of quartz with rare relict clinopyroxene and relict intergranular to diabasic texture. Metamorphic minerals include actinolite, prehnite, pumpellyite, chlorite, epidote, sphene, and calcite (Dragovich and others, 2009a,b,c, 2012, 2013). Vance and others (1980) discussed the trace-element chemistry of the metagabbro near Woods Creek west of the map area. New geochemical data from the quadrangle suggests that the arc intrusives are likely co-magmatic with arc volcanics in the area (see units KJmv_w and KJit_w). Metagabbroic rocks are in fault contact with adjacent metasedimentary and metavolcanic rocks and are primarily tectonic fragments within the mélange belt (Tabor and others, 1993; Dragovich and others, 2013).

Most metagabbro in the study area appears to be confined to the Lake Chaplain thrust sheet. For example, metagabbro in the Blue Mountain klippe is in thrust contact with lower-grade metasedimentary rocks. An important exception is the unfaulted contact between very well exposed phyllite and metagabbro in the Lakeside Quarry (significant site 18A). The rocks share a concordant metamorphic fabric suggesting they were juxtaposed prior to metamorphism and before Lake Chaplain nappe emplacement. (See *The Lake Chaplain Nappe*). Tabor and others (1993) obtained a hornblende K-Ar age date of 118 ± 7.7 Ma from

metagabbro at age site USGS-54 in the Lake Chaplain nappe west of the Sultan River. They also reported regional U-Th-Pb zircon ages of 150 to 170 Ma for metagabbro and metatonalite, indicating that the plutonic rocks are minimally the same age as or older than the enclosing Jurassic and Lower Cretaceous metasedimentary rocks but distinctly older than the 74 Ma feldspathic metasandstones reported above (see unit KJms_w).

KJit_w Metatrondhjemite—Metatrondhjemite (74% SiO₂) with minor metatonalite and flaser or chlorite gneiss; may contain minor metagabbro; typically light greenish gray; equigranular, hypidiomorphic granular, cataclastic to (proto) mylonitic meta-intrusive rock; medium to coarse grained; contains plagioclase (45–50%) and quartz (35–45%), typically with interstitial metamorphic chlorite and prehnite ± epidote that replace probably primary mafic minerals (<15%). Tabor and others (1993) report actinolized hornblende from this unit more regionally; chloritization of these rocks appears ubiquitous. The metasedimentary and metavolcanic rocks have no hornfelsic textures adjacent to the meta-intrusives (this study; Tabor and others, 1993) and, like metagabbro, this meta-intrusive rock is in high- to low-angle fault contact with other mélange belt metasedimentary and metavolcanic rocks, both locally and regionally. These meta-intrusive rocks appear to be restricted to the Lake Chaplain nappe and, similar to the metagabbro, tectonic fragments in the mélange. Mylonitized metatrondhjemitic flaser gneiss occurs at the thrust contact with underlying greenstone east of the Sultan River at significant site 48L. Here the river has eroded a structural window below the Lake Chaplain nappe and exposed the Sultan River thrust directly below the flaser gneiss. Elsewhere, north-northeast-trending elongate bodies of metatrondhjemite are transposed into the CCFZ. The kinematics of the faults and fractures along the edges of these fault-bound bodies, such as around significant site 39Q, indicate strike-slip deformation after mélange emplacement. Direct intrusive contacts between metatrondhjemite and metagabbro were not observed, but the close spatial association, similar arc geochemistry, and age suggests a cogenetic intrusive history. Tabor and others (1993) obtained a U-Pb zircon age from metatonalite of ~164 Ma at age site USGS-55 in the north-central part of the map area. Tabor and others (1993, p. 10) also state that, “metagabbro and metatrondhjemite masses yield U-Th-Pb zircon ages of 170 to 150 Ma, which indicate that the plutonic rocks are minimally about the same age as or older than the enclosing Jurassic and Lower Cretaceous sedimentary rocks”. For comparison, see fossil ages for the WMB presented above with unit KJph_w and our new detrital zircon maximum depositional age of ~74 Ma for the arkosic petrofacies (unit KJms_w).

Holocene to Tertiary Tectonic Zones

tz, tz_h Tectonic zone—Cataclasite, fault breccia, clay-rich fault gouge, protomylonite, and moderately to strongly slickenlined, fractured, and veined rocks in fault zones; green and yellow to orange to variously colored, mottled, and altered. Dragovich and others (2007, 2009a,b,c, 2010a,b, 2011a,b, 2012, 2013) mapped similar tectonic zones along faults south-southwest of the map area. Broadly, unit tz is mapped along faults representing two distinct types of brittle or brittle–ductile deformation: (1) along high-angle faults representing Tertiary and younger deformation, such as the Cherry Creek fault zone (CCFZ), and (2) along WMB thrust faults, such as the Lake Chaplain thrust, where thick zones of unit tz are prominently exposed in many areas. In some of these latter zones, unit tz contains mylonitized rocks indicative of more semi-ductile shear mechanisms. Deformed rocks and mylonites along thrusts contain retrogressive chloritic low-temperature shear foliation with sutured quartz and plagioclase. Widespread calcite-quartz veining is prominent within most mapped tectonic zones, particularly along thrust and reverse faults. Shear fabrics along high-angle faults vary from brittle gouge to chloritized protomylonite in a few zones.

Unit tz_h represents mappable zones of hydrothermal alteration within tectonic zones common to the area; these zones are yellowish or reddish brown, white, or red to dark red. Alteration minerals include chlorite and calcite. Locally the alteration includes some opal or secondary quartz, zeolite, white mica, biotite, and clay. K-spar with sulfide mineralization is locally conspicuous. Alteration mineral assemblages are principally propylitic but may rarely include phyllic and potassic zone assemblages. Alteration within unit tz_h is structurally controlled. For example, alteration along the CCFZ was noted

by Dragovich and others (2012, 2013) south of the map area, and it continues northwestward along the CCFZ into the present study area. Northeast-trending structural control of hydrothermal alteration zones has been noted regionally, including the northeast-trending transverse structural belts of Grant (1969). We suspect that much of the mineralization in and around the Sultan basin is related to hydrothermal alteration in the broad TCFZ and CCFZ (Fig. 1). Quaternary deformation is also inferred in the subsurface on Cross Section B, adjacent to potentially active faults such as the Sultan River fault.

GEOCHEMISTRY

We obtained major and trace element geochemistry of 19 Quaternary sand and 14 rock samples to study the composition, provenance, original tectonic setting, and depositional environment of Quaternary deposits and the WMB in and around the study area. See Appendix D for analytical methods and geochemical data.

Quaternary Sand Deposits

We compiled a large geochemical dataset from our previously published mapping studies ($n = 117$) covering an area from North Bend quadrangle to the current study area (Dragovich and others, 2007a,b, 2008a,b, 2010a,b, 2011a,b, 2012, 2013). These sand samples include ancient and modern nonglacial alluvium as well as various glacial deposits. Dragovich and others (2010a,b, 2011a,b) were able to discriminate modern and ancient alluviums that have a locally derived provenance from samples that have a Skykomish/Snoqualmie river basin provenance (SP) based on their Sc and V composition (Fig. 8). In addition, Dragovich and others (2010a,b, 2011a,b) were able to discriminate between glacial and nonglacial sediments using trace element ratios (Fig. 9).

The modern and ancient Skykomish and Pilchuck alluviums (units Qa, Qco, Qcws, and Qcph) have a granitic provenance (Table 1). The low Sc and V of these samples suggests an intermediate igneous provenance (Bhatia and Crook, 1986). Except for one unit Qcph sample (13-36L), these samples plot with other SP-provenance samples on Figure 8. This is supported by eight of the modern and ancient Skykomish River alluvium samples plotting in the intermediate igneous field, and all unit Qcph and one sample of unit Qco plotting in the mafic igneous field on Figure 10. Units Qa, Qco, and Qcph have Pb/Yb ratios that are indicative of a plutonic source, and these samples predominantly plot in the SP field on Figure 9. The Tertiary intrusive rocks to the east of the study area (for example, the Grotto and Index batholiths) range from mafic to felsic in composition; however, they are predominantly intermediate and locally contain true granite (Tabor and others, 1993). The detrital-zircon age populations, petrography, and geochemistry all indicate that these Tertiary intrusive rocks were the source of the modern and ancient Skykomish River alluvium. Unit Qcph sample 13-36L has petrography and geochemistry suggesting it is transitional between SP and locally derived alluvium, consistent with its position in the Explorer Falls basin margin and its proximity to unit Qcphl (Figs. 8–10). The locally derived Pleistocene alluvium of unit Qcphl is along the margins of the Pleistocene Explorer Falls basin in the northwest part of the map area. This unit is dominated by WMB metasedimentary clasts that plot in the field defined by modern and ancient local alluvium on Figure 8 and have a high Sc and V content indicative of mafic protoliths (Bhatia and Crook, 1986). This is also supported by two samples plotting in the mafic igneous field on Figure 10. The low chondrite-normalized La/Lu values of unit Qcphl samples (Fig. 9) is likely the result of metasedimentary lithic clasts being more prevalent than igneous clasts, consistent with the high Ni of unit Qcphl samples (Pearce, 1996). This WMB source for the Qcphl along the Pleistocene Explorer Falls basin margin is also consistent with the similar geochemistry of the WMB metasedimentary rocks and sediments on Figures 8 and 10.

Unit Qgod deltaic glacial sand sample 13-26Y has Sc, V, and Pb/Yb values that are typical of glacial deposits from previous studies of Dragovich and others (2010a,b, 2011a,b, 2012, 2013) (Figs. 8 and 9; Table 1). The advance glacial-outwash sample (13-10H), however, is geochemically similar to locally derived alluvium (Figs. 8 and 9). This sample is rich in sedimentary lithic grains that could have been sourced by outwash reworking older locally derived alluvium deposits.

Western Mélange Belt

We analyzed 18 WMB samples, 14 of which are from this study area (Appendix D). The whole dataset includes 8 metavolcanic (greenstone/greenschist), 2 metagabbro, 3 metatuff, 2 metatrandhjemite, 2 metasandstone, and 1 metasilstone sample. The WMB has undergone prehnite-pumpellyite to greenschist-facies metamorphism. Many geochemical elements are mobile under this condition (Cann, 1970; Pearce, 1996), and thus only elements that

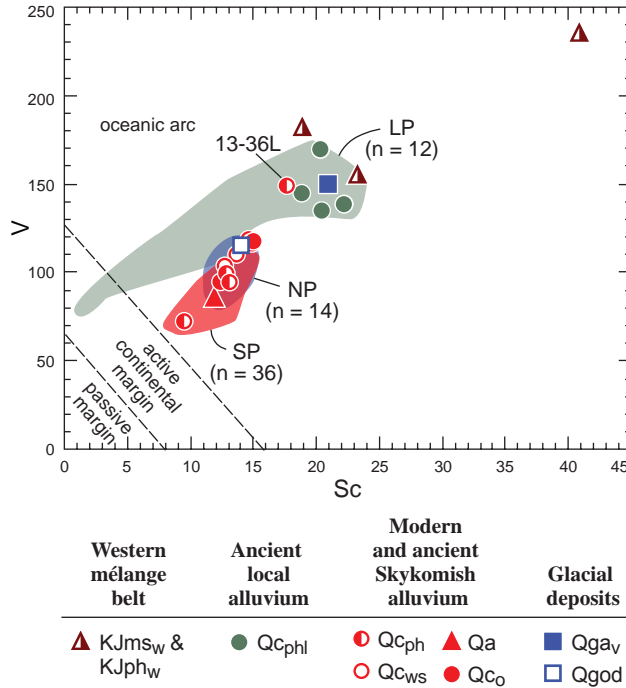


Figure 8. Vanadium (V) vs. Scandium (Sc) provenance diagram of Bhatia and Crook (1986) for Quaternary sand samples and metasedimentary rocks from the WMB. LP, local provenance from Tolt River and Youngs–Elwell Creek; NP, northern provenance deposited during continental glaciations; SP, Skykomish and Snoqualmie river basin provenance. Colored fields for NP, SP, and LP derived from previous studies (n, number of samples; Dragovich and others, 2007a,b, 2008a,b, 2009a,b, 2010a,b, 2011a,b, 2013). Compare with provenance information on Table 1.

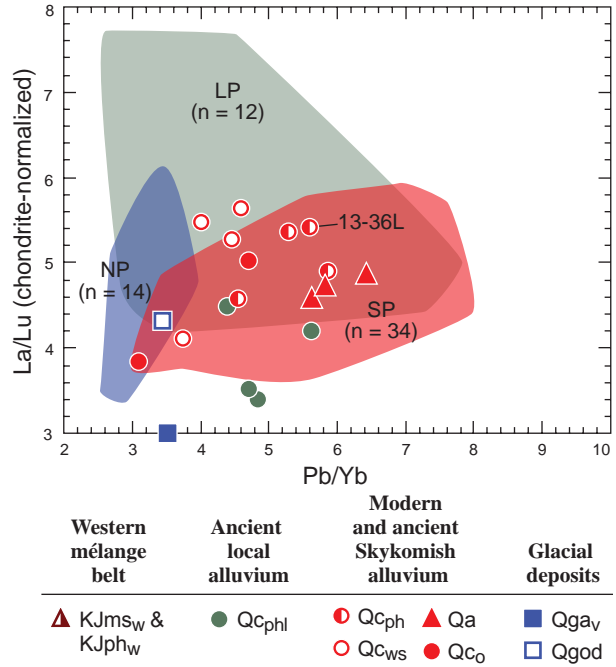


Figure 9. Chondrite-normalized Lanthanum/Lutetium (La/Lu) vs. Lead/Ytterbium (Pb/Yb) diagram for Quaternary sand samples. Chondrite normalization values are from McDonough and Sun (1995). LP, local provenance from the Tolt River and Youngs–Elwell Creek; NP, northern provenance deposited during continental glaciations; SP, modern and ancient Skykomish and Snoqualmie river basin provenance. Colored fields for NP, SP, and LP derived from previous studies (n, number of samples; Dragovich and others, 2007a,b, 2008a,b, 2010a,b, 2011a,b, 2013). Compare with provenance information on Table 1.

are immobile up to and including amphibolite-facies metamorphism were used for this study (Pearce, 1996). The metagabbro samples are plotted on Figures 11 and 12 because the element ratios for these diagrams are not greatly affected by mineral fractionation or accumulation (Wood, 1980; Pearce, 1982, 1996). Although the metagabbros analyzed for this study did not appear to have textures that suggest they are cumulates, they do display high Al and Eu values (Table D1), indicating that they do not represent melt compositions due to plagioclase accumulation (Pearce, 1996). The WMB greenstones and greenschists (units KJmv_w and KJsh_w) are basaltic to dacitic, while two metatuffs are andesitic and one is rhyolitic (Dragovich and others, 2009a,b)(Table D1). All WMB meta-igneous samples, except 12-50S, plot in the volcanic arc array on Figure 11; the greenstone, greenschist, metagabbro, and metatrandhemite have low Nb/Yb ratios (Fig. 11), indicating that they originated from a depleted mantle source (Pearce, 1982, 2008). The majority of the WMB samples plot in the island-arc tholeiite field on Figure 12. Calc-alkaline volcanic rocks include a greenstone dike that intrudes the metagabbro at Lakeside Quarry (sample 13-18D-1), a metagabbro (sample 13-23E), and the all the metatuff samples (Fig. 12). Greenstone sample 12-50S of Dragovich and others (2013) plots along the mantle array and has an Nb/Yb ratio similar to modern alkali within-plate basalts (WPB; Fig. 11) and plots in the WPB field on Figure 12 (Dragovich and others, 2013). Greenschist sample 13-19K-1 displays enriched mid-ocean-ridge basalt (E-MORB) composition, suggesting this sample may be transitional between arc and E-MORB affinities (Figs. 11 and 12). The arc geochemical affinities for the metagabbros are consistent with the primary crystallization sequence of amphibole-before-plagioclase that is commonly observed petrographically. The two metatuffs from the Snoqualmie area (Dragovich and others, 2009a,b) originated from a mantle source that was more enriched than samples from this study (Fig. 11). Metatuff 13-17E-1 has very high Th (Figs. 11 and 12) and is peraluminous (aluminum saturation index = 1.23; Table D1). This suggests that the sample assimilated continental crust (Pearce, 1982; Frost and others, 2001). Excluding sample 13-17E-1, the metatuffs and metatrandhemite are magnesian, calcic, and metaluminous. These samples also plot in the volcanic-arc granitoid (VAG) field (Fig. 13). The Nb/Yb ratios and high Th of many WMB meta-

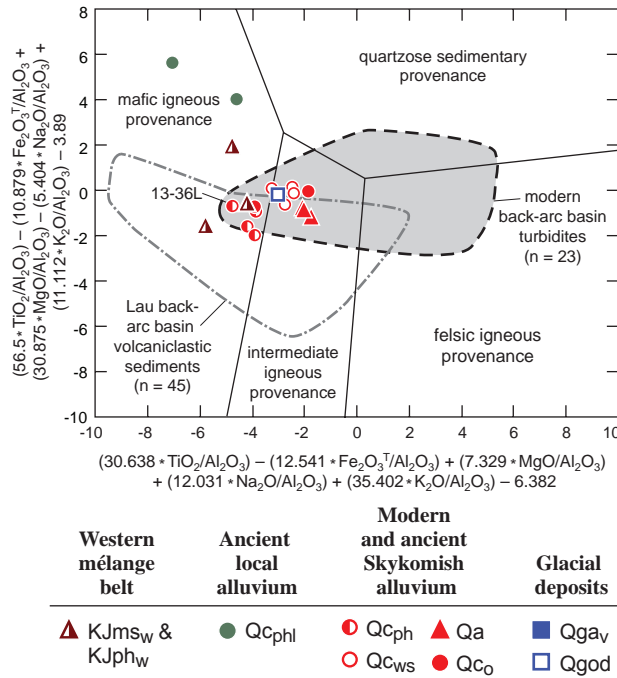


Figure 10. Roser and Korsch discriminant function diagram for Quaternary samples and metasedimentary rocks from the WMB (Roser and Korsch, 1988). Data taken from Dragovich and others (2009a,b, 2013) and this study. Note that the SP samples plot primarily in the intermediate igneous provenance field, consistent with their petrography (Table 1).

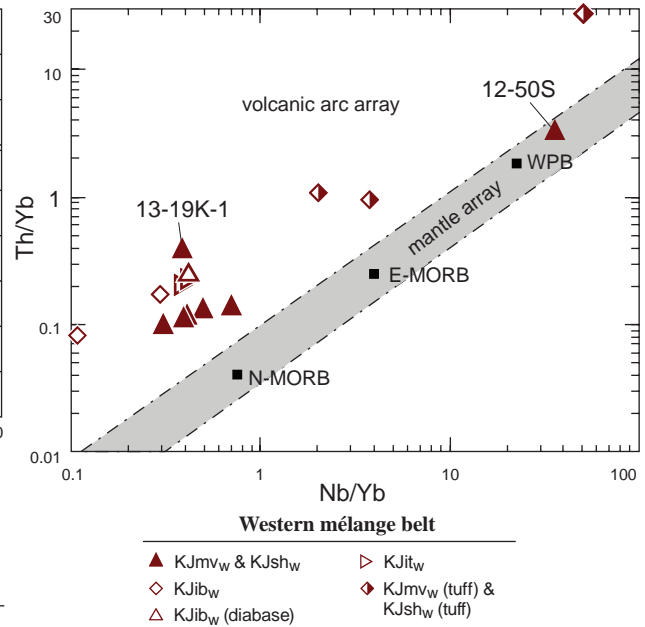


Figure 11. Thorium/Ytterbium (Th/Yb) vs. Niobium/Ytterbium (Nb/Yb) diagram of Pearce (1982, 2008) adapted for WMB meta-igneous samples. Data taken from Dragovich and others (2009a,b, 2013) and this study. E-MORB, enriched mid-ocean ridge basalt; N-MORB, normal mid-ocean ridge basalt; WPB, within-plate basalt. Note the primarily arc composition of these meta-igneous samples.

igneous samples suggests that they resulted from partial melting of a depleted mantle source, and this mantle was influenced by subduction-zone metasomatism (Pearce, 1982, 2008). The geochemistry of the meta-igneous samples suggests that they were primarily derived from a volcanic island arc (Wood, 1980; Pearce, 1982, 1996, 2008; Pearce and others, 1984; Frost and others, 2001) (Figs. 11–13). Vance and others (1980) reported trace element geochemistry from five WMB mafic metabasalt samples and one metagabbro sample. Their samples primarily have arc geochemical affinities, while one metabasalt is a normal MORB. Tabor (1994) analyzed two metabasalt samples from the WMB. One sample has arc affinities while the other plots in MORB-arc basalt overlap fields on geochemical diagrams. Greenstone sample 12-50S from the Sultan 7.5-minute quadrangle (Dragovich and others, 2013) differs geochemically from the new WMB analyses. Its elevated Yb with respect to Nb and low Hf suggests it resulted from a hotspot plume melting a deep garnet peridotite source (Figs. 11 and 12) (Pearce, 1996, 2008). This is confirmed by 12-50S plotting near the average value for WPB on Figure 11. The metatuffs from this quadrangle and the Snoqualmie 7.5-minute quadrangle (Dragovich and others, 2009a,b) were derived from a volcanic arc that had a more enriched mantle source than most WMB samples (Fig. 11) (Pearce, 1982, 2008). This suggests that these meta-igneous samples originated in a complex Jura-Cretaceous volcanic island arc system that may have evolved over time. The large amount of assimilation that metatuff 13-17E-1 underwent suggests that some arc rocks are highly evolved (Frost and others, 2001).

Metasandstone and meta-argillite from the WMB were derived from a volcanic island-arc as shown by their high V and Sc (Fig. 8) and position in the mafic igneous provenance field on a discriminant function diagram of Roser and Korsch (1988) (Fig. 10). The low Th and Zr values suggest that recycled or cratonic detritus was not a major component of these metasediments (McLennan and others, 1990), in contrast to the arkosic facies of Jett and Heller (1988), which were not geochemically analyzed in this study. Overall, the geochemistry of the WMB metasedimentary rocks is consistent with deposition in a back-arc basin or forearc setting within an accretionary prism.

Field, petrologic, and geochemical information indicate that the WMB is a structural mixture of various tectonic environments. These tectonic settings primarily consisted of volcanic island-arcs, with oceanic island (hotspot) and oceanic ridge deposits locally (MacDonald and others, 2014). This predominantly arc setting is

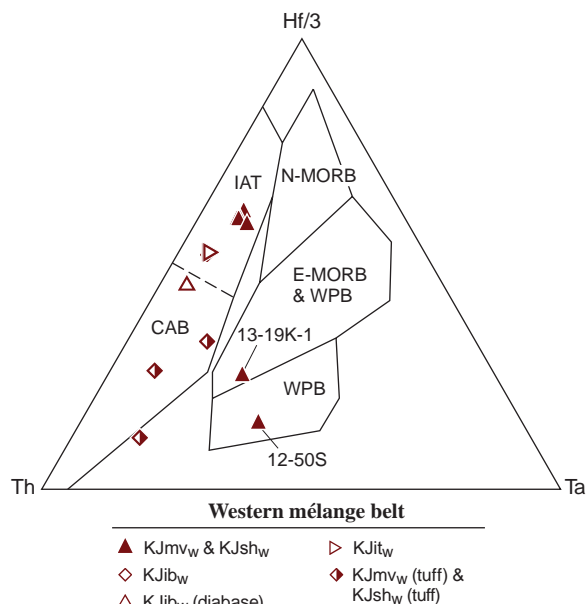


Figure 12. Thorium (Th)-Hafnium (Hf)-Tantalum (Ta) discrimination diagram of Wood (1980) adapted for WMB meta-igneous samples. Data taken from Dragovich and others (2009a,b, 2013) and this study. CAB, calc-alkaline basalt; E-MORB, enriched mid-ocean ridge basalt; IAT, island-arc tholeiite, N-MORB, normal mid-ocean ridge basalt; WPB, within-plate basalt. Note that the samples plot primarily in the arc fields.

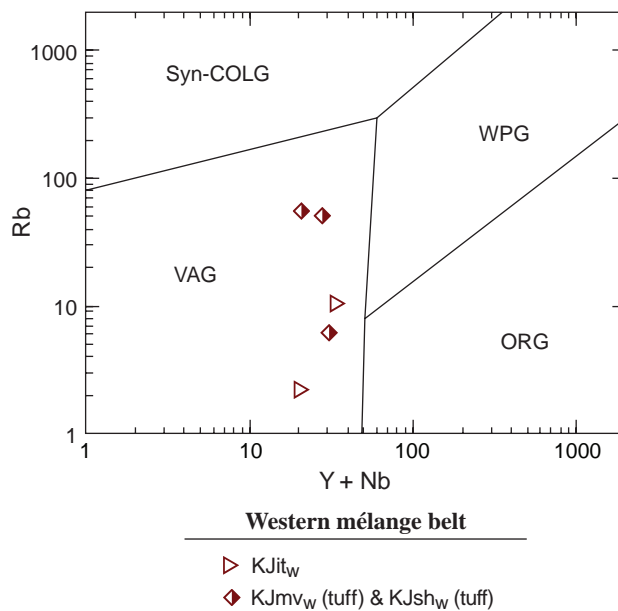


Figure 13. Rubidium (Rb) vs. [Yttrium (Y)+Niobium (Nb)] discrimination diagram for granitoid rocks of Pearce and others (1984) adapted for WMB "granitic" samples. Data taken from Dragovich and others (2009a,b) and this study. ORG, ocean-ridge granite; Syn-COLG, syn-collisional granite; VAG, volcanic-arc granite; WPG, within-plate granite. Note that the samples plot in the arc field.

consistent with previous WMB studies and the likely correlative De Roux unit and Russell Ranch complex, central Washington Cascades (Vance and others, 1980; Miller, 1985; Frizzell and others, 1987; Jett and Heller, 1988; Miller, 1989; Tabor, 1994; MacDonald and others, 2009).

ISOSTATIC GRAVITY AND AEROMAGNETIC ANALYSES

High-quality aeromagnetic data that define the geomagnetic anomalies in the quadrangle (Figs. M1 and M2, map sheet; Blakely and others, 1999) and an unpublished regional database of gravity data that constrains isostatic gravity anomalies support our structural interpretations. See Anderson and others (2006) for an overview of the gravity database. Gravity data collected in 2013 define anomalies in the quadrangle in greater detail than the regional database. Extensive sampling and measurement of density and magnetic susceptibility for units in this and neighboring quadrangles (Dragovich and others, 2010a,b, 2011a,b, 2012, 2013) aid the modeling of our cross sections and provide a means for interpreting map-view anomalies in terms of subsurface geologic units and faults. Overall, rocks of the Western mélangé belt (WMB) largely control the geophysical map and models—an assertion that is supported by multiple geophysical observations from outcrops across the map region. We greatly increased the number of WMB hand-sample properties measured for density and magnetic susceptibility during this study (Fig. M2); therefore we used a large database of WMB physical properties to interpret this map and create the geophysical models.

Models support the general trend that metagabbroic rocks are thicker and shallower to the southwest (higher-amplitude anomalies) and thinner and deeper to the northeast (lower-amplitude anomalies). This relationship is especially apparent in Figure M2, which models metagabbro within the Lake Chaplain nappe as shown on stratigraphic Cross Section A. Note that while the general distribution of the metagabbro map unit shown on the cross sections is required to match the aeromagnetic data, the exact shape and precise depth of each metagabbro body is flexible, and several geometries are plausible. This uncertainty is compounded by the observations that hand-sample magnetic susceptibility measurements have a wide variation and that weathering and deformation lead to lower susceptibilities in hand samples as compared to susceptibilities required in the deep subsurface for geologically reasonable structural models (compare values in Fig. M2). Hence, a range of susceptibilities is possible

for deeply buried metagabbroic rocks. One notable exception to uncertainty about shape are the abrupt and vertical boundaries of the metagabbro map unit within the Woods Creek fault zone in the southwest corner of the map. These boundaries are required to fit abrupt lateral changes in the magnetic anomalies (Cross Section A; Fig. M2).

Other WMB units add a more subtle contribution to the mapped gravity and magnetic anomalies. For example, unit $KJms_w$ metasedimentary rocks generally coincide with gravity lows, in accordance with slightly lower density measured from hand samples. The best example is on the eastern end of Figure M2, which shows a substantial syncline containing unit $KJms_w$ that matches a dip in the gravity values. Greenstone (unit $KJmv_w$) is also included in this syncline, but these rocks are not resolvable with the geophysical data. The gravity high around the Blue Mountain klippe (labeled BMK on Fig. M1) is not well explained by the unit KJm subunits used in the geophysical models. Although the metagabbro is collocated with a moderately high magnetic anomaly, the gravity anomaly is too high in amplitude to be explained by such a relatively thin metagabbro klippe atop mostly low-grade metasedimentary rocks. Therefore we have interpreted a relatively dense body of rock at depth, that, when added to the klippe, could account for such a large anomaly. This could be consistent with the existence of an intrusion at depth—the Young’s Creek intrusive complex, for instance—which is east and south of the map area and is supported by past gravity modeling of Dragovich and others (2013) and Anderson and others (2011). Alternatively, the dense body could be higher grade WMB phyllite, gneiss, or greenschist residing below and to the north and east of the map area as supported by regional-scale geologic maps (Tabor and others, 1993).

One prominent exception to the general relation of magnetic highs with unit $KJigb_w$ is a low-amplitude magnetic high collocated with a gravity low thought to be part of the Monroe syncline (Fig. 14). This relationship—high magnetism with low gravity (clearly evident in data for Figure M2)—could reflect deeply buried metagabbroic rocks, as we interpreted a similar relationship in the Sultan map analysis (Dragovich and others, 2013). However, this anomaly is magnified by the high-resolution aeromagnetic data (upward continued and differenced with original grid), suggesting a very near-surface magnetic source rock. A simpler interpretation is that this relationship is due to the moderately magnetic and thick Pleistocene nonglacial SP deposits (Table 1) filling the Monroe synclinal basin. This allows an easy fit of the lower-amplitude magnetic anomalies along Figure M2 and is supported by past susceptibility measurements of unit Qc_o in the Fall City quadrangle (Dragovich and others, 2007) that showed moderate magnetic values¹ for those SP-provenance deposits. Moderate magnetic susceptibility also seems reasonable, given the significant percentage of detrital magnetite grains found in this ancient alluvium. In the Sultan quadrangle (Dragovich and others, 2013), uneven gravity data precluded defining a relationship between sediment thickness and magnetic SP deposits. Instead, we interpreted metagabbro as the source rock for high magnetic anomalies over the Monroe syncline. However, with our newly acquired data, we now believe that a low-amplitude magnetic high over the Monroe syncline in the Sultan quadrangle is also related to mildly magnetic SP-provenance sediments (Fig. 14).

Several steep gradients in both the magnetic and gravity data coincide with faults. The northeastern edge of gravity low MS1 (Fig. M1) is a steep gravity gradient coincident with the 124th St. reverse fault. Figure M2 shows that an abrupt edge of the Quaternary-sediment-filled Monroe syncline is predominantly responsible for this gradient, a result that is also consistent with passive seismic data (Hayashi, 2013). A similarly strong gradient north of MS2 (Fig. M1) indicates reverse motion along the Woods Creek fault, although this gradient is influenced by high-density unit $KJigb_w$ existing within the fault zone; therefore the spatial relationship of the steep magnetic gradient with the fault location is less clear. However, an abrupt increase in Quaternary sediment thickness is needed to fit gravity data in Figure M2.

In the cross sections, we model tectonic zones (units tz and tz_h) as regions with low density, which is consistent with our approach for other models in the region (for example, Dragovich and others, 2013) and the observation that damage zones along the major strike-slip faults are highly faulted or fractured and have broad regions of sub-vertical low density rock. The lowest-density unit tz is in the Woods Creek fault zone, which suggests more pervasive deformation there compared to other faults in the map area. Past geophysical modeling, particularly in the Sultan quadrangle (Dragovich and others, 2013) supported a very low density region—and thus more extensive development of unit tz —along the Cherry Creek fault zone (CCFZ). We suggest that the apparent reduction in accumulated strain along the CCFZ in the current map area may indicate that significant slip has been transferred to the Woods Creek fault zone. This is consistent with the abrupt vertical boundaries that are required of the metagabbro (unit $KJigb_w$) within the Woods Creek fault zone (GB1 in Fig. M1 and Fig. M2). Strain transfer

¹ $3.6 \times 10^{-3} \chi$ (SI units for magnetic susceptibility) in outcrop to $1.1 \times 10^{-2} \chi$ in hand sample

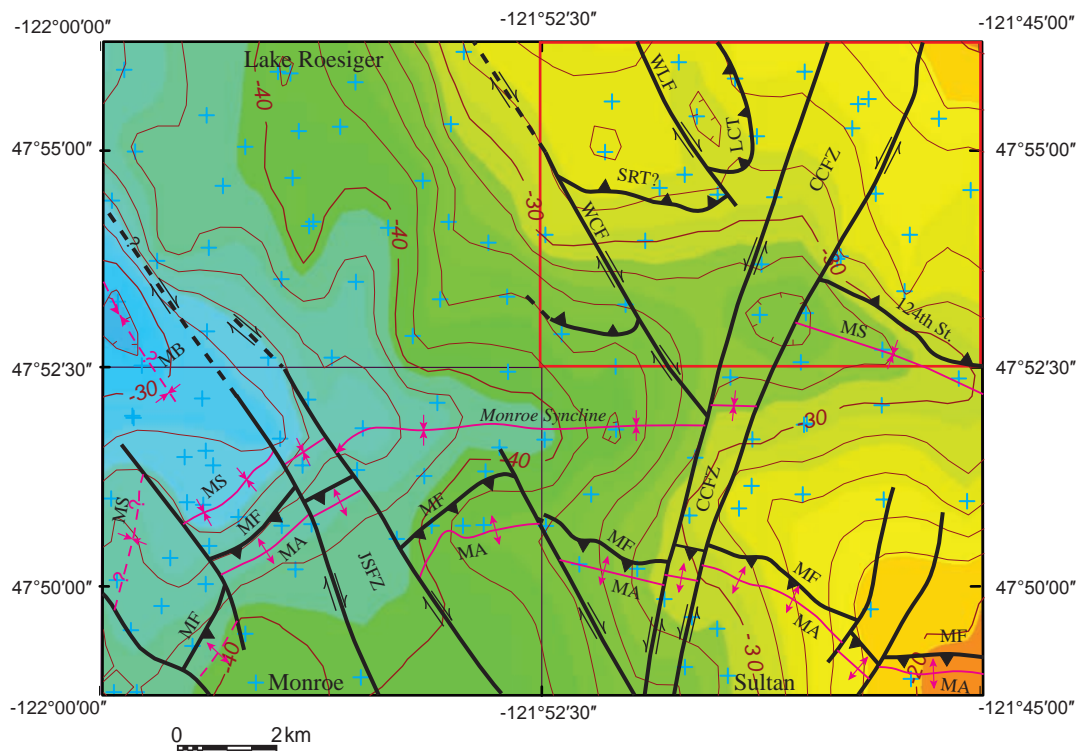


Figure 14. Isostatic gravity map of the northern halves of the Monroe and Sultan 7.5-minute quadrangles and the southern halves of the Lake Roesiger and Lake Chaplain (red outline) quadrangles. Cooler colors indicate lower gravity values, and warmer colors, higher values. Gravity contour interval is 2 mGal; small hachures indicate closed lows. Approximately 135 gravity measurements (blue crosses) constrain the contours. Gravity data in the Lake Roesiger quadrangle is preliminary. Superimposed fault and fold structures are simplified from Dragovich and others (2011a,b, 2013, this study). To simplify the illustration, we show some reverse faults as thrusts. MF, Monroe fault; MS, Monroe syncline; MA, Monroe anticline; MB, Monroe basin; CCFZ, Cherry Creek fault zone; JSFZ, Johnson's Swamp fault zone; 124th St., 124th Street reverse fault; WCF, Woods Creek fault; WLF, Woods Lake fault. Note the regional gravity low formed by the Monroe synclinal basin as well as offset of the syncline by the CCFZ. Continued study of the extension of the JSFZ in the southwestern corner of the Lake Roesiger quadrangle are warranted, especially near the more northerly gravity low on the west side of the fault zone that we informally here term the Monroe basin (MB).

to the Woods Creek fault zone is also consistent with in-progress mapping directly west, in the Lake Roesiger quadrangle, that indicates the Woods Creek fault zone is a broad strike-slip fault.

Gravity lows associated with the Monroe syncline (MS1 and MS2 in Fig. M1) have an apparent left-lateral relationship; the lowest gravity observation near MS2 is south of this label (and is on the Sultan quadrangle), as shown on Figure 14. This apparent left-lateral offset is consistent with the interpreted motion across the CCFZ, which separates the two lows, and is also supported by earthquake focal mechanisms and meso-scale structures (Dragovich and others, 2013). Gravity gradients observed along the Woods Creek fault (WC), Sultan River fault (SR), and Woods Lake fault (WL) seem to correspond with mapped faults, but not conclusively (Fig. M1). A low-amplitude gravity and magnetic low (WLL) in the central part of the map area is spatially associated with, or just east of, the Woods Lake fault (Fig. M1). We believe this low could be due to: (1) relatively thick Quaternary sediments in a basin around Woods Lake, and (or) (2) dip-slip or oblique motion on the Woods Lake fault that resulted in preservation of a relatively thick sequence of metasedimentary rocks (unit KJmsw) that we infer structurally overlie the Lake Chaplain nappe (Fig. 15; Cross Section B). Finally, we note that there is no expression of the Explorer Falls basin in the gravity data. Even its maximum thickness—200 to 250 m (656–820 ft) of sediment (see section below on the *Explorer Falls Basin*)—would only create an anomaly of ~1 mGal or less. Given our sparse gravity data coverage in the northwest corner of the map area, an anomaly of this amplitude could be easily missed. In addition, westward tilt and eastward thinning of the basin, combined with local denudation, all suggest that a thickness of less than 200 m (656 ft) is more likely and would therefore further decrease the magnitude of the expected anomaly; it would be on the edge of our detection limits, even if we had more data coverage.

METAMORPHISM AND STRUCTURE OF THE WESTERN MÉLANGE BELT

The Western mélangé belt (WMB) is a low- to medium-grade sequence of highly disrupted oceanic and arc rocks mapped widely in the region. “The eastern part of the Western [mélangé] belt is more thoroughly metamorphosed than the rest of the belt; in the general area of the lower Sultan Basin the disrupted rocks grade to slate, phyllite,

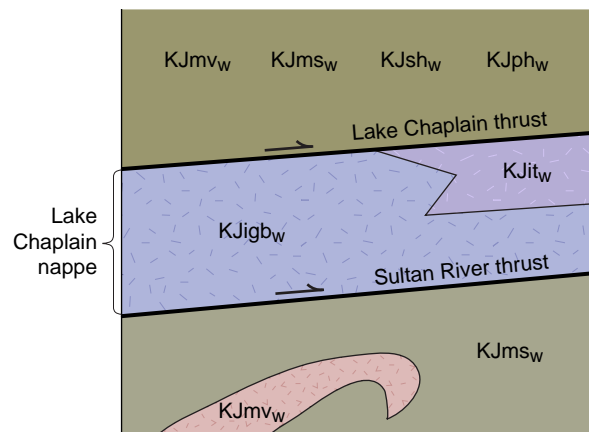


Figure 15. Structural column-block diagram showing the Lake Chaplain nappe (LCN) and the Sultan River and Lake Chaplain thrusts. The LCN contains disrupted arc metagabbroic (unit KJigbw) and metatonalite (KJitw) rocks in the map area. Low-grade metasedimentary and metavolcanic rocks (KJmsw and KJmvw) underlie the LCN in the Sultan River area. Similar low-grade, well-stratified rocks on Blue Mountain underlie the Blue Mountain klippe, implying that the underlying contact could be the elevated Sultan River thrust. Low-grade metasedimentary and metavolcanic rocks (KJmsw and KJmvw) overlie the LCN. Although strongly disrupted by the Cherry Creek fault zone, some of the higher grade phyllitic or schistose metasedimentary and metavolcanic rocks (KJphw and KJshw) in the northeastern part of the map area might be above the LCN.

and semischist and contain minor greenschist and chert” (Tabor and others, 1993, p. 12). This higher-grade part of the belt extends into the northeast corner of the study area, where phyllite and greenschist are common. In the study area, the primary cleavage increases in intensity with metamorphic grade generally from prehnite-pumpellyite facies in the southeast to greenschist facies in the northeast, with amphibolite facies found in the highest grade part of the WMB outside of the map area.

The Western mélangé belt contains outcrop- to mountain-sized phacoids of metagabbro, metadiabase, and metatonalite. Commonly the meta-argillite matrix is not well exposed, and disruption of beds, crude foliation, or pervasive cataclasis is apparent in most outcrops (Frizzell and others, 1987). A moderate to strong syn-metamorphic foliation is subparallel to bedding and likely resulted from shearing of turbidites in an accretionary prism. This primary foliation commonly dips steeply to the northeast, and we assume it is broadly synchronous with progressive deformation during the first accretionary shear deformation across the belt; variation in foliation orientation is related to post-metamorphism folding and fault-block rotation (Fig. 16).

The lack of internal deformation at outcrop scale in the WMB is noteworthy because, at a regional scale, the belt is highly disrupted—many locations (for example, near Blue Mountain) contain continuous stratigraphic sequences of well-bedded rocks (see Dragovich and others, 2013). These intact stratigraphic sections suggest that some mélangé belt components record little tectonic mixing of lithologies, and that the scale of mixing is beyond the outcrop scale and locally may occur at the scale of mountains. An exception to these relatively undeformed exposures is the intense internal disruption of the meta-igneous rocks and phyllite within the Lake Chaplain nappe, discussed below. Although internal deformation and tectonic mixing of lithologies is minimal in many areas, large overturned folds record significant local shortening. Such deformation is recorded in the turbidite sequence in the northeast part of the map area around significant sites 19R and 19T, where metasedimentary rocks are overturned and form large isoclinal folds. We noted poorly developed microfolding and crenulation lineations parallel to the axial traces of folded bedding and cleavage intersections. Although much more work is warranted, the orientation of the Cretaceous structures—including isoclinal folds and incipient crenulations of the metamorphic foliation—all suggest east- to northeast-directed thrusting during progressive formation of the accretionary prism. This direction is also supported by west-southwest-trending mineral stretching lineations in a mylonitized metatonalite at the Sultan River thrust (significant site 48L).

The Lake Chaplain Nappe

Our mapping suggests that some or all of the meta-intrusive rocks (mostly metagabbro) lie within the Lake Chaplain nappe, a structural unit bound by the newly named Sultan River and Lake Chaplain thrusts (Fig. 15). This nappe also includes strongly foliated phyllitic metasedimentary rocks. Structural relationships indicate that the thrusts are late- to post-metamorphic in age; faults in the map area juxtapose rocks of contrasting metamorphic grade—specifically, the Lake Chaplain nappe rocks are thrust over low-grade rocks. The intensity of deformation

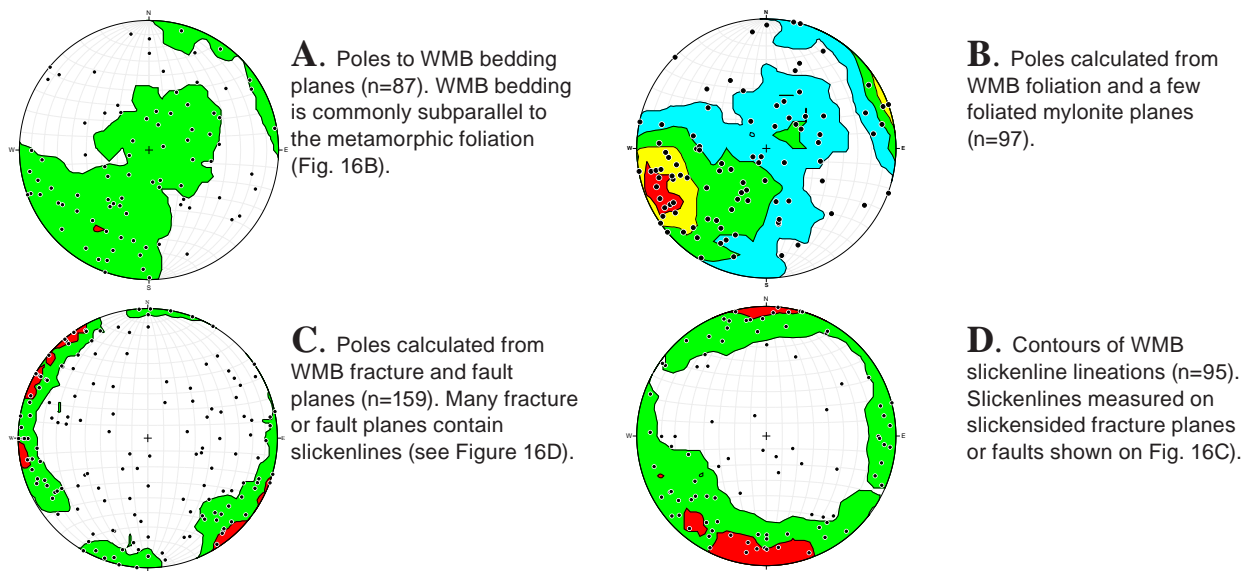


Figure 16A–D. Equal area stereonet of Western mélangé belt (WMB) structural data for the Lake Chaplain quadrangle. The Kamb contour plot offers a density distribution of the plotted poles or lineations. WMB bedding (Fig. 16A) is mostly transposed subparallel to the metamorphic foliation (Fig. 16B) in most outcrops and dominantly dips steep northeast. Later small-scale F2 folds disperse bedding and metamorphic foliation around mostly subhorizontal northwest–southeast-trending axes. Slickenlines (Fig. 16D) are observed on variably oriented fractures and faults, including a northwest-trending fault along the Woods Creek fault and east–west-trending fault zones such as the Explorer Falls basin. The dominant zone in the map area is the Cherry Creek fault zone. This zone is dominated by north-northeast-trending fractures and faults with slickenlines that most commonly plunge shallowly north-northeast–south-southwest.

in the mélangé is greater in the Lake Chaplain nappe where the meta-intrusive rocks appear to be deformed at all scales. This contrasts with the lower intensity of deformation noted above for thick sequences of metasedimentary and metamorphic rocks that lie above and below the Lake Chaplain nappe (Fig. 15).

We are unsure if the meta-igneous rocks away from the Lake Chaplain area—where thrust faults are well-exposed—are also confined to this nappe or structurally dispersed above and below it. If the meta-intrusives are confined to the nappe, then the Blue Mountain klippe lies above the Sultan River thrust on the eastern edge of the quadrangle, and indicates substantial vertical uplift of rocks to the east of the Blue Mountain fault. East-side up movement across the CCFZ is generally indicated by (1) the increase in metamorphic grade of the mélangé belt to the east and northeast across the CCFZ strands, and (2) the westerly tilt of the Explorer Falls basin. The westerly tilt of the basin, and the uplift to the east of the quadrangle, seem to be at least partially due to vertical offset along the CCFZ. The Lake Chaplain nappe is composed of Jurassic (~150–170 Ma) meta-igneous rocks and probably lies in a structurally higher position than the latest Cretaceous (~74 Ma) arkosic metasedimentary rocks (unit KJms_w), which have a strong granitic provenance. These relationships suggest a structural architecture where younger accretionary-wedge metasediments with granitic provenance underlie one or more nappes of older volcanic-arc rocks—such as the Lake Chaplain nappe which is dominated by Jurassic meta-igneous rocks. Further work is required to determine if: (1) the Lake Chaplain nappe is a structural entity of regional significance in the WMB, and (2) the arkosic petrofacies consistently occupy a structurally low position in the WMB.

We also suspect that some of the faults in the southwestern part of the quadrangle are extensions of the bounding faults of the Lake Chaplain nappe (Cross Section A). In the Lakeside quarry at significant site 18A in the southwest part of the map area, we noted a rare exposure where metagabbro and phyllite are not separated by a fault. Although we did not observe distinctive apophyses of gabbro or other intrusive structures in the phyllite, the contact might be a rare gabbro intrusion into the sedimentary mélangé belt country rock; further work is warranted in this area. Also, because metagabbro and phyllite apparently share the regional S1 cleavage fabric, this possible intrusive activity occurred before or during metamorphism and probably within an accretionary prism shear complex.

Further work is required to clearly define the tectonic stratigraphy of the WMB and test these hypotheses, including the relationships between metamorphism, structural fabrics, and thrust vergence. Tabor (1994) and other workers suggest that the Northwest Cascades System was thrust over the Eastern and Western mélangé belts during

mid-Cretaceous regional thrusting at ~90 Ma. The new ~74 Ma maximum depositional age, along with other regional considerations, appears to indicate that thrusting of the Northwest Cascade System and the structural emergence of mélange belts is younger than the previously accepted ~90 Ma age (Tabor, 1994; Dragovich and others, 2009a,b; Brown, 2012; Sauer and others, 2014).

TERTIARY TO RECENT FAULTS AND FOLDS

Overview

Geologic mapping of the Lake Chaplain quadrangle continues our efforts to better understand the southern Whidbey Island fault zone (SWIF) and its relation to the CCFZ and Monroe fault zone. West of the map area, Sherrod and others (2008) mapped the SWIF southeastward from Whidbey Island to the Maltby quadrangle west of the Lake Chaplain area (Fig. 1). In a series of geologic maps, Dragovich and others (2007, 2009a,b,c, 2010a,b, 2011a,b, 2012) mapped the Rattlesnake Mountain fault zone (RMFZ) from the North Bend, Snoqualmie, and Fall City quadrangles northwestward through the Carnation, Monroe, and Lake Joy quadrangles and correlated this broad fault zone with the SWIF. All of these studies indicate that the SWIF is a strike-slip fault zone containing several active or potentially active segments. Some of the segments align with probable active fault strands mapped by Sherrod and others (2008) to the west. Dragovich and others (2010a,b) correlated the main strand of the RMFZ with the Cottage Lake lineament of the SWIF from Sherrod and others (2008).

We informally name several faults in the Lake Chaplain quadrangle to facilitate description and communication. The CCFZ has been mapped northeastward from previous geologic mapping studies (Fig. 1). Major CCFZ fault strands in the current map area are (1) the main strand of the CCFZ and the Sultan River fault of Dragovich and others (2012), and (2) the newly named Blue Mountain fault. The main strand of the Cherry Creek fault merges with the Sultan River fault in the southern part of the map. We map the Sultan River fault as it follows straight portions of the Sultan River and into the northeastern part of the map area. We suspect that this structure is the main strand of the CCFZ in the southern part of the map area because the Sultan River fault appears to control two long, straight, north–northeast-trending segments of the river associated with a wide strike-slip damage zone. The Blue Mountain fault appears to be the eastern part of the CCFZ, at least locally. The Woods Creek fault is a northwest-striking fault defined by geophysical lineaments in the southeastern part of the map area. This structure appears to splay off the CCFZ and continues as a strong geomorphic and geophysical lineament into the Lake Roesiger quadrangle where it is associated with seismicity (Appendix B; Fig. B1; Cross Section A). The Woods Lake fault (Cross Section A) is a geomorphic lineament that is moderately defined by geophysical anomalies and might be located above shallow seismicity northwest of the map area.

Mapping in the Sultan quadrangle by Dragovich and others (2013) confirmed that the contact between the Mount Persis unit and the WMB directly south of the Skykomish River is a reverse fault. This structure was named the Monroe fault by Dragovich and others (2011a,b). The Monroe anticline and syncline were first mapped in the Monroe and Sultan quadrangles directly southwest and south of the present map area. We interpret these folds as north-verging flexural-slip folds that parallel the Monroe fault and accommodate the current north–south compression in the Puget Lowland. We base this interpretation on (1) the parallelism of the Monroe fault and the Monroe anticline and syncline (2) geophysical data documenting the geometry and thickness of the Monroe synclinal basin, and (3) fault kinematic data. The Carnation fault (Dragovich and others, 2010b, 2012) and kinematically linked Tolt River anticline (Dragovich and others, 2012) verge south, opposite to the Monroe fault, and together, displacement along these opposing structures may be responsible for the emergent bedrock between them (Dragovich and others, 2011a,b, 2012, 2013)(Fig. 1). We tentatively interpret these faults as restraining-bend duplex structures within the SWIF (Dragovich and others, 2012, 2013), but how this uplift relates to regional tectonics is unresolved. For part of its history, the Monroe fault was likely an extensional Eocene structure that was later rejuvenated as a reverse fault in the Tertiary (Dragovich and others, 2013). We note the structural similarity between the Seattle fault, Seattle uplift, and Seattle basin and the Monroe fault, Monroe uplift, and the Monroe synclinal basin (Figs. 1 and 14). Both systems trend east–west and each is bound by a southward-dipping reverse fault that elevates older rocks over Quaternary basins to the north. Finally, we suspect that the Monroe fault has a pre-Eocene history and may have originated as a Cretaceous thrust fault emanating from the WMB basement rocks below the volcanic rocks of Mount Persis.

Cherry Creek Fault Zone

The Cherry Creek fault zone (CCFZ) is a northeast-striking left-lateral strike-slip fault zone that is conjugate to the right-lateral SWIF, a geometry shared by the Tolt Creek fault zone farther southeast (Fig. 1)(Dragovich and others, 2009a,b, 2012). The CCFZ was originally mapped in the Carnation quadrangle and later mapped through the Sultan quadrangle (Dragovich and others 2010a,b, 2011a,b, 2012, 2013). The CCFZ is a probable active fault zone as indicated by faulted Vashon Stade glacial deposits and the distribution and kinematics of the shallow 1996 Duvall earthquake and aftershocks (Dragovich and others, 2012, 2013; Bradford and Waters, 1934). We mapped the CCFZ into the Lake Chaplain quadrangle as a series of high-angle north–northeast-striking strike-slip faults. Outcrops near most of the fault strands are cataclastic to fractured, and locally have hydrothermal alteration (units tz and tz_h). As observed to the south, most kinematic indicators along the CCFZ, such as en echelon vein arrays and shallowly raking slickenlines on steep fracture and fault planes, suggest left-lateral strike-slip or oblique-slip offset. Fractures and faults generally strike northeast and have subhorizontal slickenlines, consistent with brittle strike-slip deformation (Fig. 16C–D). These brittle structures also cut or displace older Cretaceous features, such as the mélangé belt cleavage fabric—including well-bedded metasedimentary rocks with prominent Cretaceous-age foliation (Figs. 17 and 18). CCFZ high-angle brittle structures displace older mélangé belt structures at significant sites 6A, 26L, 29S, 30W, 55G, 30AA, 39Q, and 19X.

The CCFZ offsets the Monroe syncline with left-lateral separation (Fig. 14). As with other Tertiary to recent high-angle faults, some CCFZ strands might also left-laterally displace older thrusts and reverse faults. For example, note the left-lateral separation of some unit KJit_w rocks across some CCFZ fault strands. The ~5km-wide CCFZ contains several long (>15 km) strands, including the Sultan River and Blue Mountain faults. These long faults locally merge with shorter transfer-fault segments that together bound tectonic blocks within the CCFZ. In some of the fault-bound CCFZ sub-domains, the high internal strain/rotation has resulted in the rotation of the older foliation into the northeast trend of the CCFZ. Elsewhere, brittle strain is less and the foliation remains

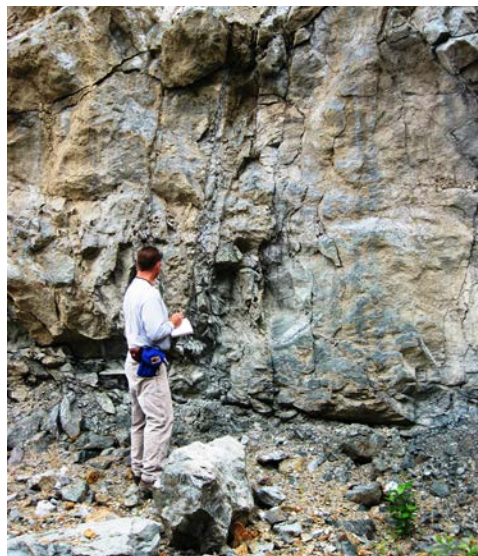


Figure 17. Greenschist facies, volcanoclastic to tuffaceous phyllite, and semischist (unit KJphw) at site 6A rock quarry in the north-central part of the map area directly west of the Sultan fault east of the Sultan River. These rocks are compositionally immature metasediments with a strong cleavage that parallels bedding (Fig.18). Note the steep fractures and small faults spaced on a scale of centimeters to meters in this photo. These faults strike north-northeast and dip subvertically. Many of the small faults contain thin gouge zones. (Photo looks NNE.) Slickenlines on the fracture and fault faces consistently plunge shallowly to the south-southeast at this site, and some faults have left-lateral offset consistent with the kinematics of the translational CCFZ. The faults and fractures distinctly cut older foliation/bedding planes that dip shallowly to the north–northeast at this site.



Figure 18. Strong metamorphic fabric in this volcanic or tuffaceous phyllite or semischist at significant site 6A. (See Fig. 17 for location and other site information.) Note the parallelism of the strong metamorphic fabric and bedding, as well as the boudinage of some of the thin relict metasedimentary beds. Some of the light colored bands are quartzose metamorphic segregations parallel to the cleavage; locally some of the quartzose segregations are more than 1 cm thick, indicating that the rocks are locally gneissose. The foliation in this quarry strikes N50 to 65°E and dips 38 to 41°NE; it is clearly cut by northeast-trending CCFZ fractures and faults shown in Figure 17. (Photo looks to the northeast and slightly oblique to the foliation.) The finger points to a steeply dipping northeast-trending fracture with an apparent left-lateral sense of offset of a dark bedding plane.

strongly oblique to the CCFZ—cleavage strikes along the more regional northwest–southeast direction. A distinct metamorphic grade change occurs across some of the CCFZ strands, particularly in the northeast part of the map area. The change in metamorphic grade is accompanied by a change in metamorphic fabric intensity—such as the change of greenstone to greenschist or meta-argillite to phyllite—and implies a component of vertical displacement on some strike-slip fault segments. This is particularly true along portions of the Sultan River fault where these distinct lithologic changes occur in close proximity across fault strands. We favor an oblique strike-slip model for juxtaposition of these blocks consistent with other evidence of general east-side up displacement along or near the CCFZ including: (1) the high elevation of the Blue Mountain klippe which is likely correlative with the Lake Chaplain nappe (Fig 15), and (2) easterly uplift/tilting of the Explorer Falls basin in the northwest corner of the map area. This oblique slip offset along the CCFZ might be part of a family of structures that accommodate on-going uplift of the Cascade Range.

ANCIENT ALLUVIUM AND THE NEOTECTONICS OF THE SKYKOMISH RIVER VALLEY

Pleistocene Alluvium

Ancient alluvium from several Pleistocene nonglacial intervals is widespread in the lower Skykomish River valley (Dragovich and others, 2011a,b, 2013). These Pleistocene alluvial deposits have a composition, sedimentology and general stratigraphic architecture that mirrors modern alluvium (SP in Table 1). The stratigraphy of these deposits is similar to the nonglacial stratigraphy in the Snoqualmie River valley to the southwest (Dragovich, 2007; Dragovich and others, 2007, 2009a,b,c, 2010a,b, 2012). SP-provenance sediments typically have liquefaction features, including contorted or chaotic bedding and (or) sand dikes; intense liquefaction features occur at significant sites 17A (sec. 32, T28N R8E), 37B (sec. 11, T28N R8E), 46G (sec. 16, T28N R8E), 28W (sec. 29, T28N R8E), 45F (sec. 32, T28N R8E), 47P (sec. 32, T28N R8E), and 109F (sec. 23, T29N R7E)(Figs. 5 and 6). Analyses in the adjacent Monroe quadrangle show that ancient and modern Skykomish River alluvial deposits are similar to their counterparts in the Snoqualmie River valley (Qm₅₉₋₆₅Qp₁₂₋₂₉PF₁₂₋₂₆)(Dragovich and others, 2011a,b). These sediments are derived from an intermediate, continental arc and are predominately from Tertiary granitic to granodioritic erosional sources, such as the Index, Grotto, and Snoqualmie batholiths (Dragovich and others, 2011a,b, 2012, 2013). SP-provenance sediments contain detrital grains of monocrystalline quartz (~10–20%), plagioclase, K-spar, hornblende, pyroxene, and mica with some granitic lithic clasts; these Pleistocene SP sequences are correlated with the Olympia nonglacial interval, Whidbey Formation, or the older Hamm Creek interglacial interval. The Cascade provenance of the SP deposits in the Monroe syncline is supported in this study by a detrital zircon study from Olympia bed SP sand at age site 37A (40–48 ka)(Appendices A and C), as well as the geochemistry of sand sample 30U, also at site 37A. The detrital zircon spectra shows a strong correlation with the age and distribution of geologic units presently exposed in the Skykomish basin east of the study area (Table C2). Most compelling are the large number of 32 to 36 Ma zircon ages, consistent with erosion of the widespread 33 to 34 Ma Index batholith (Tabor and others, 1993; Yeats and Engels, 1971) in the Cascades directly to the east. SP-provenance sand from site 37A has the ‘grus’ appearance typical of SP deposits regionally, with much subangular to angular monocrystalline quartz, plagioclase, and K-spar (~8%) and lesser hornblende with granitic lithic grains and epidote. Most important is the relative abundance of K-spar, which is largely derived from Tertiary to Cretaceous granite, granodiorite, and tonalite, particularly of the Index batholith.

We correlate deposits in the Explorer Falls basin with a pre-Hamm Creek interglacial interval. These deposits also have a granitic Cascade provenance similar to SP, but likely represent ancient Pilchuck River alluvium as discussed below. Locally derived alluvium along the margins of this graben structure is similar to other locally derived alluvium mapped regionally, such as the Olympia beds (unit QCoI) directly south of the map area (Dragovich and others, 2010a,b, 2012, 2013).

Structural Control of the Skykomish River Valley

REGIONAL OVERVIEW

Mapping of regional structures and Quaternary stratigraphy indicates that the lower Snoqualmie and Skykomish River valleys are structurally controlled by potentially active faults, folds, and fault-bounded basins. Holocene to Pleistocene basin sediments with an SP provenance have distinct and mappable facies architecture. South and west of the current map area, ancient SP sediments are observed at many stratigraphic levels in the Snoqualmie, Skykomish, and Tolt River valleys, where the sediments are commonly tilted or broadly folded. This deformation,

combined with the vertical and lateral distribution of these deposits, implies significant tectonic control of Pleistocene nonglacial river deposits by the SWIF, Carnation, and Monroe fault zones.

Dragovich and others (2007, 2009a,b,c, 2010a,b, 2011a,b, 2012, 2013), and Littke and others (2009) applied growth-folding, pull-apart, and inverted basin models to the observed structures and stratigraphic relations. These studies documented Quaternary inversion of sub-basins along the length of the SWIF in the Snoqualmie valley, where the Snoqualmie River has been structurally trapped within fault-controlled transpressional or transtensional basins during the Quaternary. In this model, formerly extensional pull-apart basins are uplifted as a result of kinematic changes along the fault zones and are now tilted, folded, and (or) raised in blocks between subparallel faults. A transition from transtensional to transpressional basins is supported by the exceptional thickness of some of the SP alluvial basins. At the south-verging Carnation fault, ancient SP sediments (Whidbey Formation) are folded by the Tolt River anticline and uplifted to an elevation of about 900 ft (275 m). Ancient SP sediments are also mapped in the synclinal basin south of this reverse fault, where basin sediments are as much as 400 ft (122 m) thick (Dragovich and others, 2012), and in the Fall City area, where SP sediments in probable SWIF pull-apart basins are as much as 800 ft (250 m) thick (Dragovich and others, 2007). In all of these settings, the exceptional thickness of SP fluvial sediment appears to be the result of subsidence within Quaternary basins.

Dragovich and others (2011a,b, 2013) mapped the Monroe fault directly south of the map area. This north-verging reverse bedrock fault parallels the east–west trending Monroe anticlinal and synclinal structures. These folds have deformed Olympia beds—compression above the fault has likely uplifted and folded these latest Pleistocene SP beds in the hanging wall of Monroe fault. Age, stratigraphy, and structural information suggest that the Monroe fault, anticline, and syncline are potentially active structures (Dragovich and others, 2014). Evidence for Pleistocene activity is inferred from the progressive tightening of the Monroe syncline—a process that has resulted in tighter folding of the Whidbey Formation compared to the younger Olympia beds in the core of the fold.

The Olympia beds were mapped widely across several quadrangles using surface and subsurface information; we obtained several 22.0 to >43.5 ka radiocarbon and OSL/IRSL ages for these ancient fluvial deposits. The ages and structural information also support the earlier contentions of Dragovich and others (2011a,b) that the elevation difference between dated ancient Skykomish River alluvial deposits (unit Qc₀) is at least partially the result of folding and uplift across the Monroe fault and anticline. Likewise, the orientation of bedding in the Olympia beds—and other SP deposits mapped below the Olympia beds north of the Skykomish River—indicate that these ancient deposits are folded by the Monroe syncline (Dragovich and others, 2011a,b). Further investigation may prove that some of the elevation differences for the Olympia bed fluvial successions may be related to complex grading and inset relations of the Skykomish River during and after the Olympia nonglacial interval.

Riedel and others (2010) document alpine ice advances in the Skagit Valley between 30.3 and 19.5 cal ka BP, with an intervening period of glacial recession at about 24.9 cal ka BP. Given the general bedrock geology of the Spada Lake area east of the Lake Chaplain quadrangle, westerly alpine advance from the Spada Lake area would send Cascade provenance outwash to the Marsh Creek area, consistent with our new OSL ages of 29.8 to 32.4 ka from SP-provenance Olympia beds at site 37B by Marsh Creek. Although Evans Creek alpine advance has not been documented in the Skykomish Valley, the SP composition (Table 1) of the 29.8 to 32.4 ka sediments in a geographic position directly west of a large Cascade Range U-shaped alpine valley may provide the setting required for this discovery. For further assessment of this alpine-advance hypothesis see the USGS topographic map of the Wallace Lake quadrangle, and the general geology of the Olney Creek U-shaped valley, Lake Stickney cirque basin, and the Sultan basin (Tabor and others, 1993).

MONROE SYNCLINE

New geologic mapping of the Sultan, Monroe and Lake Chaplain 7.5-minute quadrangles reveals a major reverse fault in the lower Skykomish River valley that juxtaposes Eocene Mount Persis volcanic rocks with the Jurassic–Cretaceous Western mélange belt. We term this east-trending fault the Monroe fault and it is flanked by the Monroe anticline and syncline. The Monroe fault was likely an Eocene extensional fault that was later rejuvenated as a north-verging reverse fault driven by regional north-south compression (Dragovich and others, 2014). The Monroe syncline is a structural basin north of the Monroe fault and may have originally formed in the Eocene. In the Lake Chaplain quadrangle, the Monroe syncline appears to be a plunging fold cored by the Olympia beds, similar to the Monroe syncline in adjacent quadrangles to the southwest and west. SP-provenance sediment in the core of the Monroe synclinal basin north of the Skykomish River is at least 450 ft (137 m) thick where Dragovich and others (2013) obtained ages between 30 and 215 ka and >300 ka (OSL/IRSL data) in the Sultan quadrangle. The Holocene to Pleistocene stratigraphy and sedimentary provenance of the basin suggest Quaternary structural control of

sedimentation in the Skykomish valley over several nonglacial intervals. The basin likely formed as a result of flexural slip in the footwall of the Monroe fault system.

Stratigraphic relations indicate that the Skykomish River valley has been structurally-controlled since at least the middle Pleistocene (>300 ka; Dragovich and others, 2014). Olympia beds occupy the core of the synclinal axis at three prominent locations: (1) east of the Blue Mountain fault, in the southwest part of the Lake Chaplain quadrangle (Cross Section B); (2) west of the Sultan River fault in the northwestern corner of the Sultan quadrangle (Dragovich and others, 2013), and; (3) near the city of Monroe (Dragovich and others, 2011a,b). Olympia beds overlie Whidbey Formation SP deposits and older pre-Hamm Creek SP deposits in the southern part of the Lake Chaplain quadrangle (for example, Cross Section B), and in the Monroe quadrangle to the southwest. Olympia beds thus reside at an intermediate stratigraphic level relative to other nonglacial intervals or formations in the valley. The continuation of the Whidbey Formation (unit Qc_{ws}) across the Monroe syncline is supported by our new OSL age obtained directly south of the quadrangle. The stratigraphic position of the older pre-Hamm Creek SP deposits (unit Qc_{ph}) is indicated by an IRSL >300 ka age in the core of the Monroe syncline directly west of the Sultan River (south of the Lake Chaplain quadrangle). See unit Qc_{pf} in Cross Section A of the Sultan quadrangle, and unit Qc_{ph} in Cross Sections A and B below unit Qc_{ws} (this study). The geometry of the syncline is constrained by bedding in SP deposits towards the synclinal axis in the map area (southerly dips), and bedding orientations presented in the Monroe and Sultan maps (Dragovich and others, 2011a,b, 2013). The Monroe syncline is also observed in the gravity data from four quadrangles—including Lake Chaplain, which shows an elongate, east-trending gravity low. The lowest values coincide with the inferred location of the syncline axis (Fig. 14).

Our new mapping and geophysical data (Fig. M1) indicate that the synclinal axis is apparently offset horizontally by ~7,500 ft (~2,286 m) along strands of the CCFZ (this study, Dragovich and others, 2013). This apparent left-lateral offset is consistent with the strike-slip kinematics of the CCFZ determined from outcrop-scale structural data and earthquake focal mechanisms. Currently, we are unsure how much, if any, CCFZ displacement offsets the Olympia beds in the core of the syncline. It is possible that the river system followed the synclinal basin axis without substantial horizontal offset of the Olympia beds, although Dragovich and others (2013) document that one or more of the CCFZ segments are active or potentially active south of the current map area. In this scenario, either the general synclinal warping of the valley during the Olympia nonglacial interval, and (or) the north-northeast-trending CCFZ may have controlled fluvial deposition. Dragovich and others (2014) postulate that the Monroe fault and RMFZ—primarily a reverse fault and strike-slip fault, respectively—may partition the oblique slip of the SWIF.

THE EXPLORER FALLS BASIN

A fault-bounded graben structure in the northwest part of the Lake Chaplain quadrangle is here named the Explorer Falls basin. This basin preserves Tertiary sedimentary rocks (unit ΦEc) and a thick succession of Pleistocene nonglacial basin strata. Deformation of the basin after deposition of the Pleistocene basin fill—including tilting, uplift, and warping—has resulted in local basin inversion. The basin is bound by normal or oblique-slip faults that strike east-northeast. The most compelling evidence for the age and evolution of the basin are the thickness and stratigraphy of Pleistocene deposits, and their subsequent deformation within the fault zone. Quaternary deposits were first mapped by Booth (1990) as pre-Fraser Pleistocene sediment, but sedimentology and differences in provenance allow two distinct units to be mapped, a fluvial unit (Qc_{ph}) that contains SP provenance sediment of the ancient Pilchuck River (Cascade Range), and a locally derived alluvial fan unit (Qc_{phi}) that contains sediment derived from WMB sources. The weathering characteristics of these units, and an IRSL sample >500 ka, indicate an early to middle Pleistocene or older age (Appendix A). Our mapping and cross sections indicate that the fluvial SP-provenance deposits are restricted to the axis of the basin whereas the locally derived alluvial fans were shed from basin margins that seem to parallel the faults of the Explorer Falls basin. These two units—longitudinal fluvial deposits and transverse alluvial fans—are distinctly interbedded near the basin center. The thickness of these early to middle Pleistocene deposits (700–800 ft) compared to elsewhere in the region requires significant subsidence during this time interval. Taken together, we use these data to suggest that the Explorer Falls basin was active during the Pleistocene and controlled the deposition of these units. Subsequent tilting of these strata (~5–15° to the west), and their anomalously high elevation compared to regions of modern deposition, suggest that deformation of the Explorer Falls basin continued after the middle Pleistocene. This later episode of deformation appears to have ‘inverted’ the former basin and may reflect a change in the kinematics of the bounding faults. We speculate that the Explorer Falls basin may be part of a conjugate set of Tertiary normal faults (along with the Pilchuck River fault), but further study is warranted. Overall, the strong structural control on valley location during

the Pleistocene documented here adds to a growing list of structurally controlled river valleys in the area, including the Snoqualmie River (SWIF and RMFZ) and Skykomish River (Monroe fault and folds).

Finally, it is worth noting that in-progress mapping of the adjacent Lake Roesiger 7.5-minute quadrangle has directly supported the interpretation of the Explorer Falls basin presented here. Mapping in this quadrangle appears to confirm that: (1) deposits with Cascade Range provenance (unit Qc_{ph}) are confined to the basin and form ancient alluvial sequences at least 700 ft thick in some locations, (2) alluvial deposits with a local provenance (unit Qc_{phi}) occur in a mappable band along the east–northeast-striking basin-bounding faults on both the northern and southern sides of the basin, (3) Tertiary strata of unit ØEc are preserved only in the Explorer Falls basin and locally form the basement for units Qc_{ph} and unit Qc_{phi}, and (4) basin deposits are tilted or folded—and locally uplifted—to form an inverted basin similar to deposits in the Lake Chaplain quadrangle. Also noteworthy is the strong local provenance of unit Qc_{phi}—with as much as 80 to 90 percent distinctive meta-argillite clasts derived from the Western mélange belt. In total, mapping in both quadrangles indicates that the Explorer Falls basin is at least 5 mi wide and 9 mi long, and only the eastern end of the basin is exposed in the northwestern part of the Lake Chaplain quadrangle.

ACKNOWLEDGMENTS

This geologic map was funded in part by the U.S. Geological Survey (USGS) National Cooperative Geologic Mapping Program under award no. G13AC00173. We thank: Patrick Schreiner (Everett Water Filtration Plant) for help in the field and providing historical information; Maddie Jones (student, Colorado College) and George Kwok (Univ. of Wash.) for help in the field; Earl Calkins for granting access to Lake Bronson and neighboring trails; Lakeside Industries Inc. for access to the Lakeside quarry; Laureen Wagoner, Scott Boroughs, Rick Conrey, and Charles Knaack (all WSU) for geochemical analyses of samples and Harrison Gray (USGS) for preparation of luminescence samples; Jeff Jones (Snohomish County), and Sue Kahle and Theresa Olsen (USGS, Water Resources Division) for subsurface geologic information; Rowland Tabor (USGS emeritus) for field notes. We also thank our Washington Division of Geology and Earth Resources colleagues: Tim Walsh for a review; Tara Salzer for logistical support, Daniel Eungard for well data, and Patty Newman and Joseph Schilter for passive-seismic field support.

REFERENCES CITED

- Anderson, M. L.; Blakely, R. J.; Brocher, T. M.; Pratt, T. L.; Wells, R. E.; Haugerud, R.; Bush, M., 2006, Structure of the Seattle uplift from seismic, gravity, magnetic, geologic, and geomorphic data [abstract]: *Eos (American Geophysics Union Transactions)*, v. 87, no. 52, Supplement, T41A-1554.
- Anderson, M. L.; Blakely, R. J.; Wells, R. E.; Dragovich, J., 2011, Eastern boundary of the Siletz terrane in the Puget Lowland from gravity and magnetic modeling with implications for seismic hazard analysis [abstract]: *Eos (American Geophysical Union Transactions)*, Fall Meeting, Abstract GP33B-06. [<http://adsabs.harvard.edu/abs/2011AGUFMGP33B..06A>]
- Associated Earth Sciences, Inc., 2001, Proposed borrow pit dewatering impact analysis—Trilogy at Redmond Ridge, King County, Washington: Associated Earth Sciences, Inc., 1 v.
- Associated Earth Sciences, Inc., 2002, Final hydrogeologic and geotechnical assessment report—Pegasus Thoroughbred Training Center, King County, Washington: Associated Earth Sciences, Inc., 1 v.
- Associated Earth Sciences, Inc., 2003, Proposed Snoqualmie Ridge II project—Environmental impact statement—Technical report on geology, soils, and groundwater: Associated Earth Sciences, Inc., [Kirkland, Wash., under contract to] Quadrant Corporation, 1 v.
- Associated Earth Sciences, Inc., 2004, Environmental impact statement—Technical report on geology, soils and ground water, Redmond Ridge East UPD/FCC and Panhandle preliminary plat, King County, Washington: Associated Earth Sciences, Inc., 1 v.
- Associated Earth Sciences, Inc., 2007, Summary of SRS-1 No. 1 infiltration pond, general geologic hazard, and geotechnical engineering recommendations, recreation complex, Redmond Ridge East, King County, Washington: Associated Earth Sciences, Inc., 1 v.
- Bateman, M. D.; Swift, D. A.; Piotrowski, J. A.; Sanderson, D. C. W., 2012, Investigating the effects of glacial shearing of sediment on luminescence: *Quaternary Geochronology*, v. 10, p. 230-236. doi:10.1016/j.quageo.2011.11.012.
- Bhatia, M. R.; Crook, K. A. W., 1986, Trace element characteristics of graywackes and tectonic setting discrimination of sedimentary basins: *Contributions to Mineralogy and Petrology*, v. 92, no. 2, p. 181-193.
- Blakely, R. J.; Wells, R. E.; Weaver, C. S., 1999, Puget Sound aeromagnetic maps and data: U.S. Geological Survey Open-File Report 99-514, version 1.0. [<http://pubs.usgs.gov/of/1999/of99-514/>]

- Booth, D. B., 1984, Glacier dynamics and the development of glacial landforms in the eastern Puget Lowland, Washington: University of Washington Doctor of Philosophy thesis, 217 p., 1 plate. [<http://hdl.handle.net/1773/6696>]
- Booth, D. B., 1986, The formation of ice-marginal embankments into ice-dammed lakes in the eastern Puget Lowland, Washington, U.S.A., during the late Pleistocene: *Boreas*, v. 15, no. 3, p. 247-263.
- Booth, D. B., 1990, Surficial geologic map of the Skykomish and Snoqualmie Rivers area, Snohomish and King Counties, Washington: U.S. Geological Survey Miscellaneous Investigations Series Map I-1745, 2 sheets, scale 1:50,000, with 22 p. text. [<http://pubs.er.usgs.gov/publication/i1745>]
- Bradford, D. C.; Waters, A. C., 1934, The Tolt River earthquake and its bearing on the structure of the Cascade Range: *Seismological Society of America Bulletin*, v. 24, no. 1, p. 51-62.
- Broecker, W. S.; Kulp, J. L.; Tucek, C. S., 1956, Lamont natural radiocarbon measurements, III: *Science*, v. 124, no. 3213, p. 154-165.
- Brown, E. H., 2012, Obducted nappe sequence in the San Juan Islands–Northwest Cascades thrust system, Washington and British Columbia: *Canadian Journal of Earth Sciences* v. 49, no. 7, p. 796-817.
- Cann, J. R., 1970, Rb, Sr, Y, Zr, and Nb in some ocean floor basaltic rocks: *Earth and Planetary Science Letters*, v. 10, no. 1, p. 7-11.
- Capps, Gerald; Simmons, J. D.; Videgar, F. D., 1973, Geology of southern Snohomish County for land-use planning: Western Washington State College Department of Geology, 1 v.
- Colman, S. M.; Pierce, K. L., 1981, Weathering rinds on andesitic and basaltic stones as a Quaternary age indicator, western United States: U.S. Geological Survey Professional Paper 1210, 56 p. [<http://pubs.er.usgs.gov/publication/pp1210>]
- Danner, W. R., 1957, A stratigraphic reconnaissance in the northwestern Cascade mountains and San Juan Islands of Washington State: University of Washington Doctor of Philosophy thesis, 3 v. [562 p.], 7 plates.
- Dickinson, W. R., 1970, Interpreting detrital modes of graywacke and arkose: *Journal of Sedimentary Petrology*, v. 40, no. 2, p. 695-707.
- Dragovich, J. D., 2007, Sand point count and geochemical data in the Fall City and Carnation 7.5-minute quadrangles, King County, Washington: Washington Division of Geology and Earth Resources Open File Report 2007-3, 2 Microsoft Excel files and 6 p. text. [http://www.dnr.wa.gov/publications/ger_ofr2007-3_fallcity_supplement.zip]
- Dragovich, J. D.; Anderson, M. L.; MacDonald, J. H., Jr.; Mahan, S. A.; DuFrane, S. A.; Littke, H. A.; Wessel, G. R.; Saltonstall, J. H.; Koger, C. J.; Cakir, Recep, 2010a, Supplement to the geologic map of the Carnation 7.5-minute quadrangle, King County, Washington—Geochronologic, geochemical, point count, geophysical, earthquake, fault, and neotectonic data: Washington Division of Geology and Earth Resources Open File Report 2010-2, 42 p., 8 digital appendices. [http://www.dnr.wa.gov/publications/ger_ofr2010-2_carnation_supplement.zip]
- Dragovich, J. D.; Anderson, M. L.; Mahan, S. A.; Koger, C. J.; Saltonstall, J. H.; MacDonald, J. H., Jr.; Wessel, G. R.; Stoker, B. A.; Bethel, J. P.; Labadie, J. E.; Cakir, Recep; Bowman, J. D.; DuFrane, S. A., 2011a, Geologic map of the Monroe 7.5-minute quadrangle, King and Snohomish Counties, Washington: Washington Division of Geology and Earth Resources Open File Report 2011-1, 1 sheet, scale 1:24,000, with 24 p. text. [http://www.dnr.wa.gov/publications/ger_ofr2011-1_geol_map_monroe_24k.zip]
- Dragovich, J. D.; Anderson, M. L.; Mahan, S. A.; MacDonald, J. H., Jr.; McCabe, C. P.; Cakir, Recep; Stoker, B. A.; Villeneuve, N. M.; Smith, D. T.; Bethel, J. P., 2012, Geologic map of the Lake Joy 7.5-minute quadrangle, King County, Washington: Washington Division of Geology and Earth Resources Map Series 2012-01, 2 sheets, scale 1:24,000, with 79 p. text and 1 Excel file. [http://www.dnr.wa.gov/publications/ger_ms2012-01_geol_map_lake_joy_24k.zip]
- Dragovich, J. D.; Anderson, M. L.; Walsh, T. J.; Johnson, B. L.; Adams, T. L., 2007, Geologic map of the Fall City 7.5-minute quadrangle, King County, Washington: Washington Division of Geology and Earth Resources Geologic Map GM-67, 1 sheet, scale 1:24,000. [http://www.dnr.wa.gov/publications/ger_gm67_geol_map_fallcity_24k.zip]
- Dragovich, J. D.; Littke, H. A.; Anderson, M. L.; Hartog, Renate; Wessel, G. R.; DuFrane, S. A.; Walsh, T. J.; MacDonald, J. H., Jr.; Mangano, J. F.; Cakir, Recep, 2009a, Geologic map of the Snoqualmie 7.5-minute quadrangle, King County, Washington: Washington Division of Geology and Earth Resources Geologic Map GM-75, 2 sheets, scale 1:24,000. [http://www.dnr.wa.gov/publications/ger_gm75_snoqualmie_24k.zip]
- Dragovich, J. D.; Littke, H. A.; Anderson, M. L.; Wessel, G. R.; Koger, C. J.; Saltonstall, J. H.; MacDonald, J. H., Jr.; Mahan, S. A.; DuFrane, S. A., 2010b, Geologic map of the Carnation 7.5-minute quadrangle, King County, Washington: Washington Division of Geology and Earth Resources Open File Report 2010-1, 1 sheet, scale 1:24,000, with 21 p. text. [http://www.dnr.wa.gov/Publications/ger_ofr2010-1_geol_map_carnation_24k.zip]
- Dragovich, J. D.; Littke, H. A.; MacDonald, J. H., Jr.; DuFrane, S. A.; Anderson, M. L.; Wessel, G. R.; Hartog, Renate, 2009b, Geochemistry, geochronology, and sand point count data for the Snoqualmie 7.5-minute quadrangle, King County, Washington: Washington Division of Geology and Earth Resources Open File Report 2009-4, 35 p. text, with 3 Microsoft Excel files. [http://www.dnr.wa.gov/Publications/ger_ofr2009-4_snoqualmie_suppl.zip]

- Dragovich, J. D.; Littke, H. A.; Mahan, S. A.; Anderson, M. L.; MacDonald, J. H., Jr.; Cakir, Recep; Stoker, B. A.; Koger, C. J.; Bethel, J. P.; Dufrane, S. A.; Smith, D. T.; Villeneuve, N. M., 2013, Geologic map of the Sultan 7.5-minute quadrangle, King and Snohomish Counties, Washington: Washington Division of Geology and Earth Resources Map Series 2013-01, 1 sheet, scale 1:24,000, with 52 p. text. [http://www.dnr.wa.gov/publications/ger_ms2013-01_geol_map_sultan_24k.zip]
- Dragovich, J. D.; Logan, R. L.; Schasse, H. W.; Walsh, T. J.; Lingley, W. S., Jr.; Norman, D. K.; Gerstel, W. J.; Lapen, T. J.; Schuster, J. E.; Meyers, K. D., 2002, Geologic map of Washington—Northwest quadrant: Washington Division of Geology and Earth Resources Geologic Map GM-50, 3 sheets, scale 1:250,000, with 72 p. text. [http://www.dnr.wa.gov/publications/ger_gm50_geol_map_nw_wa_250k.pdf]
- Dragovich, J. D.; Mahan, S. A.; Anderson, M.; Macdonald, J. H., Jr.; Frattali, C.; Littke, H. A.; Stoker, H. A.; Koger, C. J.; Smith, D. T.; Dufrane, S. A., 2014, The Monroe fault, anticline, and synclinal basin—A potentially active fault and fold system in the Skykomish River Valley, Snohomish County, Washington: Geological Society of America Abstracts with Programs, v. 46, no. 6, p. 779.
- Dragovich, J. D.; Mahan, S. A.; Anderson, M. L.; MacDonald, J. H., Jr.; Wessel, G. R.; DuFrane, S. A.; Cakir, Recep; Bowman, J. D.; Littke, H. A., 2011b, Analytical data from the Monroe 7.5-minute quadrangle, King and Snohomish Counties, Washington—Supplement to Open File Report 2011-1: Washington Division of Geology and Earth Resources Open File Report 2011-2, 58 p., 2 plates, 2 Microsoft Excel files. [http://www.dnr.wa.gov/publications/ger_ofr2011-2_monroe_supplement.zip]
- Dragovich, J. D.; Walsh, T. J.; Anderson, M. L.; Hartog, Renate; DuFrane, S. A.; Vervoot, Jeff; Williams, S. A.; Cakir, Recep; Stanton, K. D.; Wolff, F. E.; Norman, D. K.; Czajkowski, J. L., 2009c, Geologic map of the North Bend 7.5-minute quadrangle, King County, Washington, with a discussion of major faults, folds, and basins in the map area: Washington Division of Geology and Earth Resources Geologic Map GM-73, 1 sheet, scale 1:24,000. [http://www.dnr.wa.gov/publications/ger_gm73_geol_map_northbend_24k.zip]
- Evans, J. E.; Ristow, R. J., Jr., 1994, Depositional history of the southeastern outcrop belt of the Chuckanut Formation—Implications for the Darrington–Devil’s Mountain and Straight Creek fault zones, Washington (U.S.A.): Canadian Journal of Earth Sciences, v. 31, no. 12, p. 1727-1743.
- Frizzell, V. A., Jr.; Tabor, R. W.; Zartman, R. E.; Blome, C. D., 1987, Late Mesozoic or early Tertiary mélanges in the western Cascades of Washington. In Schuster, J. E., editor, Selected papers on the geology of Washington: Washington Division of Geology and Earth Resources Bulletin 77, p. 129-148. [http://www.dnr.wa.gov/Publications/ger_b77_papers_on_wa_geology_pt2of3.pdf]
- Frost, B. R.; Barnes, C. G.; Collins, W. J.; Arculus, R. J.; Ellis, D. J.; Frost, C. D., 2001, A geochemical classification for granitic rocks: Journal of Petrology, v. 42, no. 11, p. 2033-2048.
- Fuller, R. E., 1925, The geology of the northeastern part of Cedar Lake quadrangle with special reference to the de-roofed Snoqualmie batholith: University of Washington Master of Science thesis, 96 p., 4 plates.
- Harland, W. B.; Cox, A. V.; Llewellyn, P. G.; Pickton, C. A. G.; Smith, A. G.; Walters, R., 1982, A geologic time scale: Cambridge University Press, 131 p.
- Hayashi, K.; Cakir, R.; Dragovich, J. D.; Stoker, B. A.; Walsh, T. J.; Littke, H. A., 2013, Passive seismic analyses in the Sultan 7.5-minute quadrangle, King and Snohomish Counties, Washington: Washington Division of Geology and Earth Resources Open File Report 2013-04, 9 p. [http://www.dnr.wa.gov/publications/ger_ofr2013-04_seismic_analysis_sultan_quad.pdf]
- Jett, G. A., 1986, Sedimentary petrology of the western mélange belt, north Cascade Range, Washington: University of Wyoming Master of Science thesis, 85 p.
- Jett, G. A.; Heller, P. L., 1988, Tectonic significance of polymodal compositions in mélange sandstones, western mélange belt, north Cascade Range, Washington: Journal of Sedimentary Petrology, v. 58, no. 1, p. 52-61.
- Johnson, D. M.; Hooper, P. R.; Conrey, R. M., 1999, XRF analysis of rocks and minerals for major and trace elements on a single low dilution Li-tetraborate fused bead: Advances in X-ray Analysis, v. 41, p. 843-867. [http://www.sees.wsu.edu/Geolab/note/V41_91.pdf]
- Knaack, C.; Cornelius, S.; Hooper, P., 1994, Trace element analysis of rocks and minerals by ICP/MS: Department of Geology Washington State University Open-file Report, December 1994, 18 p.
- Knoll, K. M., 1967, Surficial geology of the Tolt River area, Washington: University of Washington Master of Science thesis, 91 p., 1 plate.
- Le Maitre, R. W.; Streckeisen, A.; Zanettin, B.; Le Bas, M. J.; Bonin, B.; Bateman, P., eds., 2002, Igneous rocks—A classification and glossary of terms; 2nd ed.: Cambridge University Press, Cambridge, U.K., 256 p.
- Lees, J. M., 1999, Geotouch—Software for three and four-dimensional GIS in the earth sciences: Computers & Geosciences, v. 26, no. 7, p. 751-761.
- Lees, J. M., 2007, RFOC—Graphics for spherical distributions and earthquake focal mechanisms, graphics for statistics on a sphere, as applied to geological fault data, crystallography, earthquake focal mechanisms, radiation patterns, ternary plots and geographical/geological maps: Comprehensive R Archive Network (CRAN). [accessed May 31, 2011, at <http://streaming.stat.iastate.edu/CRAN/web/packages/RFOC/index.html>].

- Lees, J. M., 2008, GEOMap—Topographic and geologic mapping: Comprehensive R Archive Network (CRAN) [accessed May 31, 2011, at <http://streaming.stat.iastate.edu/CRAN/web/packages/GEOMap/index.html>].
- Littke, H. A.; Dragovich, J. D.; Anderson, Megan; Hartog, Renate; Wessel, G. R.; DuFrane, S. A.; Walsh, T. J.; MacDonald, J. H., Jr.; Cakir, Recep, 2009, Geologic map of the Snoqualmie 7.5-minute quadrangle, King County, Washington—Active faulting, basin inversion and Miocene volcanic extrusion of the Snoqualmie batholith along the Rattlesnake Mountain fault zone [abstract]: Geological Society of America Abstracts with Programs, v. 41, no. 7, p. 457.
- Lovseth, T. P., 1975, The Devils Mountain fault zone, northwestern Washington: University of Washington Master of Science thesis, 29 p.
- MacDonald, J. H., Jr.; Miller, R. B.; Dragovich, J. D.; Metzger, E. P.; Miller, J. S.; Harper, G. D., 2009, Geology and geochemistry of the De Roux unit and possibly correlative tectonostratigraphic terranes within the Cascade mountains, Washington: Geological Society of America Abstracts with Programs, v. 41, no. 7, p. 518.
- MacDonald, J. H., Jr.; Dragovich, J. D.; Frattali, C. L.; Anderson, M.; Stoker, B. A.; Littke, H. A.; Dufrane, S. A.; Sauer, K.; Smith, D. T.; Koger, C. J., 2014, Geochemistry and metaigneous rocks from the western mélange belt, Lake Chaplain, Snoqualmie, and Sultan 7.5-minute quadrangles, western Cascades, Washington: Evidence for a predominantly volcanic arc setting: Geological Society of America, Abstracts with Programs, v. 46, no. 6, p. 363.
- Mackin, J. H., 1941, Glacial geology of the Snoqualmie—Cedar area, Washington: Journal of Geology, v. 49, no. 5, p. 449-481.
- McDonough, W. F.; Sun, S. S., 1995, The composition of the Earth: Chemical Geology, v. 120, issue 3-4 p. 223-253.
- McLennan, S. M.; Taylor, S. R.; McCulloch M. T.; Maynard, J. B., 1990, Geochemical and Nd-Sr isotopic composition of deep-sea turbidites—Crustal evolution and plate tectonic associations: Geochimica et Cosmochimica Acta, v. 54, p. 2015-2050.
- Miller, R. B., 1985, The ophiolitic Ingalls Complex, north-central Cascades Mountains, Washington: Geological Society of America Bulletin, v. 96, no. 1, p. 27-42.
- Miller, R. B., 1989, The Mesozoic Rimrock Lake inlier, southern Washington Cascades—Implications for the basement to the Columbia Embayment: Geological Society of America Bulletin, v. 101, no. 10, p. 1289-1305.
- Minard, J. P., 1981, Distribution and description of the geologic units in the Maltby quadrangle, Washington: U.S. Geological Survey Open-File Report 81-100, 4 p., 1 plate, scale 1:24,000.
- Morrison, R. B., ed., 1991, Quaternary nonglacial geology—Conterminous U.S.: Geological Society of America DNAG Geology of North America, v. K-2, 672 p., 8 plates in accompanying case.
- Pearce, J. A., 1982, Trace element characteristics of lavas from destructive plate boundaries. In Thorpe, R. S., ed., Andesites—Orogenic andesites and related rocks: John Wiley & Sons [Chichester, U.K.], p. 525-548.
- Pearce, J. A., 1996, A user's guide to basalt discrimination diagrams. In Wyman, D. A., ed., Trace element geochemistry of volcanic rocks—Applications for massive sulphide exploration: Geological Association of Canada Short Course Notes, v. 12, p. 79-113.
- Pearce, J. A. 2008, Geochemical fingerprinting of oceanic basalts with applications to ophiolite classification and the search for Archean oceanic crust: Lithos, v. 100, no. 1-4, p. 14-48.
- Pearce, J.A.; Harris, N.B.W.; Tindle, A.G., 1984, Trace element discrimination diagrams for the tectonic interpretation of granitic rocks: Journal of Petrology, v. 25, issue 4, p. 956-983.
- Pessl, Fred, Jr.; Dethier, D. P.; Booth, D. B.; Minard, J. P., 1989, Surficial geologic map of the Port Townsend 30- by 60-minute quadrangle, Puget Sound region, Washington: U.S. Geological Survey Miscellaneous Investigations Series Map I-1198-F, 1 sheet, scale 1:100,000, 13 p. text. [http://ngmdb.usgs.gov/Prodesc/proddesc_9029.htm]
- Pettijohn, F. J., 1957, Sedimentary rocks; 2nd ed.: Harper & Row, 718 p.
- Porter, S. C.; Swanson, T. W., 1998, Radiocarbon age constraints on rates of advance and retreat of the Puget lobe of the Cordilleran ice sheet during the last glaciation: Quaternary Research, v. 50, no. 3, p. 205-213.
- Prescott, J. R.; Hutton, J. T., 1994, Cosmic ray contributions to dose rates for luminescence and ESR dating—Large depths and long-term time variations: Radiation Measurements, v. 23, p. 497-500.
- Riedel, J. L.; Clague, J. J.; Ward, B. C., 2010, Timing and extent of early marine oxygen isotope stage 2 alpine glaciation in Skagit Valley, Washington: Quaternary Research, v. 73, no. 2, p. 313-323.
- Rigg, G. B., 1958, Peat resources of Washington: Washington Division of Mines and Geology Bulletin 44, 272 p. [http://www.dnr.wa.gov/publications/ger_b44_peat_reasources_wa_1.pdf; http://www.dnr.wa.gov/publications/ger_b44_peat_reasources_wa_2.pdf; http://www.dnr.wa.gov/publications/ger_b44_peat_reasources_wa_3.pdf]
- Roser, B. P.; Korsch, R. J., 1988, Provenance signatures of sandstone-mudstone suites determined using discriminant function analysis of major-element data: Chemical Geology, v. 67, no. 1-2 p. 119-139.
- Sarikhan, I. Y.; Pringle, P. T., 2005, Landslide hazard zonation project—Mass wasting assessment—Sultan River watershed: Washington Department of Natural Resources, Forest Practices Division, 22 p., 2 plates, scale 1:24,000. [http://www.dnr.wa.gov/BusinessPermits/Topics/LandslideHazardZonation/Pages/fp_lhz_completed.aspx]

- Sarikhan, I. Y.; Vaugeois, L. M., 2007, Landslide hazard zonation mapping—Quantification of landslide response to severe storms and forest management in the Sultan basin, Washington. In Schaefer, V. R.; Schuster, R. L.; Turner, A. K., editors, 1st North American Landslide Conference—Conference presentations: Association of Engineering Geologists AEG Special Publication 23, p. 558-568.
- Sauer, K.; Dragovich, J. D.; Macdonald, J. H., Jr.; Frattali, C.; Anderson, M.; Dufrane, S. A.; Gordon, S. M., 2014, Tectonic implications of detrital zircon geochronology and neodymium isotopes of the arkosic petrofacies of the western mélange belt, Lake Chaplain quadrangle, western Cascades, Washington: Geological Society of America Abstracts with Programs, v. 46, no. 6, p. 363.
- Sherrod, B. L.; Blakely, R. J.; Weaver, C. S.; Kelsey, H. M.; Barnett, Elizabeth; Liberty, Lee; Meagher, K. L.; Pape, Kristin, 2008, Finding concealed active faults—Extending the southern Whidbey Island fault across the Puget Lowland, Washington: Journal of Geophysical Research, v. 113. [B05313, doi:10.1029/2007JB005060, 2008]
- Singarayer, J. S.; Bailey, R. M., 2003, Further investigations of the quartz optically stimulated luminescence components using linear modulation: Radiation Measurements, v. 37, p. 451-458.
- Tabor, R. W., 1994, Late Mesozoic and possible early Tertiary accretion in western Washington State—The Helena–Haystack mélange and the Darrington–Devils Mountain fault zone: Geological Society of America Bulletin, v. 106, no. 2, p. 217-232.
- Tabor, R. W.; Booth, D. B.; Vance, J. A.; Ford, A. B., 2002, Geologic map of the Sauk River 30- by 60-minute quadrangle, Washington: U.S. Geological Survey Geologic Investigations Series Map I-2592, 2 sheets, scale 1:100,000, with 67 p. text. [<http://pubs.er.usgs.gov/usgspubs/i/i2592>]
- Tabor, R. W.; Frizzell, V. A., Jr.; Booth, D. B.; Waitt, R. B., 2000, Geologic map of the Snoqualmie Pass 30 x 60 minute quadrangle, Washington: U.S. Geological Survey Geologic Investigations Series Map I-2538, 1 sheet, scale 1:100,000, 57 p. text. [<http://geopubs.wr.usgs.gov/i-map/i2538/>]
- Tabor, R. W.; Frizzell, V. A., Jr.; Booth, D. B.; Waitt, R. B.; Whetten, J. T.; Zartman, R. E., 1993, Geologic map of the Skykomish River 30- by 60-minute quadrangle, Washington: U.S. Geological Survey Miscellaneous Investigations Series Map I-1963, 1 sheet, scale 1:100,000, 42 p. text. [<http://pubs.usgs.gov/imap/i1963/>]
- Troost, K. G.; Booth, D. B.; Wisher, A. P.; Shimel, S. A., 2005, The geologic map of Seattle—A progress report: U.S. Geological Survey Open-File Report 2005-1252, version 1.0, 1 sheet, scale 1:24,000. [<http://pubs.usgs.gov/of/2005/1252/>]
- U.S. Geological Survey Geologic Names Committee, 2010, Divisions of geologic time—Major chronostratigraphic and geochronologic units: U.S. Geological Survey Fact Sheet 2010-3059, 2 p. [<http://pubs.usgs.gov/fs/2010/3059/>]
- Vance, J. A.; Dungan, M. A.; Blanchard, D. P.; Rhodes, J. M., 1980, Tectonic setting and trace element geochemistry of Mesozoic ophiolitic rocks in western Washington: American Journal of Science, v. 280-A, p. 359-388.
- Varnes, D. J., 1978a, repr. 1995, Landslide classification system. In Dragovich, J. D.; Brunengo, M. J., Landslide map and inventory, Tilton River–Mineral Creek area, Lewis County, Washington: Washington Division of Geology and Earth Resources Open File Report 95-1, 165 p., Plate 3. [http://www.dnr.wa.gov/publications/ger_ofr95-1_lewis_co_landslides_plates.pdf; http://www.dnr.wa.gov/publications/ger_ofr95-1_lewis_co_landslides_text.pdf]
- Varnes, D. J., 1978b, Slope movement types and processes. In Schuster, R. L.; Krizek, R. J., eds., Landslides—Analysis and control: National Academy of Sciences Transportation Research Board Special Report 176, p. 11-33, 1 plate.
- Wells, R. E.; Blakely, R. J.; Weaver, C. S., 1998, Tectonics and earthquake potential of Cascadia—Effects of rotation and northward transport of fore-arc crustal blocks in Oregon and Washington [abstract]: Eos (American Geophysical Union Transactions), v. 79, no. 24, Supplement, p. W115.
- Whetten, J. T.; Carroll, P. R.; Gower, H. D.; Brown, E. H.; Pessl, Fred, Jr., 1988, Bedrock geologic map of the Port Townsend quadrangle, Washington: U.S. Geological Survey Miscellaneous Investigations Series Map I-1988-G, scale 1:100,000. [http://ngmdb.usgs.gov/Prodesc/proddesc_9030.htm]
- Wolfe, J. A.; Forest, C. E.; Molnar, Peter, 1998, Paleobotanical evidence of Eocene and Oligocene paleoaltitudes in midlatitude western North America: Geological Society of America Bulletin, v. 110, no. 5, p. 664-678.
- Wood, D. A., 1980, The application of a Th–Hf–Ta diagram to problems of tectonomagmatic classification and to establishing the nature of crustal contamination of basaltic lavas of the British Tertiary volcanic province: Earth and Planetary Science Letters v. 50, no. 1, p. 11–30.
- Yeats, R. S.; Engels, J. C., 1971, Potassium-argon ages of plutons in the Skykomish–Stillaguamish areas, North Cascades, Washington: U.S. Geological Survey Professional Paper 750-D, p. D34-D38. [<http://pubs.er.usgs.gov/publication/pp750D>]

Appendix A. Infrared and Optically Stimulated Luminescence Age Data

Sample ID (geologic unit)	Water content (%) ^a	K (%) ^b	U (ppm) ^b	Th (ppm) ^b	Cosmic dose ^c (Gy/ka)	Total dose rate (Gy/ka)	Equivalent dose (Gy)	N ^d	Age (ka) ^e
38A (unit Q _{CWS})	20 (37)	1.24 ±0.02	1.91 ±0.09	4.54 ±0.22	0.12 ±0.01	1.75 ±0.05 2.52 ±0.07 ^f	132 ±1.72 202 ±16.9 ^f	21 (30) —	75.4 ±2.3 80.4 ±7.0 ^f

A 15-ft-high road cut along an abandoned domestic access road in the northern part of the Sultan 7.5-minute quadrangle ~2,700 ft (823 m) directly south of the present study area. The sand is distinctly liquefied with rootless overturned folds and flame structures (Fig. 7). Ancient Skykomish SP provenance well-sorted sand with angular to subangular fine sand grains dominated by monocrystalline quartz, plagioclase, hornblende, pyroxenes and mica. K-spar content ~10% and substantial mica in this overbank sand facies. Significant opaque mineral content observed at this location (unit Q_{CWS}). See site 17A in Appendix D for geochemical analyses. Latitude and longitude of site are 47.866912°, -121.804463°; elevation = 300 ft (91 m).

^a Field moisture, with Figures in parentheses indicating the complete sample saturation %. Ages calculated using approximately 60% of saturation values.

^b Analyses obtained using high-resolution gamma spectrometry (HPGe detector).

^c Cosmic doses and attenuation with depth were calculated using the methods of Prescott and Hutton (1994). See text for details.

^d Number of replicated equivalent dose (De) estimates used to calculate the equivalent dose. Figures in parentheses indicate total number of measurements included in calculating the represented equivalent dose and age using the minimum age model (MAM). All aliquots passed methodology tests but there was large dispersion between analyses.

^e Dose rate and age for fine-grained 250–180 micron sized quartz. Exponential + linear fit used on single aliquot regeneration equivalent doses; errors to one sigma; ages and errors rounded.











^f Feldspar from fine-grains of 4–11 micron polymineral silt. Exponential fit used for multiple aliquot additive doses. Errors to one sigma. Fade tests indicate ~2 g/decade correction.

Appendix B. Seismicity in and near the Lake Chaplain 7.5-minute Quadrangle

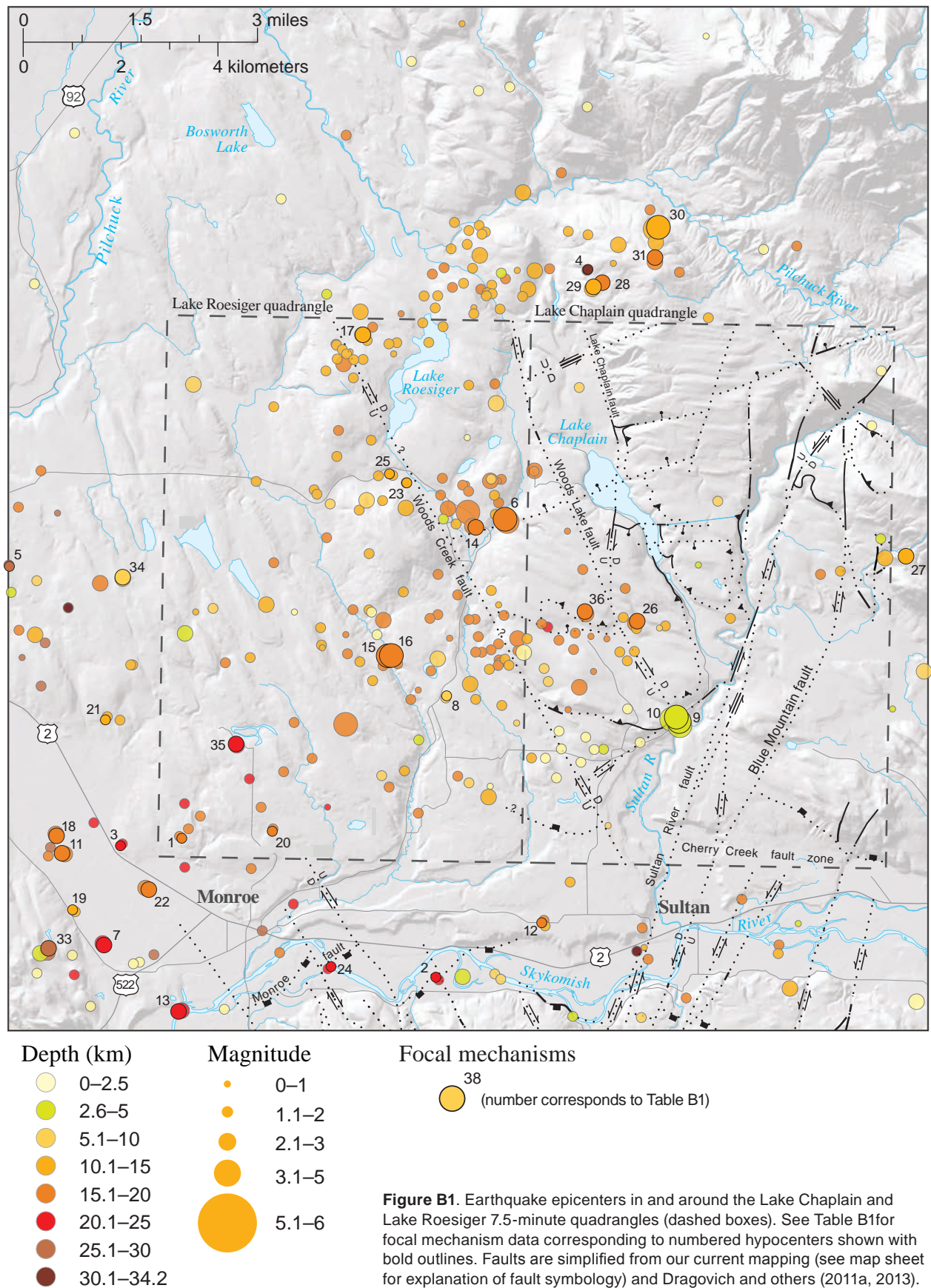
Recorded earthquake epicenters obtained from the Pacific Northwest Seismic Network (PNSN) (<http://www.pnsn.org>) in and around the Lake Chaplain and Lake Roesiger quadrangles provide a sense of fault movement at depth. This broader study area (Fig. B1) encompasses 324 epicenters and 35 focal mechanisms. Hypocenter depths are less than 25 mi (40 km) and are interpreted as crustal events. The focal-mechanism stereonets are shown as icons in Table B1 and were prepared using the RFOC package of Lees (1999, 2007, and 2008). These stereonets provide information on the geometry of the earthquake-generating fault, including the potential fault plane solutions. Each focal mechanism provides two potential fault plane solutions.

There are substantially fewer earthquakes associated with the Cherry Creek fault zone (CCFZ) in the present Lake Chaplain quadrangle study area than in previously mapped quadrangles to the south. Noteworthy exceptions are earthquakes associated with focal mechanisms FM9 and FM10 (Table B1) near the Sultan River fault that may be located along that structure. The 1996 Duvall earthquake ($M_l = 5.3$ or $M_d = 5.4$, local and duration magnitudes, respectively, <http://www.pnsn.org/event/10389973>) occurred as a mainshock and its aftershock sequence was roughly centered on the intersection of the Lake Joy, Monroe, Carnation, and Sultan quadrangles within the CCFZ, with most hypocenters originating at a shallow depth (1.2–5 mi [2–8 km]). See Dragovich and others (2010a,b, 2011a,b, 2012, 2013) for further information, including detailed mapping of the Duvall earthquake epicenters that yielded strong structural and spatial correlations between the kinematics of the northeast-trending, left-lateral CCFZ and the earthquake focal mechanisms. The informally named Woods Creek fault in the southwest part of the map area is tentatively projected to the northwest on Figure B1. This lineament is also spatially associated with clusters or linear arrays of earthquakes and suggests active tectonism along a fault. Finally, we speculate that some generally east-west striking reverse fault focal mechanisms on Table B1 might be related to active rejuvenation of Cretaceous accretionary faults common in the Western mélangé belt (for example, FM_27).

Table B1. Earthquake focal mechanisms in the Lake Chaplain and surrounding area. This table provides the focal mechanism ID number, the strike, dip, and rake for both of the focal mechanism solutions' nodal planes. Reported focal mechanisms are labeled with the focal mechanism ID number on Figure B1. The earthquake identification number gives the date (yr/month) and time (day, hr., decimal second) in sequential order without spaces; it is a unique identifier to link its original data reported on the PNSN I website (<http://www.pnsn.org>). See Figure B1 for earthquake locations.

Focal mechanism ID no.	Lat. & long. (decimal degrees)	Strike (°) 1	Dip (°) 1	Rake (°) 1	Strike (°) 2	Dip (°) 2	Rake (°) 2	Preferred fault type	Focal mechanism illustration	Earthquake ID no.; depth (km); magnitude	Location (quadrangle)
FM_1	47.8790 -121.9930	50	25	150	168	78	68	reverse-oblique strike-slip		60432732; 17.76; 1.1	Lake Roesiger
FM_2	47.8480 -121.9050	120	40	50	348	61	118	oblique reverse		60434667; 23.07; 1.5	Monroe
FM_3	47.8770 -122.0140	180	40	140	303	66	57	reverse-oblique strike-slip		60434917; 21.59; 1.2	Snohomish
FM_4	48.0120 -121.8570	330	20	50	192	75	103	oblique reverse		60458026; 66.61; 1.6	Verlot
FM_5	47.9410 -122.0540	40	65	-80	197	27	-110	normal		60517947; 27.80; 1.6	Snohomish
FM_6	47.9540 -121.8840	0	80	70	244	22	152	oblique reverse		10858833; 17.84; 3.3	Lake Roesiger
FM_7	47.8540 -122.0190	5	90	-20	95	70	180	normal-oblique strike-slip		10840748; 24.70; 2.5	Maltby
FM_8	47.9130 -121.9030	70	70	110	203	28	47	oblique reverse		10846918; 5.98; 1.8	Lake Roesiger
FM_9	47.9080 -121.8230	15	60	50	254	48	138	oblique reverse		10088068; 4.40; 3.8	Lake Chaplain
FM_10	47.9090 -121.8240	90	90	-40	180	50	180	normal-oblique strike-slip		10088198; 3.15; 3.5	Lake Chaplain

Focal mechanism ID no.	Lat. & long. (decimal degrees)	Strike (°) 1	Dip (°) 1	Rake (°) 1	Strike (°) 2	Dip (°) 2	Rake (°) 2	Preferred fault type	Focal mechanism illustration	Earthquake ID no.; depth (km); magnitude	Location (quadrangle)
FM_11	47.8750 -122.0340	60	15	140	189	80	78	reverse- oblique strike-slip		10179728; 17.37; 2.2	Maltby
FM_12	47.8610 -121.8690	165	45	110	318	48	71	oblique reverse		10214853; 18.54; 2.0	Sultan
FM_13	47.8390 -121.9930	25	35	110	181	57	77	oblique reverse		10226628; 24.06; 2.3	Monroe
FM_14	47.9520 -121.8940	50	45	100	216	46	80	reverse		10245558; 17.83; 2.6	Lake Roesiger
FM_16	47.9220 -121.9230	15	55	40	259	58	137	reverse- oblique strike-slip		10254553; 16.34; 3.4	Lake Roesiger
FM_17	47.9960 -121.9340	25	35	90	205	55	90	reverse		10280373; 11.50; 2.2	Lake Roesiger
FM_18	47.8790 -122.0360	80	55	90	260	35	90	reverse		10294663; 18.81; 2.5	Snohomish
FM_19	47.8620 -122.0300	100	50	130	227	54	52	oblique reverse		10304783; 14.04; 1.3	Maltby
FM_20	47.8810 -121.9620	195	80	150	291	61	12	reverse- oblique strike-slip		10337608; 17.01; 1.8	Lake Roesiger
FM_21	47.9060 -122.0200	155	50	90	335	40	90	reverse		10337923; 13.83; 1.8	Snohomish
FM_22	47.8670 -122.0040	5	40	100	172	51	82	reverse		10485948; 19.72; 2.5	Maltby
FM_23	47.9620 -121.9180	135	20	-160	26	83	-71	normal-oblique strike-slip		10518933; 11.22; 1.9	Lake Roesiger
FM_24	47.8500 -121.9410	65	55	-120	290	45	-55	oblique normal		10540763; 24.45; 1.9	Monroe
FM_25	47.9640 -121.9240	290	65	-130	173	46	-36	oblique normal		10536458; 11.10; 1.9	Lake Roesiger
FM_26	47.9310 -121.8380	105	25	80	296	65	95	reverse		10587458; 15.68; 2.4	Lake Chaplain
FM_27	47.9470 -121.7460	95	50	100	260	41	79	reverse		10587608; 11.58; 2.3	Wallace Lake
FM_28	48.0090 -121.8520	50	85	100	166	11	26	reverse		10621193; 17.11; 2.3	Verlot
FM_29	48.0080 -121.8550	175	40	110	330	53	74	oblique reverse		10646943; 13.06; 2.7	Verlot
FM_30	48.0220 -121.8330	0	65	120	126	38	43	oblique reverse		10647093; 13.57; 3.5	Verlot
FM_31	48.0150 -121.8340	130	50	50	3	54	128	oblique reverse		10662698; 17.00; 2.6	Verlot
FM_32	47.9000 -122.0600	105	55	140	221	58	43	reverse- oblique strike-slip		10684883; 26.00; 1.8	Snohomish
FM_33	47.8530 -122.0380	65	50	90	245	40	90	reverse		10698348; 26.02; 2.5	Maltby
FM_34	47.9390 -122.0150	55	60	80	254	31	106	reverse		10785083; 8.45; 2.2	Snohomish
FM_35	47.9010 -121.9750	50	45	100	216	46	80	reverse		10793748; 22.71; 2.5	Lake Roesiger
FM_36	47.9330 -121.8560	55	40	90	235	50	90	reverse		10813778; 19.90; 2.4	Lake Chaplain



Appendix C. U-Pb Detrital Zircon Geochronology

Sand Sample 37A

We obtained detrital zircon U-Pb age data from nonglacial sand from the southwestern part of the map area at age site 37A (map sheet). See unit Qc₀ for the outcrop and petrographic description of this SP sand sample (Table 1) from the deposits of the Olympia nonglacial interval, ancient Skykomish River facies (Olympia beds). See *Pleistocene Alluvium* where the local and regional significance of the age distribution of this sample is further discussed. In that discussion, we highlight the agreement between (1) the age distribution of the zircons of this sample, (2) Cascade or SP provenance of this sample, (3) other age information in and around the Monroe syncline, and (4) geochemistry of this sample and other SP sediments. See Appendix A for the 40.5 and 48.3 ka OSL and IRSL ages for sample 37A. See sample 30U in Appendix D for the geochemistry of sand at this age site. Table C1 presents basic age information for the 158 zircons analyzed. Figure C1 provides the age-distribution plots and concordia chart for the sand sample. Note the age peaks at ~34 and 90 Ma. Table C2 gives the area percentage of major geologic units in the Skykomish River basin and documents the strong correlation between the major geologic units of the basin, such as Oligocene and mid-Cretaceous intrusive rocks, and the age spectrum of the sand zircon grains in the sample. It is noteworthy that neither the Olympia nonglacial interval age of the sample nor most of the zircon peaks are consistent with a glacial provenance (see Table 1). The detrital zircons were transported to the sample site by ancient rivers during the Olympia nonglacial interval (20–60 ka) and deposited 40.5 to 48.3 ka as indicated by the IRSL and OSL samples from site 37A (Appendix A). Important in this general analysis is the observation that some units are zircon rich (for example, felsic igneous rocks) whereas some units are zircon poor (for example, many sedimentary or metasedimentary rock types).

Table C1. Sample 37A U-Pb zircon data from Olympia beds (unit Qc₀) in the Lake Chaplain 7.5-minute quadrangle. We obtained U-Pb age information for 158 zircons from a well-sorted sand deposit. Out of 170 analyzed grains, 12 analyses (not shown) were rejected because of insufficient count rates, a high common Pb component, apparent ablation of subsurface inclusions, or the grain apparently not being zircon. cps, counts per second.

Zircon Grain No.	²⁰⁶ Pb (cps)	²⁰⁴ (Pb +Hg) (cps)	²³⁸ U/ ²⁰⁶ Pb	2σ	²⁰⁷ Pb/ ²⁰⁶ Pb	2σ	²⁰⁶ Pb/ ²³⁸ U age (Ma)	2σ error (Ma)
1	35653	375	194.2	6.0	0.046	0.001	33	1
2	6408	337	199.0	5.9	0.044	0.002	32	1
3	109919	320	68.9	2.0	0.048	0.000	93	3
4	15192	296	189.5	4.9	0.047	0.001	34	1
5	10646	286	193.2	5.2	0.044	0.001	33	1
6	43892	287	65.3	1.8	0.049	0.001	98	3
7	23045	270	66.9	1.8	0.048	0.001	96	3
8	25495	269	65.4	1.8	0.049	0.001	98	3
9	131856	266	60.8	1.7	0.049	0.000	105	3
10	9353	255	195.0	5.2	0.049	0.001	33	1
11	18746	236	71.8	2.0	0.048	0.001	89	2
12	26746	233	69.0	2.6	0.048	0.001	93	3
13	610283	246	68.9	1.8	0.049	0.000	93	2
14	8839	245	189.6	7.0	0.051	0.001	34	1
15	225009	220	71.3	2.0	0.049	0.000	90	3
16	51321	229	86.1	2.3	0.049	0.001	74	2
17	25989	207	176.9	4.7	0.046	0.001	36	1
18	31428	215	190.7	5.4	0.047	0.001	34	1
19	5006	211	282.8	8.5	0.045	0.002	23	1
20	17345	205	191.8	5.8	0.050	0.001	34	1
21	27423	165	190.0	5.5	0.050	0.001	34	1
22	13402	170	192.3	6.4	0.052	0.001	33	1
24	75920	198	66.9	2.0	0.050	0.001	96	3
25	11545	233	192.5	5.9	0.055	0.003	33	1
26	18494	207	176.0	4.9	0.058	0.003	37	1
55	20466	239	71.1	2.0	0.051	0.001	90	3
27	39031	228	236.8	6.5	0.049	0.001	27	1
28	4553	249	187.4	5.1	0.062	0.003	34	1
29	42226	236	64.7	2.7	0.054	0.003	99	4
30	4517	220	189.0	5.8	0.059	0.002	34	1
31	5297	219	212.7	7.8	0.057	0.003	30	1
32	8867	233	57.7	2.1	0.056	0.001	111	4
33	5389	247	177.4	5.3	0.057	0.002	36	1
34	61287	256	79.7	2.1	0.050	0.001	80	2
36	6744	250	189.3	6.6	0.059	0.002	34	1
38	13860	222	192.1	5.1	0.054	0.001	33	1
39	27887	212	190.7	5.9	0.050	0.001	34	1
40	7369	225	187.0	6.2	0.057	0.002	34	1
41	12943	213	175.3	4.7	0.050	0.001	37	1
43	82067	247	71.2	1.8	0.049	0.001	90	2
44	10531	225	189.7	5.5	0.054	0.001	34	1
45	36863	249	72.0	1.8	0.052	0.001	89	2
46	83798	219	30.1	0.9	0.052	0.000	211	6
47	80690	223	71.0	2.0	0.049	0.000	90	3
48	41808	212	71.1	2.5	0.051	0.001	90	3
49	64196	248	69.6	2.2	0.050	0.001	92	3
50	6709	249	181.0	4.9	0.059	0.002	36	1
51	12704	220	191.7	5.2	0.051	0.001	34	1
52	72431	233	65.7	2.0	0.050	0.001	97	3
53	23622	243	71.8	2.1	0.051	0.001	89	3
54	11220	237	67.5	1.8	0.054	0.002	95	3
117	8144	129	189.0	4.5	0.046	0.001	34	1

Zircon Grain No.	²⁰⁶ Pb (cps)	²⁰⁴ (Pb +Hg) (cps)	²³⁸ U/ ²⁰⁶ Pb	2σ	²⁰⁷ Pb/ ²⁰⁶ Pb	2σ	²⁰⁶ Pb/ ²³⁸ U age (Ma)	2σ error (Ma)	Zircon Grain No.	²⁰⁶ Pb (cps)	²⁰⁴ (Pb +Hg) (cps)	²³⁸ U/ ²⁰⁶ Pb	2σ	²⁰⁷ Pb/ ²⁰⁶ Pb	2σ	²⁰⁶ Pb/ ²³⁸ U age (Ma)	2σ error (Ma)
56	27785	239	105.0	3.5	0.050	0.001	61	2	118	101428	113	68.8	2.7	0.049	0.001	93	4
57	31027	229	71.4	2.0	0.051	0.001	90	3	119	29257	131	186.6	4.5	0.047	0.001	34	1
58	89661	236	64.9	1.9	0.050	0.001	99	3	120	12796	121	197.4	5.6	0.046	0.001	33	1
59	8056	260	183.8	5.2	0.055	0.003	35	1	121	97042	115	86.1	2.5	0.048	0.001	74	2
60	156871	233	88.2	2.7	0.048	0.000	73	2	122	20239	112	70.9	1.8	0.048	0.001	90	2
61	111504	195	30.0	0.7	0.052	0.000	212	5	123	12852	124	190.6	5.8	0.054	0.003	34	1
62	15236	199	188.1	4.4	0.050	0.001	34	1	124	117938	109	68.9	2.4	0.048	0.001	93	3
63	38837	196	71.3	1.8	0.050	0.001	90	2	125	18443	115	231.7	9.6	0.048	0.001	28	1
64	30582	217	81.7	2.5	0.050	0.001	78	2	126	34481	113	70.0	1.7	0.049	0.001	91	2
65	57387	232	65.8	1.9	0.049	0.000	97	3	127	32373	115	71.9	1.8	0.048	0.001	89	2
66	26628	211	235.3	6.3	0.049	0.001	27	1	128	17824	122	73.1	2.1	0.049	0.001	88	2
67	27852	215	289.8	7.9	0.050	0.001	22	1	130	3968	148	192.6	5.6	0.045	0.003	33	1
68	57273	208	70.2	1.9	0.049	0.000	91	2	131	7408	162	186.403	4.8	0.050	0.002	34	1
69	70256	214	85.6	2.3	0.049	0.000	75	2	132	7549	158	194.3	5.3	0.046	0.001	33	1
70	90748	208	30.9	0.7	0.051	0.001	206	5	133	5219	166	191.5	4.3	0.052	0.002	34	1
71	52648	214	66.3	2.1	0.049	0.001	96	3	134	23981	160	75.3	2.2	0.050	0.001	85	2
72	9125	191	191.3	5.0	0.051	0.001	34	1	135	7564	170	93.6	2.0	0.051	0.001	69	1
73	22638	191	67.8	2.1	0.050	0.001	94	3	136	32153	158	71.4	1.5	0.048	0.001	90	2
74	7164	198	205.6	6.0	0.052	0.002	31	1	137	6710	182	197.3	5.0	0.047	0.002	33	1
75	4972	205	181.5	5.3	0.055	0.002	35	1	138	14545	191	60.4	1.4	0.049	0.001	106	2
76	42032	201	30.2	0.7	0.052	0.001	210	5	139	58180	193	71.8	2.2	0.049	0.001	89	3
77	10761	181	166.9	5.2	0.053	0.001	38	1	140	63853	185	70.5	1.6	0.049	0.001	91	2
78	62623	182	37.1	0.9	0.051	0.001	171	4	141	20804	185	69.3	2.1	0.048	0.001	92	3
79	8320	165	288.2	8.3	0.056	0.001	22	1	143	18956	182	72.2	2.3	0.050	0.001	89	3
80	56018	178	82.9	2.3	0.050	0.001	77	2	146	8943	204	192.6	4.4	0.052	0.001	33	1
81	22434	182	72.5	2.0	0.051	0.001	88	2	147	8066	198	195.3	6.2	0.051	0.001	33	1
82	27213	186	70.1	2.3	0.050	0.001	91	3	148	56180	177	76.8	1.9	0.048	0.001	83	2
83	10274	186	192.5	5.6	0.051	0.001	33	1	149	106656	175	69.1	1.6	0.049	0.001	93	2
84	72222	192	29.5	1.2	0.052	0.001	215	8	150	17134	157	71.0	1.8	0.047	0.001	90	2
86	27164	224	187.9	5.6	0.049	0.001	34	1	151	183265	192	66.7	1.5	0.048	0.001	96	2
87	14058	206	181.9	5.5	0.054	0.002	35	1	152	70167	181	232.6	5.1	0.047	0.001	28	1
88	14889	208	66.7	2.0	0.051	0.001	96	3	153	11786	185	193.3	4.9	0.051	0.002	33	1
89	25988	214	73.3	1.9	0.054	0.002	87	2	154	16374	180	70.9	1.6	0.051	0.001	90	2
90	19772	203	196.1	5.1	0.050	0.001	33	1	155	20944	176	72.2	1.5	0.050	0.001	89	2
91	13724	78	190.7	7.7	0.053	0.002	34	1	156	25518	177	72.9	1.9	0.050	0.001	88	2
92	15673	52	185.5	8.2	0.051	0.001	35	2	157	8697	176	178.6	3.9	0.048	0.002	36	1
93	29419	38	70.8	3.0	0.050	0.001	90	4	158	71811	184	42.4	1.7	0.050	0.001	150	6
94	16029	28	69.4	2.8	0.051	0.001	92	4	159	3667	197	187.3	5.1	0.054	0.003	34	1
95	19338	33	188.2	7.6	0.052	0.001	34	1	160	27134	174	69.8	1.6	0.050	0.001	92	2
97	16171	41	188.8	7.3	0.053	0.001	34	1	161	9220	189	173.9	5.0	0.049	0.002	37	1
98	58462	38	66.5	2.8	0.050	0.001	96	4	162	43978	186	72.3	2.1	0.049	0.001	89	3
99	11141	12	163.5	6.3	0.052	0.002	39	2	163	31023	180	184.2	4.2	0.048	0.001	35	1
100	10300	19	193.0	7.5	0.054	0.001	33	1	164	22387	175	189.9	4.9	0.048	0.001	34	1
102	194200	10	68.2	2.7	0.048	0.001	94	4	165	7042	183	81.1	2.2	0.053	0.002	79	2
103	83367	15	72.9	2.9	0.049	0.001	88	3	166	29099	182	73.6	1.9	0.051	0.001	87	2
104	76919	18	72.7	2.9	0.050	0.001	88	3	167	7876	194	192.9	5.2	0.051	0.001	33	1
105	25283	12	72.4	2.9	0.049	0.001	88	4	169	7646	201	171.6	5.1	0.053	0.002	37	1
106	85111	3	93.7	3.6	0.048	0.001	68	3	170	9927	193	196.8	5.7	0.050	0.002	33	1
107	12526	8	177.0	7.2	0.048	0.002	36	1									
108	92808	7	199.3	8.3	0.047	0.001	32	1									
109	20535	3	109.4	4.9	0.048	0.001	59	3									
110	14360	1	192.8	7.8	0.047	0.001	33	1									
111	21070	144	183.9	4.6	0.048	0.001	35	1									
112	24694	139	175.4	4.2	0.048	0.001	37	1									
113	35839	135	73.6	2.0	0.049	0.001	87	2									
114	45931	121	30.8	1.0	0.051	0.001	206	7									
115	39082	132	74.4	1.9	0.049	0.001	86	2									
116	4260	136	196.9	6.1	0.044	0.002	33	1									

Table C2. Percentage area of major geologic units in the Skykomish River basin east, or 'up-basin', of the Lake Chaplain quadrangle; the western part of our basin analysis area terminates at (single U-Pb zircon) sample site 13-37A. We obtained the major geologic units from the 1:250,000-scale geologic map Washington (northwest quadrant) of Dragovich and others (2002). Sample 13-37A is ancient Skykomish River alluvium as indicated by the SP composition of the sand (Table 1, as well as the stratigraphic style and position of the strata. This provenance is supported by the detrital zircon ages, which show a strong correlation with the presently exposed Skykomish basin geology.

Major geologic units	Notes	Total area geologic units in Skykomish basin (%)	Combined total area of geologic units (%)	General distribution of zircon age data (sample 37A)
Geologic unit information				
Eocene volcanic and sedimentary rocks	Mostly sedimentary rocks such as the Sauk Formation and the volcanic rocks of Mount Persis. Significant contribution of zircons from nearby volcanic rocks of Mount Persis seems likely.	14.5	14.5	11.4% of zircons by age are Late Eocene
Cretaceous–Triassic metamorphic basement rocks	Mostly eastern and Western mélange belts as well the Tonga Formation schist and Chiwaukum Schist. See detrital zircon age data for metasandstone in the study area (Appendix C).	17.0	35.8	51.9% of zircons by age are Cretaceous to Triassic
Cretaceous intrusive rocks including orthogneiss	Plutons in the crystalline core of the North Cascades. Distinct peak at ~90 Ma is correlated with the abundant mid-Cretaceous plutonic rocks of the southern part of the crystalline core (for example, ~90 Ma Tenpeak pluton).	18.8		
Miocene–Oligocene intrusive rocks	General 1:250,000-scale unit MØig of Dragovich and others (2002) such as parts of the Snoqualmie batholith.	19.6	29.8	35.5% of zircons by age are Miocene to Oligocene
Oligocene intrusive rocks	General unit Øigd of Dragovich and others (2002).	10.1		
Pliocene–Miocene intrusive dacite	Biotite-hornblende-hypersthene dacite plugs and dikes. This unit can include altered breccia and flows.	0.1		
Quaternary deposits	Mostly alpine drift but some continental deposits as well. Much of the Quaternary sediment in the Skykomish basin is alpine drift that reworked intrabasinal deposits. However, continental glacial deposits mapped in the geographically lower part of the Skykomish basin east of Sultan likely contributed some detrital zircons from the north, including zircons from the Mesozoic Coast plutonic complex.	18.8	18.8	0% of zircons by age are Quaternary
Ice and water		1.2	1.2	Not applicable
Total		100.1	100.0	

Metasandstone Sample 35J

We obtained detrital zircon ages from feldspathic metasandstone from the southeastern part of the map area at age site 35J. The weighted average of the youngest age population ($n = 21$ zircons) is 74 ± 1 Ma and indicates that the arkosic (potassium-feldspar) sandstone petrofacies is locally as young as latest Cretaceous in age. This age is about ~13 to 26 Ma younger than previous age estimates for the Western mélange belt from detrital zircon ages (Dragovich and others, 2009a,b; Brown, 2012; Sauer and others, 2014). This metasandstone is monocrystalline quartz, plagioclase, and potassium-feldspar rich with minor but significant biotite and mica, conforming to the arkosic petrofacies of Tabor and others (1993), Jett (1986), and Jett and Heller (1988). This provenance information suggest a two-mica granitic source for this petrofacies such as the Idaho Batholith or other true granite sources. See unit KJms_w for further information.

Table C3. Detrital zircon U-Pb data for sample 35J (unit KJms_w) in the Lake Chaplain 7.5-minute quadrangle. 131 zircon grains were analyzed and 34 analyses (not shown) were rejected because of insufficient count rates, a high common Pb component, apparent ablation of subsurface inclusions, or the grain apparently not being zircon.**The final age column was determined using the $^{207}\text{Pb}/^{206}\text{Pb}$ age for grains older than 1200 Ma and the $^{206}\text{Pb}/^{238}\text{U}$ age for grains younger than 1200 Ma. The weighted average of the youngest age population is 74 ± 1 Ma (Fig. C2); cps = counts per second.

Zircon grain no.	^{206}Pb (cps)	^{204}Pb (cps)	$^{238}\text{U}/^{206}\text{Pb}$	2σ	$^{207}\text{Pb}/^{206}\text{Pb}$	2σ	Final age (Ma)**	2σ error (Ma)	Zircon grain no.	^{206}Pb (cps)	^{204}Pb (cps)	$^{238}\text{U}/^{206}\text{Pb}$	2σ	$^{207}\text{Pb}/^{206}\text{Pb}$	2σ	Final age (Ma)**	2σ error (Ma)
4_1	41700	290	58.207	1.481	0.050	0.001	110	3	4_17	387000	334	3.337	0.118	0.107	0.002	1743	35
4_2	484200	282	4.322	0.106	0.089	0.002	1402	28	4_18	372600	302	3.744	0.103	0.096	0.002	1541	31
4_3	99660	288	3.446	0.084	0.103	0.002	1676	34	4_19	204060	303	75.643	1.897	0.048	0.001	85	2
4_4	9690	307	84.746	2.048	0.050	0.002	76	2	4_21	34860	308	32.787	0.821	0.050	0.001	194	5
4_7	290400	302	82.919	2.029	0.048	0.001	77	2	4_22	12216	312	73.855	1.903	0.049	0.001	87	2
4_8	14304	308	84.962	2.096	0.049	0.001	75	2	4_25	16320	301	80.515	1.989	0.048	0.001	80	2
4_9	43980	316	38.655	0.959	0.051	0.001	165	4	4_26	8856	352	86.655	2.394	0.049	0.001	74	2
4_11	153360	397	5.225	0.134	0.089	0.002	1129	29	4_28	36660	301	13.072	0.343	0.057	0.001	475	12
4_12	586800	302	4.643	0.117	0.087	0.002	1364	27	4_29	36360	316	69.686	1.848	0.049	0.001	92	2
4_13	487800	309	4.352	0.106	0.088	0.002	1372	28	4_31	64500	303	82.919	2.154	0.048	0.001	77	2
4_14	30780	299	88.889	2.228	0.048	0.001	72	2	4_32	25482	285	64.641	1.689	0.049	0.001	99	3
4_16	45480	314	69.541	1.722	0.050	0.001	92	2	4_33	428400	317	3.295	0.085	0.104	0.002	1692	34

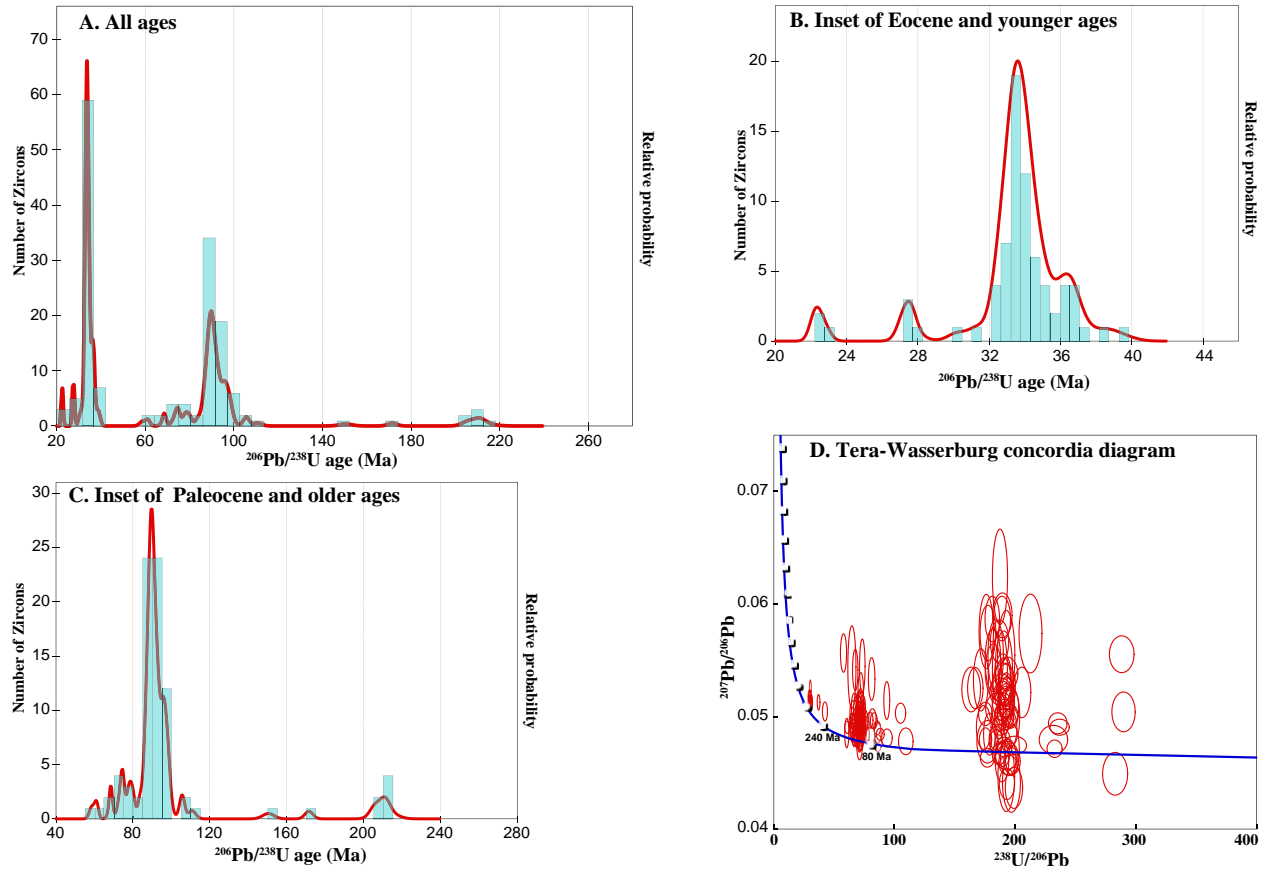


Figure C1. Age distribution plot and concordia chart for sample 37A. **A.** Probability density plot with histogram that shows the $^{206}\text{Pb}/^{238}\text{U}$ age distribution for all of the sampled zircons ($n = 158$). Ages plotted are the apparent $^{206}\text{Pb}/^{238}\text{U}$ age and not the anchored intercept age, as the difference between the two is negligible and within analytical errors. **B.** Probability density plot with histogram shows the age distribution for the younger age peak (32–36 Ma). **C.** Probability density plot with histogram shows the age distribution for the older age peak (80–100 Ma). **D.** Tera-Wasserburg concordia diagram of all sampled zircons. The white dots along the concordia curve represent ages determined by the relationship between $^{207}\text{Pb}/^{206}\text{Pb}$ and $^{238}\text{U}/^{206}\text{Pb}$ ratios. Ages increase as $^{207}\text{Pb}/^{206}\text{Pb}$ ratios increase and $^{238}\text{U}/^{206}\text{Pb}$ ratios decrease. Data-point error ellipses are 2σ . See Table C2 for the Skykomish River source-basin geology and the relationship between ‘up-basin’ source geologic units and the major age peaks.

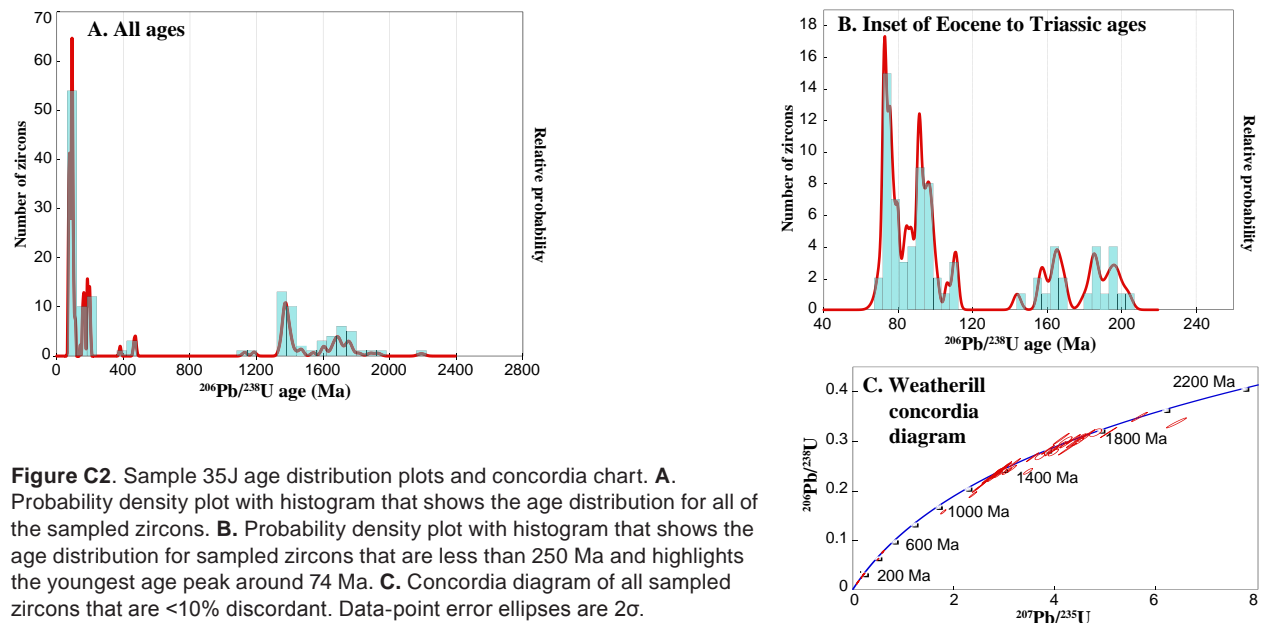


Figure C2. Sample 35J age distribution plots and concordia chart. **A.** Probability density plot with histogram that shows the age distribution for all of the sampled zircons. **B.** Probability density plot with histogram that shows the age distribution for sampled zircons that are less than 250 Ma and highlights the youngest age peak around 74 Ma. **C.** Concordia diagram of all sampled zircons that are <10% discordant. Data-point error ellipses are 2σ .

Appendix D. Geochemical Data

Whole-rock major- and trace-element analyses were performed on glacial and nonglacial sand and rock using x-ray fluorescence (XRF) and inductively coupled plasma source mass spectrometry (ICP-MS) at the GeoAnalytical Laboratory of Washington State University (WSU). Grinding of samples was completed at WSU using a tungsten carbide mill for XRF analyses and iron equipment for ICP-MS analyses. Estimates of accuracy and precision, as well as discussion of analytical methods for both XRF and ICP-MS at WSU, are given by Johnson and others (1999) and Knaack and others (1994), respectively. We prepared the Quaternary sand with 2 mm (mesh no. 10) and 0.075 mm (mesh no. 200) sieves at the DNR laboratory in Olympia, Wash. prior to grinding at WSU, so that only the sand-size fraction was chemically analyzed. Although most samples were well-sorted sand, sieving provides a better comparison between sand samples, eliminating or reducing erroneous results that may ensue from inclusion of fines and pebbles in the sand samples. As part of their quality check, WSU re-analyzed sample 13-6K2 using both XRF and ICP-MS methods. We present an average for both analyses in the tables below.

Table D1. Unnormalized x-ray fluorescence data from the Lake Chaplain 7.5-minute quadrangle. *, average of two analyses; ^L, OSL/IRSL age sample; ^T, all iron reported as Fe²⁺ (FeO); ^Z, U-Pb zircon sample. Sky-Qa, Holocene Skykomish River alluvium (unit Qa); n/a, not analyzed.

Sample	Unit	Latitude Longitude	SiO ₂ (wt %)	TiO ₂ (wt %)	Al ₂ O ₃ (wt %)	FeO ^T (wt %)	MnO (wt %)	MgO (wt %)	CaO (wt %)	Na ₂ O (wt %)	K ₂ O (wt %)	P ₂ O ₅ (wt %)	LOI (wt %)	Total (wt %)	Ni (ppm)	Cr (ppm)	Sc (ppm)	V (ppm)	LOI	ASI	CIA
6A2	Kjphw	47.968486 -121.783623	46.77	0.72	16.53	7.52	0.19	5.52	8.63	4.93	0.28	0.08	7.72	98.9	55.9	155.08	41.57	233.28	7.72	n/a	40.68
6K2*	Kjmvw	47.963311 -121.784337	52.5	1.4	16.25	10.77	0.22	7.75	2.21	3.87	0.08	0.15	4.79	100	0.66	1.56	34.31	316.02	4.79	1.58	60.81
15A-2	Kjmvw – dacite flow	47.963129 -121.770904	68.31	0.87	12.6	5.66	0.07	2.26	2.8	4.85	0.04	0.2	2.04	99.7	0.3	3.94	17.56	46.41	2.04	0.98	49.01
15J-2	Kjmvw – dacite flow	47.96418 -121.76443	65.69	0.78	11.38	7.08	0.09	5.21	2.09	2.99	0.13	0.08	3.27	98.8	16.24	8.88	21.39	227.13	3.27	1.3	56.25
15L-2	Kjmvw – flow	47.959691 -121.756448	54.32	0.59	14.68	7.91	0.06	4.63	11.1	1.45	0.01	0.06	4.42	99.23	10.29	7.26	30.67	253.46	4.42	0.65	39.44
16E	Kjltw	47.942258 -121.753854	72.07	0.3	12.88	2.63	0.06	1.02	3.36	3.7	0.78	0.04	2.43	99.27	1.72	4.24	14.13	42.08	2.43	0.99	49.7
17E	Kjshw – tuff	47.968393 -121.783396	75.37	0.04	13.88	1.36	0.02	0.09	0.33	5.4	1.68	0.03	1.14	99.35	0.3	3.94	1.41	2.12	1.14	1.23	55.11
18D-1	Kjlgbw	47.897687 -121.868764	48.77	0.41	19.1	5.86	0.14	6.71	11.38	3	0.45	0.04	2.83	98.69	40.97	147.62	38.14	158.51	2.83	0.73	42.24
18D-2	Kjlgbw – diabase	47.897687 -121.868764	50.8	0.54	17	8.62	0.15	6.2	9.81	2.24	0.19	0.06	3.02	98.62	35.11	80.82	43.08	265.37	3.02	0.79	43.91
19K-1	Kjshw	47.981402 -121.77361	45.53	0.91	15.82	13.49	0.27	5.58	8.78	1.65	0.03	0.13	5.64	97.83	9.79	33.3	50.85	350.73	5.64	0.85	45.85
23E	Kjlgbw	47.906551 -121.795799	42.18	0.47	23.08	8.96	0.15	5.6	13.09	1.51	0.15	0.01	3.54	98.74	13.22	8.17	33.8	376.16	3.54	0.87	46.61
26L-1	Kjshw	47.98199 -121.803258	46.09	1.46	16.4	12.53	0.19	4.8	9.38	3.32	0.04	0.17	4.73	99.12	14.83	10.09	35.92	327.32	4.73	0.73	42.1
39P	Kjltw	47.971565 -121.799756	74.54	0.33	12.55	3.12	0.06	1.5	0.6	5.22	0.18	0.05	1.49	99.65	3.73	8.68	16.55	57.61	1.49	1.28	55.98
53B	Kjphw	47.994063 -121.782773	65.11	0.48	14.15	6.16	0.11	2.98	2.8	3.2	0.55	0.05	3.18	98.75	17.66	45.1	23.01	152.96	3.18	n/a	56.37
3E	Qows	47.900654 -121.835441	70.3	0.51	12.59	4.38	0.08	2.37	1.87	2.43	1.35	0.11	3.58	99.57	57.92	112.71	12.92	108.87	3.58	n/a	58.69

Sample	Unit	Latitude Longitude	SiO ₂ (wt %)	TiO ₂ (wt %)	Al ₂ O ₃ (wt %)	FeO ⁺ (wt %)	MnO (wt %)	MgO (wt %)	CaO (wt %)	Na ₂ O (wt %)	K ₂ O (wt %)	P ₂ O ₅ (wt %)	LOI (wt %)	Total (wt %)	Ni (ppm)	Cr (ppm)	Sc (ppm)	V (ppm)	LOI	ASI	CIA
10H	Qgav	47.961717 -121.873169	60.5	0.65	12.47	7.5	0.13	7.15	1.91	1.84	1.12	0.12	5.58	98.96	440.93	848.87	19.88	148.12	5.58	n/a	61.81
10T	Qcphl	47.968106 -121.840503	58	0.61	11.28	7.23	0.14	9.78	2.05	1.79	0.87	0.12	6.45	98.32	574.02	868.04	20.68	132.38	6.45	n/a	59.7
16K ^L	Qco	47.933929 -121.753605	70.57	0.5	12.67	3.76	0.07	2.18	2.1	2.86	1.23	0.1	3.41	99.45	62.05	125.42	13.22	94.04	3.41	n/a	56.22
17A-2 ^L	Qco	47.866912 -121.804463	66.51	0.7	14.51	4.9	0.09	2.22	2.47	2.99	1.32	0.16	3.53	99.42	91.62	141.36	14.73	115.53	3.53	n/a	57.21
28Y	Qgos	47.886485 -121.806874	70.69	0.6	12.78	4.76	0.09	2.34	2.16	2.59	1.19	0.12	3.04	100.36	64.68	169.61	13.72	115.63	3.04	n/a	57.43
30U ^{2L}	Qows	47.883503 -121.774256	69.25	0.53	12.79	4.79	0.09	2.22	2.38	2.35	1.05	0.09	3.73	99.27	76.68	147.72	15.34	116.94	3.73	n/a	57.81
31H ^L	Qcph	47.984133 -121.873487	71.21	0.64	13.31	4.1	0.05	1.41	1.84	1.84	0.95	0.05	3.78	99.18	28.05	100.19	14.33	98.68	3.78	n/a	64.24
36 ^L	Qcph	47.977113 -121.835707	62.09	0.98	16.43	5.81	0.07	2.04	2.04	1.62	1.2	0.09	5.97	98.34	45	156.09	17.46	146	5.97	n/a	68.18
39B	Qcphl	47.968737 -121.835664	61.76	0.62	11.84	8.84	0.18	5.98	2.09	1.84	0.83	0.1	6.12	100.21	414.7	1099.2	23.41	138.23	6.12	n/a	60.42
41P	Qcphl	47.956706 -121.870131	61.2	0.62	12.91	6.92	0.13	4.79	1.5	1.97	1.17	0.13	6.83	98.18	332.34	588.28	20.04	166.68	6.83	n/a	64.13
45F	Qows	47.877627 -121.811874	68.06	0.65	13.43	4.99	0.09	2.52	2.35	2.6	1.18	0.12	3.52	99.5	95.35	229.24	14.83	117.75	3.52	n/a	57.75
47P	Qows	47.877556 -121.811847	69.06	0.54	13.27	4.32	0.08	2.33	2.05	2.71	1.29	0.12	3.23	98.99	80.01	148.02	13.22	101.71	3.23	n/a	58.07
47Q	Sky-Qa	47.837091 -121.65925	69.98	0.47	13.97	3.67	0.07	1.81	2.99	3.05	1.44	0.08	1.77	99.29	26.94	64.78	13.32	84.66	1.77	n/a	53.75
36H	Qcphl	47.97671 -121.838177	61.79	0.67	12.89	6.79	0.13	7.34	1.92	1.97	1.22	0.15	5	99.87	347.2	594.81	19.37	144.09	5	n/a	61.54
54C	Qcph	47.984402 -121.844318	74.46	0.47	11.71	3.32	0.04	1.07	1.42	1.51	0.96	0.03	3.86	98.84	22.06	82.28	9.82	70.64	3.86	n/a	65.7
54F	Qcph	47.984867 -121.841982	71.24	0.64	13.54	3.74	0.04	1.55	1.86	1.8	0.92	0.02	4.13	99.49	26.03	91.01	13.02	94.04	4.13	n/a	64.88
105A	Sky-Qa	47.85652 -121.81407	67.32	0.57	14.42	4.2	0.08	2.03	2.98	2.98	1.46	0.1	3.8	99.93	41.2	80.8	12	99.6	3.8	n/a	54.78
105B	Sky-Qa	47.85713 -121.81305	67.86	0.57	14.16	4.12	0.08	1.95	2.97	2.99	1.44	0.09	3.02	99.24	34.21	89.5	13.82	99.79	3.02	n/a	54.43

Table D2. Unnormalized inductively coupled plasma mass spectrometry data from the Lake Chaplain 7.5-minute quadrangle in parts per million (ppm). *, average of two analyses; ¹, OSL/IRSL age sample; ², U-Pb zircon sample. Sky-Qa, Holocene Skymish River alluvium (unit Qa).

Sample	Unit	Latitude Longitude	La	Ce	Pr	Nd	Sm	Eu	Gd	Tb	Dy	Ho	Er	Tm	Yb	Lu	Ba	Th	Nb	Y	Hf	Ta	U	Pb	Rb	Cs	Sr	Sc	Zr
6A2	Kjphw	47.968486 -121.783623	3.66	9.05	1.44	7.22	2.25	0.99	2.98	0.53	3.49	0.75	2.03	0.29	1.8	0.29	63.91	0.25	0.64	19.62	1.09	0.05	0.13	3	5.78	0.71	259.44	40.36	38.76
6K2*	Kjmwv	47.963311 -121.784337	4.75	12.08	1.93	9.91	3.25	1.32	4.28	0.79	5.14	1.1	3.02	0.44	2.69	0.41	43.85	0.38	1.87	27.84	2.2	0.13	0.16	3.26	1.11	0.46	63.3	33.85	77.87
15A-2	Kjmwv – dacite flow	47.963129 -121.770904	6.11	17.09	2.82	14.57	4.86	1.6	6.31	1.15	7.55	1.65	4.68	0.68	4.37	0.69	37.32	0.58	2.16	41.43	3.34	0.15	0.3	1.9	0.48	0.12	83.96	17.77	122.65
15J-2	Kjmwv – dacite flow	47.96418 -121.76443	2.17	6.29	1.09	6.03	2.29	0.8	3.31	0.63	4.21	0.88	2.39	0.32	1.8	0.28	44.58	0.18	0.55	23.07	1.02	0.05	0.19	0.71	1.93	0.45	74.42	21.49	34.18
15L-2	Kjmwv – flow	47.959691 -121.756448	1.71	4.46	0.75	4.1	1.47	0.59	2.06	0.39	2.66	0.57	1.58	0.22	1.26	0.19	8.91	0.14	0.49	13.37	0.88	0.04	0.09	0.86	0.22	0.25	61.21	27.56	27.1
16E	Kjltw	47.942258 -121.753854	4.74	11.95	1.84	9.06	3.01	0.65	4	0.81	5.53	1.26	3.72	0.58	3.81	0.62	196.94	0.79	1.48	32.89	3.01	0.12	0.33	1.11	10.25	0.45	207.16	13.62	91.88
17E	Kjshw – tuff	47.968393 -121.783396	15.56	29.96	3.75	14.89	4.34	0.78	3.54	0.43	1.63	0.2	0.4	0.05	0.27	0.04	530.94	7.38	13.77	6.79	3.42	1.32	3.11	13.4	53.99	1.15	190.2	1.22	73.39
18D-1	Kjlgbw	47.897687 -121.868764	0.88	2.45	0.41	2.29	0.85	0.41	1.19	0.23	1.49	0.32	0.87	0.12	0.75	0.12	131.4	0.13	0.22	7.71	0.47	0.02	0.03	0.66	6.93	0.86	324.28	39.32	13.51
18D-2	Kjlgbw – diabase	47.897687 -121.868764	2.22	5.47	0.89	4.5	1.52	0.57	1.91	0.34	2.28	0.47	1.38	0.2	1.26	0.21	63.47	0.33	0.52	12.27	0.92	0.04	0.11	0.39	2.87	0.44	283.29	42.85	27.92
19K-1	Kjshw	47.981402 -121.77361	3.66	8.44	1.31	6.47	1.97	0.79	2.43	0.42	2.7	0.59	1.61	0.24	1.5	0.25	113.16	0.59	0.58	14.48	0.95	0.32	0.17	2.49	1.25	1.28	545.71	51.15	30
23E	Kjlgbw	47.906551 -121.795799	0.27	0.59	0.1	0.57	0.22	0.21	0.31	0.06	0.4	0.09	0.26	0.04	0.24	0.04	67.81	0.02	0.03	2.07	0.05	0	0.01	0.23	3.68	1.02	896.49	32.36	1.24
26L-1	Kjshw	47.98189 -121.803258	3.46	9.39	1.61	8.64	3.16	1.27	4.21	0.81	5.2	1.14	3.17	0.45	2.89	0.46	14.62	0.34	1.17	28.71	1.92	0.08	0.13	1.44	0.85	0.37	50.51	36.57	63.93
39P	Kjltw	47.971565 -121.799756	2.46	6.55	1.01	4.96	1.74	0.39	2.33	0.48	3.3	0.76	2.31	0.37	2.41	0.4	68.37	0.55	1.02	19.52	2.15	0.09	0.24	1.27	2.2	0.11	110.01	16.31	64.16
53B	Kjphw	47.994063 -121.782773	4.17	9.52	1.4	6.48	1.92	0.62	2.37	0.45	2.99	0.66	1.95	0.3	1.94	0.31	150.99	0.74	1.04	16.75	2.07	0.08	0.37	4.9	10.36	1.04	208.43	22.97	69.19
3E	Qcws	47.900654 -121.835441	9.6	20.28	2.51	10.36	2.47	0.72	2.47	0.43	2.74	0.56	1.61	0.23	1.55	0.24	462.36	2.63	4.26	14.3	2.29	0.32	1	5.8	35.16	1.38	178.05	13.45	82.56
10H	Qgav	47.961717 -121.873169	10.5	21	3.2	14.06	3.8	1.16	4.01	0.65	4.06	0.83	2.33	0.33	2.19	0.36	373.92	2.55	4.65	21.26	2.23	0.32	1.04	7.7	33.11	2.17	108.14	20.7	81.13
10T	Qcphi	47.968106 -121.840503	8.7	18.48	2.49	10.61	2.74	0.88	2.98	0.52	3.2	0.66	1.81	0.26	1.66	0.27	324.2	1.98	4.03	17.3	1.96	0.28	0.86	8.02	24.3	1.79	110.32	19.97	71.24
16K	Qco	47.933929 -121.753905	10.55	21.75	2.73	10.81	2.57	0.82	2.48	0.42	2.62	0.54	1.48	0.21	1.36	0.22	481.57	2.63	3.94	13.1	2.44	0.29	0.93	6.41	28.37	1.04	267.25	12.28	89.5
17A-2 ¹	Qco	47.866912 -121.804463	16.02	33.08	4.28	17.83	4.1	1.22	4.03	0.67	4.05	0.81	2.21	0.33	2	0.3	519.51	3.71	6.26	20.49	3.43	0.46	1.42	7.99	35.35	1.72	290.69	15.03	127.32
28Y	Qgos	47.886485 -121.806874	10.74	22.12	2.92	12.29	2.96	0.89	3	0.52	3.22	0.67	1.82	0.27	1.66	0.26	441.59	2.47	4.44	17.06	2.41	0.34	0.94	5.73	29.09	1.37	210.06	13.96	88.81
30U ^{2L}	Qcws	47.883603 -121.774256	9.08	18.17	2.48	10.4	2.48	0.8	2.6	0.45	2.83	0.59	1.65	0.24	1.54	0.24	366.75	2.16	3.74	15.18	2.05	0.28	0.81	4.78	27.78	1.26	196.28	15.06	74.87
31H	Qcph	47.984133 -121.873487	10.77	20.26	2.83	11.57	2.5	0.83	2.35	0.4	2.51	0.52	1.41	0.2	1.29	0.21	394.98	2.22	4.59	13.17	2.31	0.32	0.74	6.8	31.39	2.12	242.85	12.72	85.5
36L	Qcph	47.977113 -121.835707	14.12	29.88	3.93	16.33	3.69	1.09	3.5	0.56	3.4	0.69	1.87	0.28	1.71	0.27	487.01	3.36	7.06	16.94	4.16	0.47	1.22	9.59	41	2.44	201.16	17.32	154.68
39B	Qcphi	47.968737 -121.835664	8.5	18.51	2.57	11.08	2.86	0.92	3.12	0.54	3.28	0.68	1.86	0.27	1.67	0.25	290.74	1.9	3.8	16.83	1.86	0.28	0.76	7.86	23.13	1.6	108.04	22.19	69.05

Sample	Unit	Latitude Longitude	La	Ce	Pr	Nd	Sm	Eu	Gd	Tb	Dy	Ho	Er	Tm	Yb	Lu	Ba	Th	Nb	Y	Hf	Ta	U	Pb	Rb	Cs	Sr	Sc	Zr
41P	Qcpl	47.956706 -121.870131	12.01	24.2	3.23	13.77	3.33	0.99	3.46	0.6	3.7	0.75	2.02	0.29	1.79	0.28	444.7	2.56	4.32	19.02	2.09	0.31	1.03	7.83	33.48	2.02	114.84	19.81	77.47
45F	Qcws	47.877627 -121.811874	14.04	29.28	3.58	14.4	3.31	1	3.16	0.55	3.23	0.66	1.84	0.27	1.68	0.26	476.77	3.47	5.4	17	3.19	0.73	1.17	7.68	30.38	1.43	251.54	14.48	122.64
47P	Qcws	47.877556 -121.811847	12.2	25.23	3.22	13.06	3.11	0.93	3.1	0.51	3.07	0.64	1.74	0.24	1.59	0.24	500.61	2.92	4.68	16.18	2.61	0.72	1.06	7.07	32.51	1.44	255.29	12.55	98.17
47Q	Sky-Oa	47.837091 -121.85925	10.52	21.41	2.71	10.6	2.46	0.77	2.4	0.43	2.61	0.56	1.55	0.23	1.52	0.24	451.64	3.05	4.27	14.66	2.95	0.66	1.2	8.51	39.28	2.06	277.54	11.75	106.28
36H	Qcpl	47.97671 -121.838177	11.21	23.7	3.09	13.08	3.14	0.93	3.2	0.54	3.36	0.69	1.92	0.28	1.75	0.28	412.79	2.87	5.07	17.69	2.38	0.36	1.12	9.81	36.6	2.36	121.37	18.67	88.16
54C	Qcph	47.984402 -121.844318	7.81	15.6	2.13	8.88	2.06	0.74	2.04	0.35	2.12	0.44	1.15	0.17	1.1	0.17	374.57	1.79	3.95	11.44	2.02	0.61	0.67	6.44	27.01	1.62	209.35	9.35	75.49
54F	Qcph	47.984867 -121.841982	10.3	20.04	2.78	11.42	2.62	1.01	2.79	0.47	3.02	0.63	1.67	0.24	1.51	0.23	363.48	2.13	4.73	16.72	2.46	0.68	0.74	6.89	31.01	2.5	247.22	13.03	91.4
105A	Sky-Oa	47.85652 -121.81407	12.25	24.89	3.11	12.4	2.71	0.84	2.72	0.48	2.95	0.61	1.7	0.26	1.6	0.26	459.23	3.41	5.15	16.31	3.56	0.67	1.43	10.29	42.53	2.54	268.96	12.64	132.19
105B	Sky-Oa	47.85713 -121.81305	12.01	24.1	3.02	11.93	2.72	0.79	2.64	0.45	2.92	0.63	1.71	0.27	1.67	0.26	448.46	3.31	5	16.19	3.49	0.68	1.3	9.73	41.24	2.28	268.57	12.67	128.06